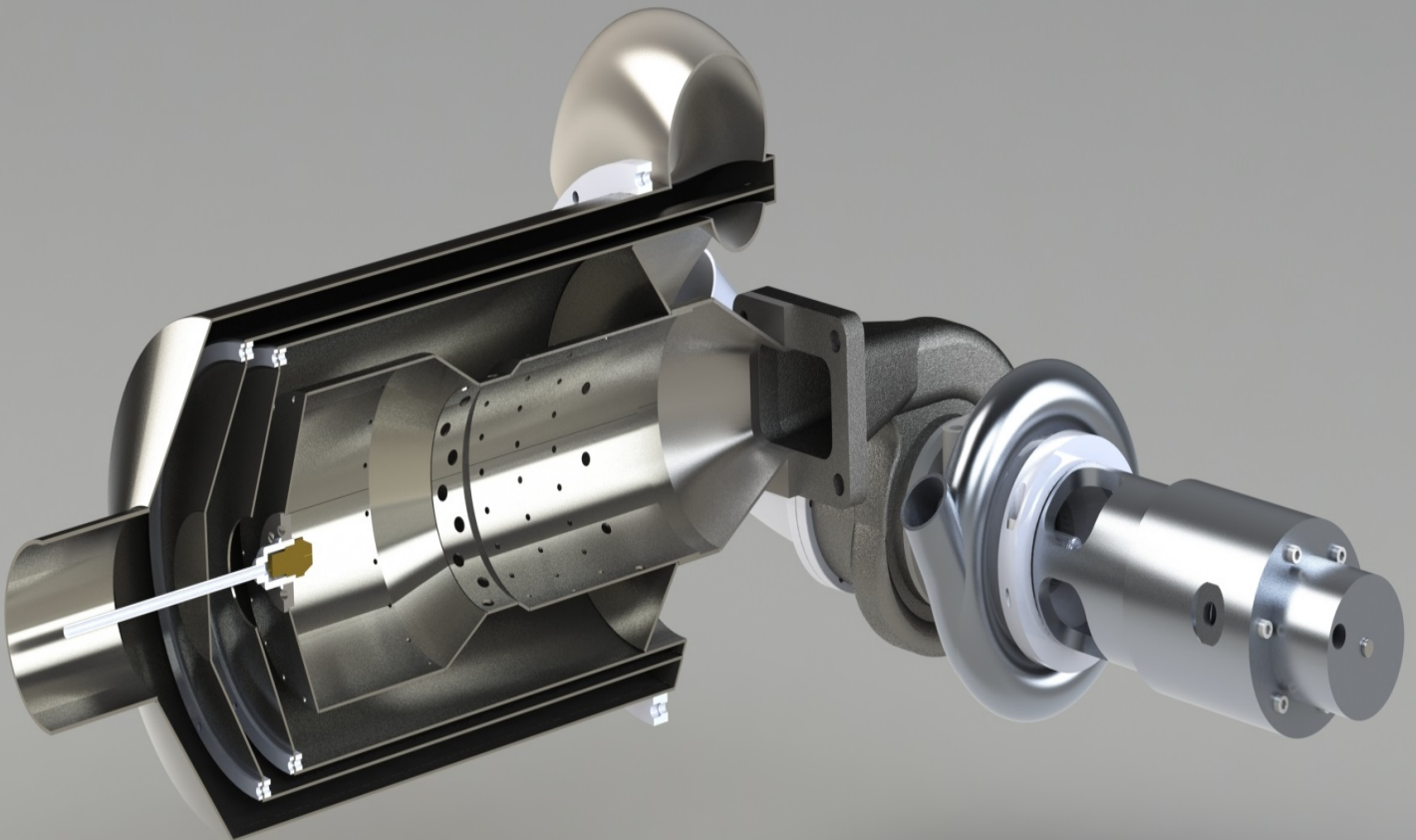


Department of Precision and Microsystems Engineering

Gas turbine range-extender for automotive applications

Patrick Dettmers

Report no : 21
Coach : Prof. dr. ir. S.A. Klein
Professor : Prof. dr. ir. B.J. Boersma
Specialisation : Engineering mechanics
Type of report : Thesis
Date : 22-09-2016



Gas turbine range-extender

For automotive applications

by

Patrick Dettmers

to obtain the degree of Master of Science
at the Delft University of Technology,
to be defended publicly on Tuesday September 22, 2016 at 10:30 AM.

Student number: 4237110
Project duration: August 17, 2015 – September 22, 2016
Thesis committee: Prof. dr. ir. S. A. Klein, TU Delft, supervisor
Prof. dr. ir. B. J. Boersma, TU Delft, supervisor
Ir. J. W. Spronck, TU Delft
Ir. E. Kamphues, Mitsubishi Turbocharger and Engines Europe B.V.

This thesis is confidential and cannot be made public until September 31, 2019.

An electronic version of this thesis is available at <http://repository.tudelft.nl/>.

Abstract

This thesis describes the design and construction of a small gas turbine engine range-extender which is meant for charging electric vehicles. While automotive emission legislation becomes more stringent every five years, the challenges for conventional cars to meet these standards increase. Therefore alternatives such as 'hybrid electric vehicles' or 'full-electric vehicles' are becoming more popular. Even though electric powered cars are gaining popularity, they still have a limited range which makes them impractical for most users. This problem can be addressed with a range-extender, a device that can be used to charge the batteries of electric vehicles while driving. When a micro gas turbine drives a generator it can be used as a range-extender.

The goal of this graduation project is to design and build a prototype range-extender. This prototype will act as a proof-of-concept, therefore for this purpose mostly off-the-shelf components will be used.

Prior to the design phase literature research and market research were conducted. Based on their outcome, the requirements of the gas turbine engine were defined. Using Matlab, a cycle and matching analysis was conducted to obtain the optimum compressor and turbine behaviour for this application. The combustion chamber is designed using a Fluent combustion model. Three different combustion chambers have been developed and simulated to compare stability and emissions when using different fuels.

Within the final phase of the graduation project, the design was tested within Mitsubishi Turbocharger and Engines Europe (MTEE). The results were compared to the results obtained from the modelling. It may be concluded that the combustion model gives a good indication on the behaviour. However, unforeseen instabilities did occur, but could be solved by minor changes to the test set-up.

After finalization of this thesis the test set-up will be used for combustion and cycle experiments. The results of these experiments can be leveraged to improve later prototypes.

Preface

From a very early age I found engines captivating technology, and quickly started to build them on my own. At age 16 I started to design and build gas turbine engines from scratch which quickly became a time consuming hobby. During my master at the University of Delft I came into contact with MTEE, and when they offered me a graduation project that involved designing and building a gas turbine engine, it didn't took long to make a decision.

The goal of the assignment is to design and build a gas turbine engine to be used for a range-extender¹ application. This test set-up can then be used for future research.

Before the design process started market research has been conducted by Clara Moreno Castán [7] and myself. Its goal was to study the potential market opportunities and challenges a gas turbine range-extender faces. Based on these results a literature research was conducted to investigate the possibilities and available technology to shape the gas turbine technology to meet the requirements derived from the market research.

After the literature research a design process started where the main focus was on the overall layout, overall design and the combustor. Therefore specific components, like the generator and recuperator, have not been optimized to their full potential. This should be done within future research.

Finally the design was built and tested within MTEE. The results of these tests are enclosed within this thesis.

¹A range-extender is a device which can charge the batteries of an electric vehicle while driving

Acknowledgement

After almost 13 months working on the gas turbine range-extender project, I want to take this opportunity to thank all the people who worked, helped and made this project possible.

First and foremost I would like to thank my academic supervisors and my company supervisors; Professor Bendiks Jan Boersma, Professor Sikke Klein, Edwin Kamphues, Rob Eling and Mark Rankenberg. Without their guidance, knowledge, efforts and support this project would have not been possible.

I also would like to thank all the people within MTEE who have helped designing, purchasing, building and testing. The whole gas turbine project is a pure group-effort and again; without all these people this project would not have been possible.

Besides the people who worked directly on this project, I would also like to thank Kurt Schreckling, Martin Stouten and Gerald Rutten as they inspired and motivated me to start designing and building gas turbines from a very young age. In addition my father always supported me with putting the idea's to practice and taught me how to machine each component.

Finally I would like to thank my parents and my girlfriend Charmaine for all the support and for giving me the opportunity to study in Delft.

Nomenclature

\dot{m}	Mass flow
η_{recup}	Recuperator efficiency
η_{comp}	Compressor efficiency
η_{turb}	Turbine efficiency
κ	Specific heat ratio
κ	Turbulent kinetic energy
ω	Specific dissipation
P	Pressure [Pa]
T	Temperature [K]
W	Work
BEV	Battery Electric Vehicle, also known as full EV
ER	Expansion Ratio
EV	Electric Vehicle
FAR	Fuel to Air Ratio
FCEV	Fuel Cell Electric Vehicle
hc	Convective heat transfer coefficient $\frac{W}{m^2K}$
HEV	Hybrid Electric Vehicle
ICE	Internal Combustion Engine
kRPM	Revolutions per minute x 1000
NVH	Noise, vibrations and harshness
OEM	Original Equipment Manufacturer

POI	Point of operation / point of interest
Pr	Prandtl number
Re	Reynolds number
REEV	Range-extended Electric Vehicle, vehicle equipped with a range-extender
RPM	Revolutions per minute
RQL	Rich-Quench-Lean, type of combustion chamber which lowers the max. temperature to decrease NO_x emissions while still making use of the stability of a rich flame
SRQL	Straight-Rich-Quench-Lean, where the RQL liner is stepped, the SRQL liner is straight along its whole length
TIT	Turbine inlet temperature

Contents

1	Market research	8
1.1	Conclusions market research	13
2	Micro gas turbines	14
2.1	Automotive history	15
2.2	Gas turbine basics	15
2.2.1	Cycle	15
2.2.2	Compressor	18
2.2.3	Combustion chamber	20
2.2.4	Emissions	27
2.2.5	Turbine	37
2.2.6	Recuperator	38
3	Modelling	41
3.1	Goals / requirements	41
3.2	Basic design	43
3.3	Matlab thermodynamic cycle model	47
3.4	Matlab matching model	51
3.5	Cycle-Tempo model	55
3.6	Fluent combustion simulation	56
3.6.1	Combustion model	56
3.6.2	Geometry & Boundary conditions	57
3.6.3	Mesh	60
3.6.4	Solver set-up	60
3.6.5	Validation	61
3.6.6	Results	63
3.6.7	Conclusion	70
4	Final Design	71
4.1	Turbomachinery	73
4.2	Combustion Chamber	74
4.3	Recuperator	77
4.4	Generator	78

5	Test Set-up	82
5.1	Engine test-stand	82
5.1.1	Oil circuit	83
5.1.2	Fuel-system	83
5.1.3	Sensor layout	84
5.2	Preliminary test	86
5.2.1	Vaporizing nozzle test	86
5.3	Engine test	87
5.3.1	Testing goals	87
6	Test Results	88
6.1	Stability tests	88
6.1.1	Rich can	88
6.1.2	RQL can	93
6.1.3	SRQL can	95
6.1.4	Fuel nozzles	96
6.1.5	Generator test	96
6.2	Measurements	97
6.2.1	Engine behaviour	97
6.2.2	Recuperator behaviour	105
6.2.3	Cycle model	106
7	Conclusions	109
8	Recommendations	110
8.1	General project recommendations	110
8.2	Engine recommendations	110
A	Morphological overviews	115
B	Test results	119
B1	Plots	120
C	Drawings	130
D	Matlab Code	146
D1	Cycle Model	146
D2	Recuperator Calculations	151
D3	Matching model	152
D4	Post-process script	152
E	Generator data	163

Introduction

Currently electric vehicles are gaining a small market share, yet the range of these electric vehicles is relatively small. The lack of range is one of the factors that hold back a large growth in market share as the electric range is often insufficient. This problem can be solved using a range extender, which is a device that can charge the batteries while driving. Currently a few gas turbine range-extendors² have been developed, these engines are all designed for maximum efficiency. This causes the engines to be large and expensive. This project approach is different from all other engines as the main focus is to reduce costs.

This thesis describes the design process of a gas turbine engine aimed for range-extender usage. The gas turbine engine should be based on turbocharger part and technology. The scope of this project includes the design, build and test process of the gas turbine range-extender. The main focus lies on the overall layout, overall design and the combustion chamber. Other systems will be designed but not optimized to their full potential.

The first part of this thesis describes the market- and literature research. The literature research compares the current technology available, the information in this section can apply to most micro gas turbines. The market research investigates the potential market opportunities and challenges for gas turbine range-extendors.

The second part of this report describes the design process of a gas turbine range-extender. The design process started by generating a rough design based on the market- and literature research. This rough design is being modelled and a detailed design has been made. The detailed design is eventually built and tested within MTEE.

The last part describes the results of the tests and compares them to the results of the previously constructed models.

²A range-extender is a device which can charge the batteries of an electric vehicle while driving

Chapter 1

Market research

Within MTEE market research is conducted to study the market opportunities and challenges of a micro gas turbine range-extender. Several studies reviewed and direct contact with OEM's is made. Besides the potential market-size, the market demands are also studied.

In past decades most cars were powered directly by 4-stroke gasoline or diesel engines. Currently alternatives are being developed and gaining small market shares. More stringent emission legislation is the major driving force for these developments. Within the European Union the emission legislation becomes more challenging for automotive manufacturers to fulfil every five years. Figure 1.1 shows the trend of CO₂ emission legislation.

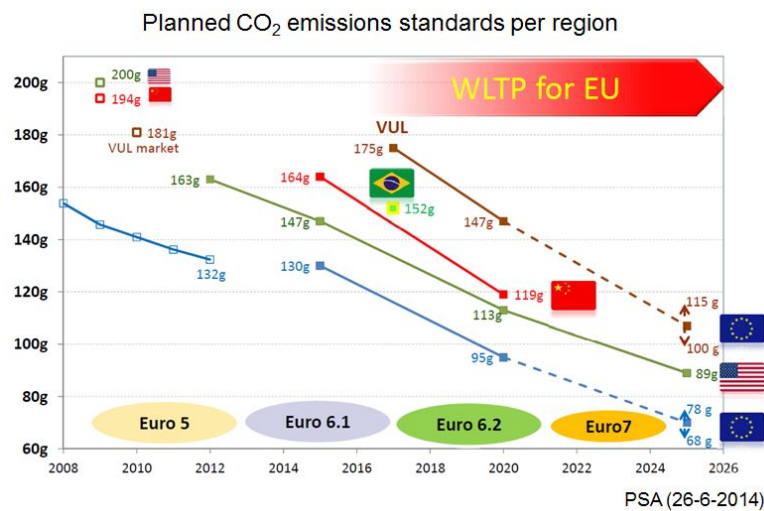


Figure 1.1: The changing CO₂ limits for different areas past and coming years

Currently the maximum allowed CO₂ emission is 130 grams per kilometre. The current allowable NO_x emissions for diesel and gasoline cars are 80 and 50 milligrams per kilometre respectively [7]. In 2020 the allowed CO₂ emission will drop to 95 grams per kilometre. It is to be expected that in 2025 the limit is decreased to 68 to 78 grams per kilometre. At

this point conventional piston-engined powered cars will struggle to comply with this legislation. Hence automotive manufacturers will need to develop alternative driving systems to be able to comply with the legislation of 2025 and beyond. Currently a trend of hybridization and electrification of vehicles is already noticeable, yet the progress of battery development is typically slow. OEM's do not expect major improvements in battery technology for the coming 10 to 20 years. This is where the range-extender's market potential arises, as long as batteries do not fulfil the needs of end-users.

Battery development plays a key role in the market potential for range-extenders. Currently batteries are relatively expensive and heavy. The majority of car batteries are Li-On¹ based, the cost of these batteries are estimated at 133 to 150 euro per kWh. The added range with range-extender use should be less expensive than an extra battery.

Figure 1.2 shows the forecast of the expected market share of cars produced worldwide when the CO₂ limit is 40 grams of CO₂ per kilometre in 2050. The y-axis shows the market share of cars sold globally in percentages, which approximately correspond to millions of cars. According to the forecast, it is to be expected that in 2050 the conventional ICE powered car is completely phased-out. The range-extender would gain a market share of 45% which corresponds to 45 million vehicles, the expectation is that REEV's would primarily be used for middle sized cars (M). The full electric vehicles (BEV) could gain a market share of 35%. The fuel-cell powered cars (FCEV) are expected to gain a market share of 20% and would primarily be used for larger cars(L). The figure shows a rapid increase of range-extenders in 2022, this years should be the aim for MTEE to enter the range-extender market.

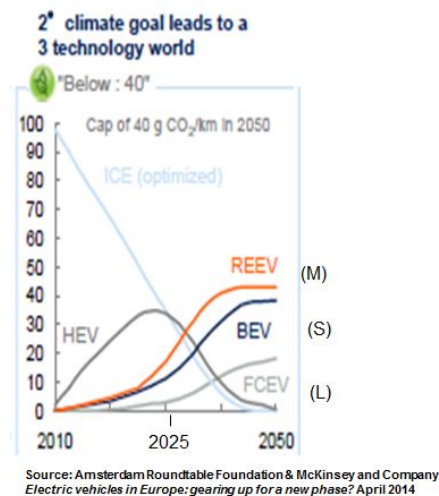


Figure 1.2: Market share of units produced each year worldwide in % (equals approximately million units)

During the market research several forecasts were reviewed, their expectations of the range-extender market's magnitude is summarized in Figure 1.3. Despite the discrepancy

¹Lithion-ion battery

in expectations, there is a consensus that a significant market share will arise for range-extenders. The average expected market share will grow from 2 million units in 2020 to almost 7 million in 2025.

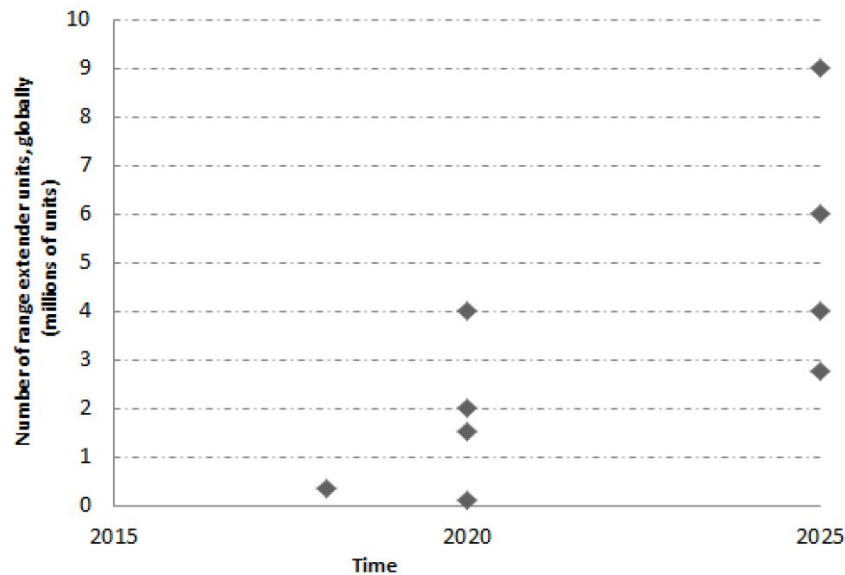


Figure 1.3: Forecast of the global range-extender market upto 2025 [7]

Customer demands

Different studies and OEM's input have been gathered to study the demands of OEM's and of end-users. The following features are mentioned by OEM's as important. The features are sorted by importance, the first being the most important.

- Cost
Volvo mentioned that a range-extender's cost should not exceed 1000 Euro while Renault stated that 800 Euro should be the target price of a range-extender [7].
- Emissions
Currently the European-Union offers no legislation for range-extender applications, they are likely reviewed as an HEV. California has laws that prescribe the maximum allowable emissions for range-extended vehicles. These could be used as a guideline and are shown in Table 1.1.
- Power output
The required power output of a range-extender depends on its function and the targeted market. The estimated power output needed is shown in Table 1.4.
- Life-time
A range-extender should have a life-time of at least 500 hours according to Volvo [7].

- Efficiency

The range-extender should only be used in emergency situations, therefore the efficiency is least important and not specified.

Power output	Functions allowed
$P < 10\text{ KWe}$	<ul style="list-style-type: none"> ▪ Urban: only charge depleting
$10\text{ KWe} \leq P < 20\text{ KWe}$	<ul style="list-style-type: none"> ▪ Urban: both charge depleting and sustaining ▪ Highway: only charge depleting
$20\text{ KWe} \leq P < 30\text{ KWe}$	<ul style="list-style-type: none"> ▪ Urban: both charge depleting and sustaining ▪ Highway: charge depleting; charge sustaining at the expense of comfort (auxiliaries off, lower speed)
$P \geq 30\text{ KWe}$	<ul style="list-style-type: none"> ▪ Urban: both charge depleting and sustaining ▪ Highway: charge depleting and charge sustaining, including hills gradients

Figure 1.4: Required power output of a range-extender [7]

Emission type	Limit [g/km]
NO _x	0.0125
CO	0.625
HC	2.5
PM	0.00625

Table 1.1: SULEV emission legislation limits. [12]

In theory any combustion engine could be used for a range-extender application. As 4-stroke piston engines are currently widely used to drive cars, it is obvious that these engines will be adapted for range-extender use. However the change of required engine behaviour when used in range-extender applications makes it interesting to study other types of engines. The use of an range-extender can be compared to a 'Series HEV' in a sense that the range-extender only outputs electrical power which is added to a buffer, in this case a battery(see Fig. 1.5). This allows the engine to run at a constant speed with a constant power output, which is significantly different from a 'Parallel HEV' where a direct drive is being used and thus a transient engine response is required. Currently competitors are studying Wankel, 4-stroke, free-piston and gas turbine engines. From the morphological overview in Appendix A and the market study conducted by C. Moreno Castán [7] it can be concluded that a micro gas turbine would suit the needs of a range-extender best due to the superb weight to power ratio and power density. Besides being a compact engine, the gas turbine engine is nearly maintenance free and has the potential to be more silent than a piston engine.

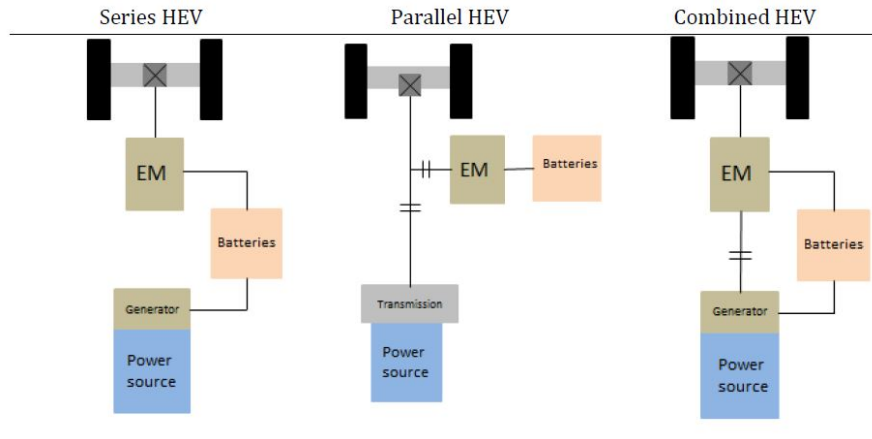


Figure 1.5: Configuration possibilities of a hybrid electric vehicle [7]

With the changing automotive market, the turbocharger market is highly influenced. The phasing out of the conventional ICE powered cars will cause the demand for turbochargers to fade. For a company like MTEE it is important to anticipate the gradual shifting turbocharger market. A product like a micro gas turbine is close to MTEE's core business and makes use of already developed technology and production facilities. This is a major advantage which other companies might not have. Therefore the main competitive advantage of MTEE would be cost, which happens to be the most important feature of a range-extender according to OEM's.

1.1 Conclusions market research

This section summarizes the conclusions that can be derived from the market-research which acts as an input for the literature research.

Market research main conclusions;

- Emission legislation development generates a market opportunity for range-extendeders. The size of this market is estimated to be 3 to 9 million units per annum in 2025.
- Currently, no range-extender specific legislation is available in the European Union. The state of California has currently the only range-extender legislation. This legislation could be taken as a reference.
- The investigation into what engine type is most suitable to drive a range-extender showed that a micro gas turbine has particular advantages over a piston engine. These advantages are mainly cost, size and weight. These advantages only hold if the concept focuses on these characteristics.
- The most important feature of the range-extender is cost, which should be the main focus of the gas turbine concept design. The least important factor is efficiency, yet the range-extender should comply with the SULEV legislation. The limitations of the SULEV legislation are shown in Table 1.1.
- A range-extender can cost up to 1.000 euro.
- An electric power output between 10 and 30 kW would be sufficient according to OEMs.

Chapter 2

Micro gas turbines

A gas turbine engine is a power plant that is known for its high power to weight ratio. In large land-based applications the efficiency of gas turbine engines can exceed the efficiency of piston engines. On smaller scale applications the efficiency is less but the high power-to-weight ratio and high power density are still advantageous.

The basis of gas turbine engines is relatively simple because there are only a few moving parts. The low number of moving parts makes the engine reliable and maintenance friendly. Besides these advantages a gas turbine engine does not have to run on a specific fuel. This multi-fuel capability makes the concept more resilient to future changes in fuel availability.

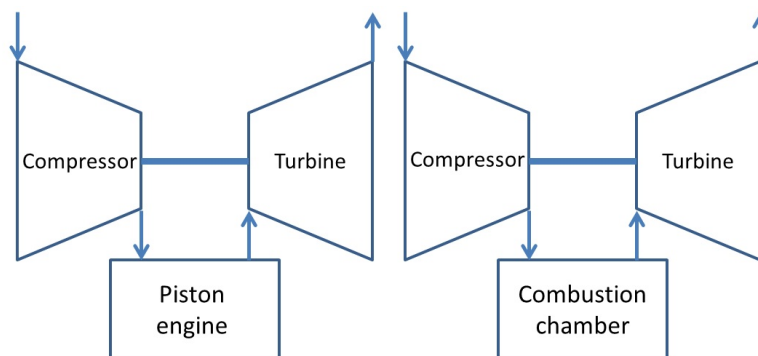


Figure 2.1: Schematic representation of the most basic Brayton cycle

A turbocharger is a device used to enhance the performance of a piston-engine. This device extracts energy from the exhaust and uses this energy to compress fresh air which is used to feed the engine. The turbocharger consists of a turbine and compressor that are typically mounted on the same shaft as shown in Figure 2.1. This explains the close relationship between turbochargers and gas turbine engines. Basically a turbocharger can be seen as a gas turbine engine without a combustion chamber. MTEE ¹ supplies turbochargers to the

¹Mitsubishi Turbocharger and Engine Europe B.V.

European car market. The transition from turbocharger manufacturing to gas turbine manufacturing is therefore a relatively small step.

2.1 Automotive history

In the late 1940's, Rover was the first car manufacturer to experiment with gas turbine powered cars. These initial tests showed the potential of these engines. The gas turbines proved to be small, lightweight and yet have a large power output. The majority of the gas turbines were direct or indirect shaft power configurations, this proved to be the Achilles-heel of the gas turbine engine. When the high-speed turbomachinery was still in its infancy, high-speed electronics did not even exist. Thus a shaft driven configuration was the only available option. The consequence of this configuration was a low throttle response, high cost and high fuel consumption. These factors finally made the gas turbine lose the battle with the piston engine [8] [21].

Times have changed, and today the emission legislation challenges the automotive industry. With high-speed electronics becoming more available, the comeback of the gas turbine engine could be feasible. These technological processes make it possible to apply a gas turbine engine in a hybrid configuration. When a gas turbine engine is used in a hybrid car, the engine can run at a constant speed, which eliminates the need for high throttle response. The combustion process within gas turbine engines can be accomplished at relatively low temperatures compared to piston engines. Therefore gas turbines have the potential to lower the emissions of vehicles, NO_x emissions in particular [8].

2.2 Gas turbine basics

2.2.1 Cycle

A gas turbine engine is based on the thermodynamic Brayton cycle. The flow-scheme of a basic configuration and the corresponding temperature-enthalpy chart can be seen in Figure 2.2 and 2.3. When non-isentropic compression and expansion are introduced the compression and expansion behaviour will follow the dashed line [4].

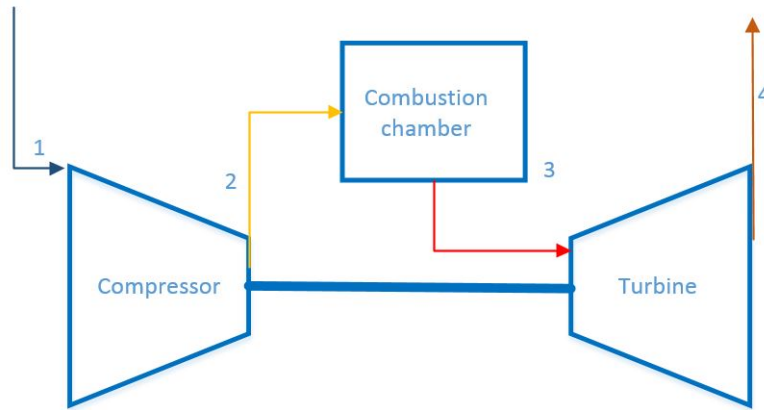


Figure 2.2: Schematic representation of the basic Brayton cycle

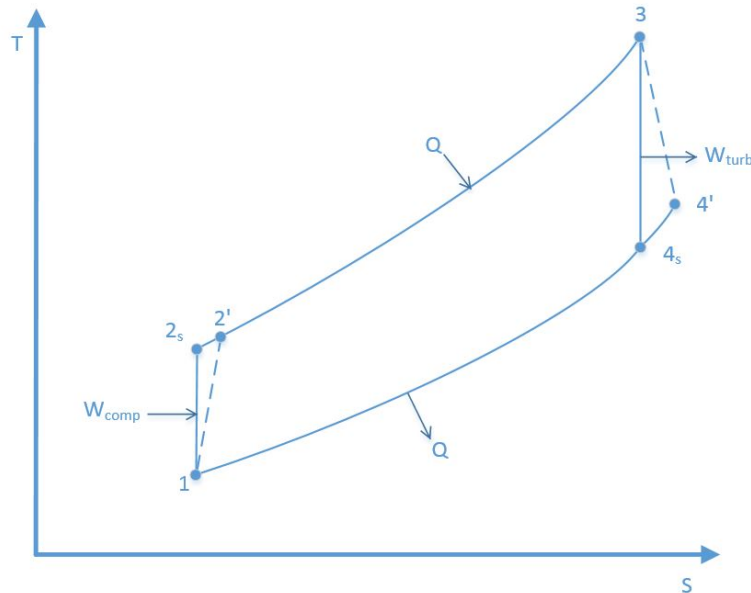


Figure 2.3: Temperature plotted against entropy from the basic Brayton cycle, with the non-isentropic path described by the dashed lines.

A more advanced configuration is the recuperated cycle. A recuperator is a device that extracts heat from the exhaust gas in order to pre-heat the compressor discharge air. The effects of this recuperator can be seen in Figure 2.5, a new point is introduced (point 3). The temperature difference between point 2' and point 3 is caused by the recuperator. Because no fuel is added to gain this temperature elevation, the systems efficiency increases [4]. The flow-scheme of the recuperated cycle can be seen in Figure 2.4, where the cold-side of the recuperator is placed between the compressor and combustor. The hot-side is placed between the turbine discharge and exhaust.

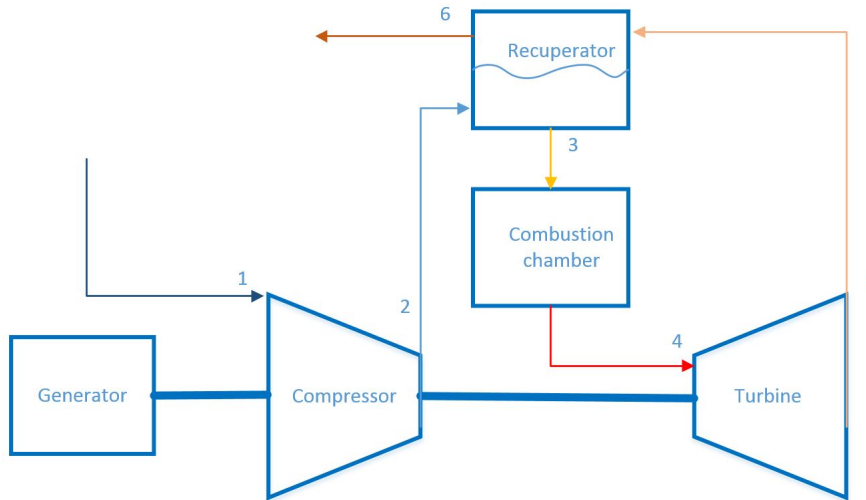


Figure 2.4: Schematic representation of recuperated Brayton cycle

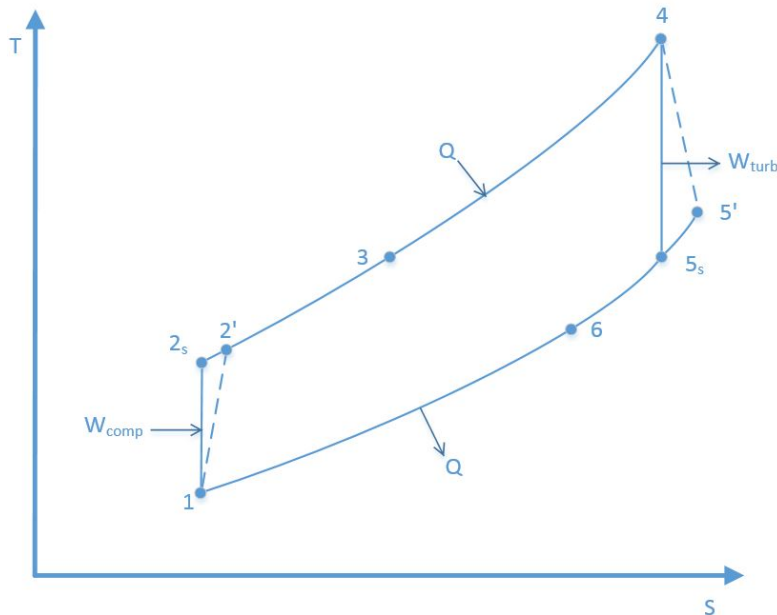


Figure 2.5: TS diagram of recuperated Brayton cycle

Within Figure 2.4 a direct driven generator is being used. This requires a generator that operates on the same RPM as the gas turbine engine. A 'free-power' or 'turbine-power' configuration can also be used, which is shown in Figure 2.6. When a free-power configuration is used the generator is driven by an extra turbine. By decoupling the gas turbine engine from the generator, the generator can run on lower RPM. The disadvantage is that the extra turbine wheel creates extra losses. This configuration should only be used if a rotational speed decoupling between output shaft and gas turbine engine is absolutely necessary. For a micro gas

turbine range extender a direct driven generator would be more suitable than a free-powered generator.

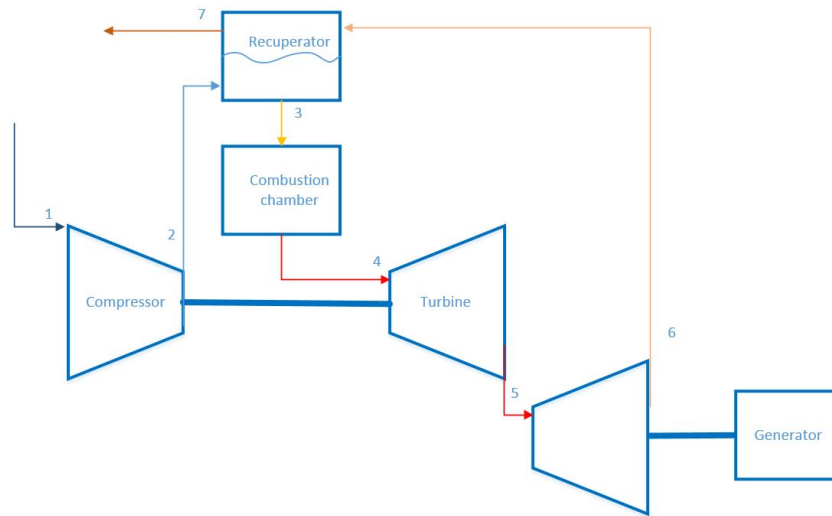


Figure 2.6: Schematic representation of recuperated Brayton cycle with free power driven generator

Further possible configurations, i.e. twin shaft, are not taken into consideration as they are not in line with the low-cost concept.

2.2.2 Compressor

The Brayton cycle starts with compressing air, a side effect of the pressure increase is temperature increase. A gas turbine engine uses radial or axial compressors or a combination of the two. The compressor stages can be divided into two groups; axial compressors and radial compressors.

2.2.2.1 Axial

Most modern gas turbines mainly use axial compressors. Within the axial compressor air is accelerated by rotating air-foils and then diffused in a row of stationary blades. The pressure ratio is relatively low, typically between 1.1 and 1.5 [4] [3]. Figure 2.7 compares different compressors on the basis of the pressure ratio (head) with respect to flow. Due to the low pressure ratio the compressor efficiency is typically high. In order to achieve high overall pressure ratio's several axial compressor stages are used; even when multiple stages are applied the peak compressor efficiency remains higher than the radial compressor's efficiency. While the efficiency of an axial compressor is high, it can only operate on a narrow speed range.

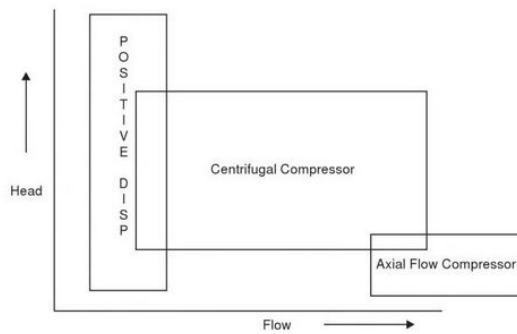


Figure 2.7: Performance characteristics of compressors [5]

2.2.2.2 Radial

In small gas turbine engines radial compressors are most often used due to their large tolerance, reliability and low cost [4] [3]. Within a radial compressor the air is forced through the impeller by the rotating blades. The velocity of the air is converted to pressure, partially in the impeller and partially in the diffuser [4]. The pressure and velocity profile through the compressor is shown in figure 2.8. The frontal area for a radial compressor is often large for a given flow. The pressure ratio of radial compressors typically range from 1.5 to 5, but pressure ratios as high as 12 have been reached with experimental test set-ups [4]. The main advantage of the radial compressor is the high pressure ratio, but the radial compressor is impractical to combine with multiple compressor stages. While the peak efficiency of a radial compressor is lower than an axial counterpart, its efficiency is acceptable over a wide range of rotational speeds [3].

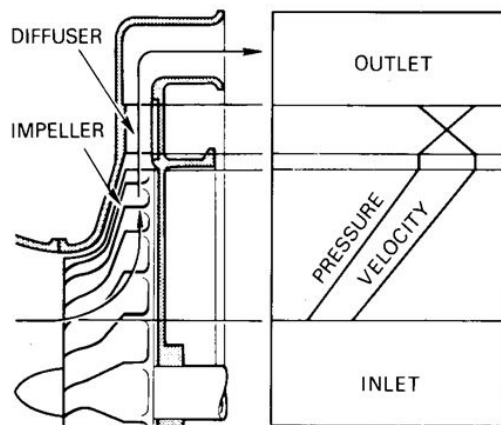


Figure 2.8: Pressure and velocity through a centrifugal compressor [4]

2.2.2.3 Summary

The benefits from the axial and radial compressor are summarized within this chapter. The use of an axial compressor has the following benefits [3];

- Smaller frontal area for given mass flow
- Flow direction of compressor discharge is convenient for multi-staging
- Higher efficiency at higher pressure ratio's

The use of a radial compressor has the following benefits [3];

- Higher stage pressure ratio
- Simple and rugged construction
- Shorter length for given pressure ratio
- Wide range of operation between surge and choke limits

The benefits mentioned above are focused on compressors for general gas turbine use. However, when gas turbines are scaled down other challenges arise. While axial compressors might seem superior for a specific goal in theory, often mechanical and production challenges make the use of axial compressors impractical.

2.2.3 Combustion chamber

Once the air is compressed by either an axial or radial compressor, the air gets heated in a combustion chamber. The source of this heat is not important for the Brayton cycle to work, which makes the gas turbine engine multi-fuelled. However the combustion chambers are only able to work with specific fuels that show resemblance in combustion behaviour. The combustion chamber can be built using several different configurations. The main combustion chamber performance parameters are as follows [3]:

- Pressure drop
Ideally the pressure drop would be almost zero, this is unfortunately never the case. The pressure drop is mainly caused obstruction placed within the flow stream providing combustion stability and proper mixing; these obstructions are needed for combustion. In the area where the flame is anchored the velocity has to be rather low to maintain the flame in the correct position.
- Combustion efficiency
The completeness of combustion can be expressed as combustion efficiency. The combustion efficiency mainly depends on the equivalence ratio, vaporization, combustor length and the evenness of the distribution of each parameter [20] [23].

- Outlet temperature distribution
When the temperature of the turbine inlet flow is not evenly distributed hot-spots occur. Besides potential mechanical damage to the turbine section, the overall TIT should be lowered to compensate for the hot-spots. A lower mean TIT lowers the cycle efficiency.
- Stability
Combustors have to operate over a wide range of operating conditions. Once the combustion is initiated, it should be maintained even when parameters, i.e. airspeed or FAR, show dynamic behaviour. The stability is often ensured by generating a sheltered or recirculating low airspeed zone [20].

2.2.3.1 Combustion process

The combustion process takes place with the combustion chamber. The simplest way a combustion process can be described is as an exothermic reaction of a fuel and its oxidizer. For gas turbine applications the oxidizer is air which is discharged from the compressor. The fuel can be gaseous, liquid or solid [4]. Each fuel can combust in various ways, this chapter describes the three main types of combustion.

Deflagration

Deflagration is a fast combustion process that often takes less than 1ms for 80% completed combustion [20]. Deflagrational combustion is characterised by a flame that propagates through unburnt fuel-air mixture. The deflagration waves travel with the flame speed which is typically lower than 5 m/s [20]. The burnt gasses have a higher temperature and larger volume than the unburnt mixture. The burnt gasses therefore gain in velocity as the pressure remains constant. Besides gas turbine engines, piston engines also make use of deflagrational combustion. Within the deflagration combustion there is a wide variety of combustion processes typically characterised by the equivalence ratio of the fuel-air mixture.

Non-premixed

Within a non-premixed combustor, fuel and air enter the combustion chamber separately. The fuel starts to combust within the primary zone as soon as it leaves the fuel nozzle. A non-premixed combustor is often referred to as a diffusion combustor [18] Within the diffusion combustor different overall equivalence ratio's can be obtained, yet localized sections of stoichiometric ratio's can often occur [18]. This causes high temperature within the primary zone which produces a large NO emission.

When the equivalence ratio², defined by equation 2.1, of the mixture is $\phi > 1$ the mixture is called rich. In the past gas turbines primarily used a rich diffusion combustion process due to its stable nature. Figure 2.9 shows a schematic representation of a rich combustor. The

²The equivalence ratio, or ϕ , represents the fuel to air ratio based on its stoichiometric ratio, where $\phi = 1$ means stoichiometric combustion

rich combustor can be divided into three main regions. The first region houses a fuel injector and stabiliser, in this case an axial swirler. Fuel is injected in the first section and combusts in the primary zone. The swirler and cone-shaped front cone ensure stability. The mixture travels through the first section and enters the second region, also known as the secondary combustion zone. Within the secondary combustion zone, the combustion process is completed. The gasses are cooled in the last zone, the dilution zone. The gasses are cooled down, till the desired TIT is reached.

While the NO emissions are unfavourable, the diffusion combustor offers stability and a wide range of operation as it is not susceptible for changing airspeed or inlet temperature. In order to reduce the NO emission while maintaining the stability of a diffusion combustor, an RQL combustor is used.

$$\phi = \frac{\frac{n_{\text{fuel}}}{n_{\text{ox}}}}{\left(\frac{n_{\text{fuel}}}{n_{\text{ox}}}\right)_{\text{st}}} \quad (2.1)$$

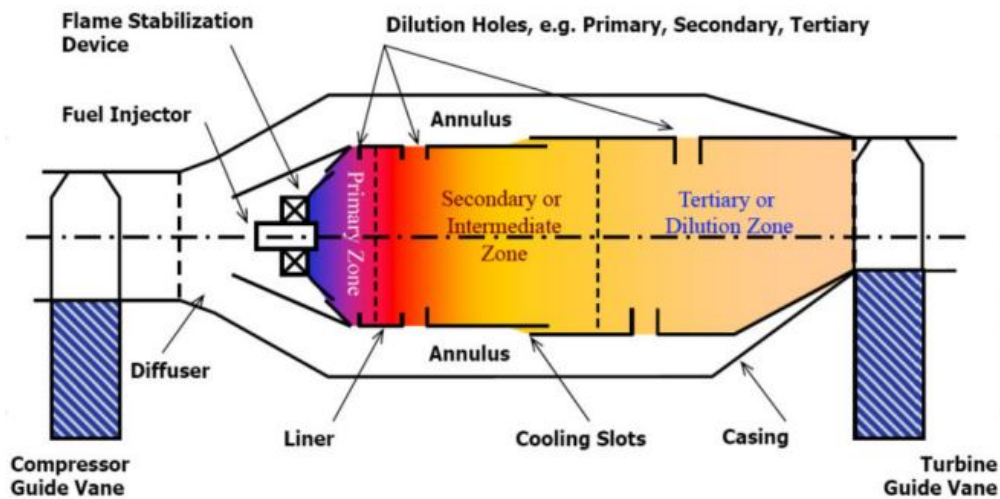


Figure 2.9: Schematic representation of rich combustor [18]

Rich-Quick Quench-Lean

The Rich-Quench-Lean, or RQL, combustor concept was introduced in the late 1980s to reduce thermal NO_x [31] [19]. This technology was further developed during the 1990s to apply the technology to aviation gas turbines. Currently most aviation gas turbines use RQL technology. The RQL technology uses staged combustion sections which are divided into a rich combustion zone, quench zone and lean combustion zone (Figure 2.10). The rich combustion zone houses a diffusion flame with an equivalence ratio of approximately $\phi = 1.8$ which causes oxygen depletion to occur. The consequence of oxygen depletion is a relatively low NO_x formation rate which maintains a stable basis for the combustion process. Further downstream of the rich combustion zone a large amount of air is added to continue the combustion process and cool down the flame. The equivalence ratio is lowered from $\phi = 1.8$ to

about $\phi = 0.6$, the transition from rich to lean should be done as fast as possible so that the gas mixture spends little time burning on a stoichiometric ratio. Thus the design and dimensioning of the quench section is of decisive importance to the success of lowering NO_x emissions. The lean zone completes the combustion with an equivalence ratio of $\phi = 0.3$, the low equivalence ratio has a relatively low NO_x formation rate.

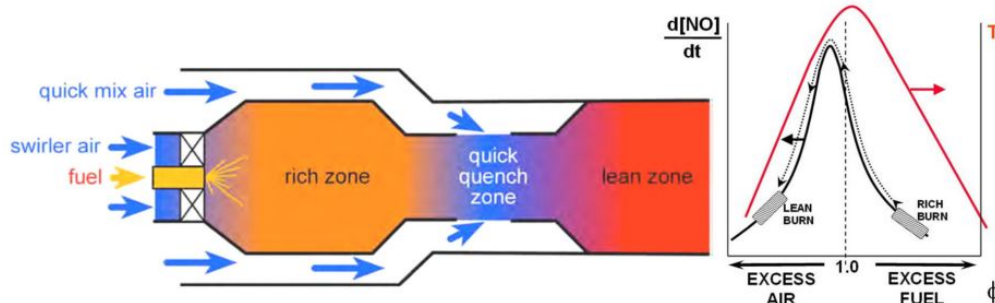


Figure 2.10: Schematic representation of RQL combustor [18]

As mentioned before, the quenching zone plays a vital role in the RQL combustor. When the quenching effect is designed to be too conservative, not enough mixing takes place which causes a high NO_x formation rate due to lack of mixing and potentially local stoichiometric combustion. When the quenching effect is designed to be too strong the quenching jets could partially blow-off the flame which would lower the combustion efficiency. The lean combustion zone is prone to instabilities, therefore a rich flame is used to ensure combustion stability. The ruggedness of the combustion stability can be influenced by altering the dimensions of the combustion chamber. When the rich combustion zone is shorter it combusts less fuel and the combustion chamber relies more on the lean combustion zone.

Premixed

Within a premixed combustor, fuel is premixed or pre-vaporized with air before it enters the combustion chamber. By premixing the fuel the equivalence ratio can be controlled, often it is controlled such that it approaches the lower-flammability limit of the fuel. These low equivalence ratio's lower the NO_x emission [4]. As premixed combustors are used to ensure a low equivalence ratio, there are often referred to as 'lean-premixed' combustors. Lean-premixed combustors come in a wide variety, the most commonly used is the LPP combustor. The LPP combustor offers a lean combustion of a premixed pre-vaporized air-fuel mixture. A typical LPP combustor consists of three sections [20]. When a liquid fuel is being used, the first section houses the premixer. Within the premixer fuel is injected and vaporized. This mixture should be well mixed/homogeneous to reduce the chances of droplet combustion and/or autoignition. The second zone combusts the mixture, due to the low equivalence ratio the temperature and therefore the NO_x formation is relatively low. The last section mixes and dilutes the combusted mixture to lower the temperature to the required TIT.

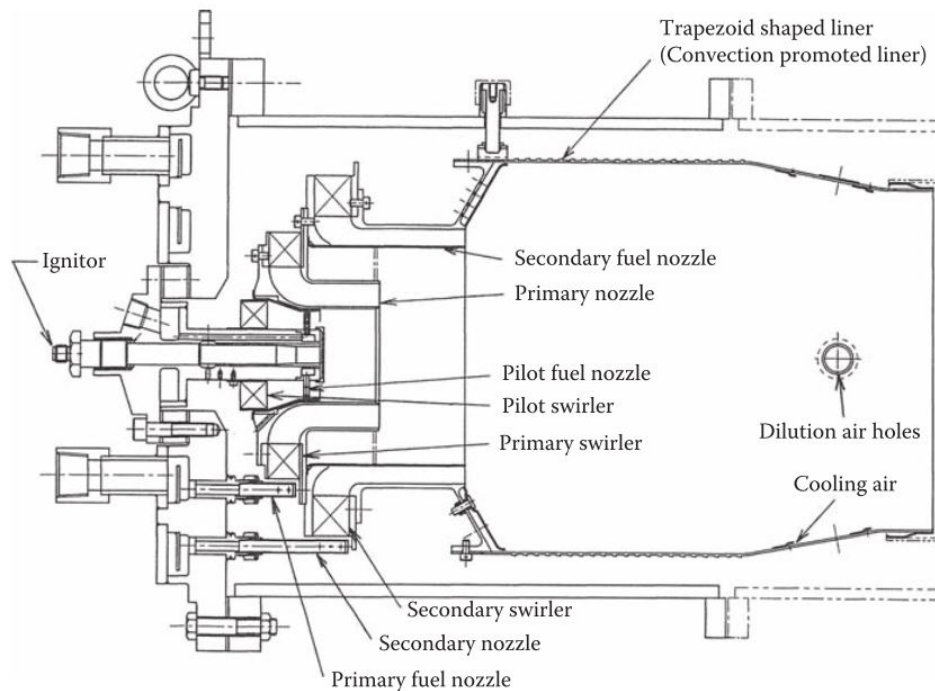


Figure 2.11: Schematic representation of a catalytic combustor [20]

A lean-premixed combustor is often prone to instabilities, the airspeed is critical in the different zones of the combustor. An airspeed lower than the flame speed can cause flashback. During flashback the flame can propagate towards the premixer. When the airspeed is too high blow-out can occur. Besides critical speeds, lean-premixed combustors often suffer from acoustic instabilities [20]. The operational bandwidth of the lean-premixed combustor is therefore rather small.

Catalytic combustion

The catalytic combustor can achieve lower NO_x emissions than any deflagration combustor [4]. A catalytic combustor pre-vaporizes fuel and air to an equivalence ratio that is below the flammability limit of the fuel used. The mixture travels over a bed of catalytic material. The presence of the catalytic material enables the oxidizing reaction to occur. The maximum temperature of a catalytic combustor is very low which means NO_x formation is minimal [20]. Most catalytic combustor designs use a thermal reaction zone to raise the temperature to the required TIT. Figure 2.12 shows a schematic layout of a typical catalytic combustor.

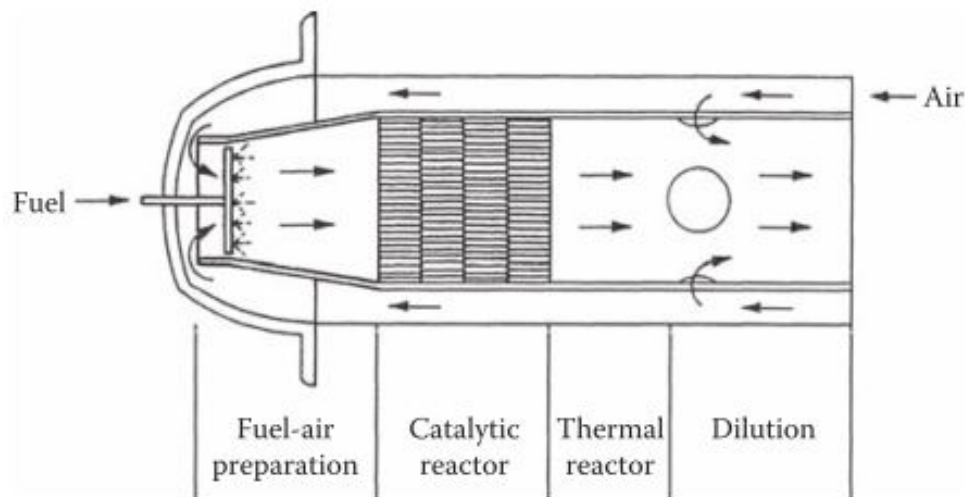


Figure 2.12: Schematic representation of a catalytic combustor [20]

The catalytic combustion process is rarely applied in the field due to the small bandwidth the combustion process operates. This disadvantage is magnified when the gas turbine needs a transient behaviour. Besides the lack of transient behaviour the high cost and low durability of catalytic materials are clear disadvantages.

Detonation

When detonating combustion is used, a shock wave travels through the combustion chamber at supersonic speed (up to 4km/s) [20] [27]. Detonation cannot occur when conventional equivalence ratio's are used, but arises when extra oxygen is supplied so lower a equivalence ratio is reached. The detonation combustion is more efficient than deflagration combustion when an equal number of species is considered. The NO_x emissions are reduced as the residence time is reduced to a minimum. An extra benefit it is the pressure gain in the combustion chamber, which would increase the overall efficiency [28].

The detonation gas turbine use 'receivers', which are basically valves, to control the air-flow. The detonation combustion chamber can use one receiver in front of the chamber or two receiver at either end. By controlling the inlet receiver the shockwave is sent in the direction of the turbine. A rear receiver can build up pressure from the detonation cycle before it is released into the turbine [29].

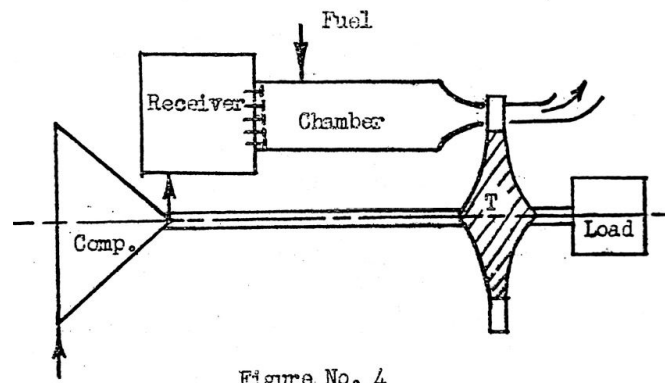


Figure 2.13: Gas turbine with 'open end' detonation combustion chamber [29]

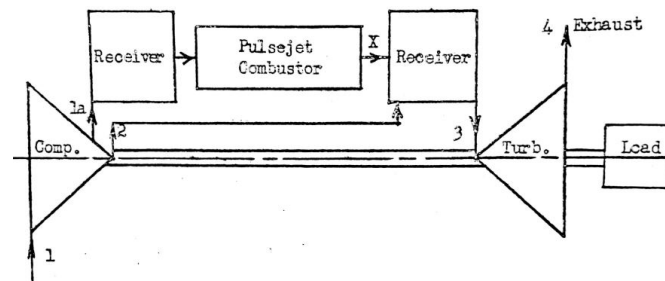


Figure 2.14: Gas turbine with detonation combustion chamber using the pulse-jet set-up [29]

If a single receiver, or blown-down set-up, is used the combustion process is more efficient than a deflagration process. But due to shock waves generated by the supersonic flame speed, the turbine efficiency is lowered [13]. The overall efficiency of the engine drops by several percent [29]. When a double receiver, also known as pulse-jet set-up is used, pressure can build up inside the combustion chamber. Even though shockwaves will be sent to the turbine, the turbine output increases due to the higher pressure. The flue gas is diluted using high-pressure air which can be seen in Figure 2.14. This set-up increases the engine efficiency but can only be used when several compressor stages are used. The main challenge of the detonating combustion chamber is the development of high temperature and high pressure resistant valves.

Flameless (FLOX)

The combustion processes described above all have one thing in common, a flame front is clearly distinguishable which moves with an certain flame speed. The flameless oxidation, or FLOX, process lacks this flame-front. Within flameless oxidation the gasses recirculate and thus the flame front is lost. The flame-front is the area where the temperature rises most, without this flame front the temperature peaks are removed and emissions are reduced significantly [35]. A FLOX combustor can even reduce the NO_x emissions when highly pre-heated inlet air is being used.

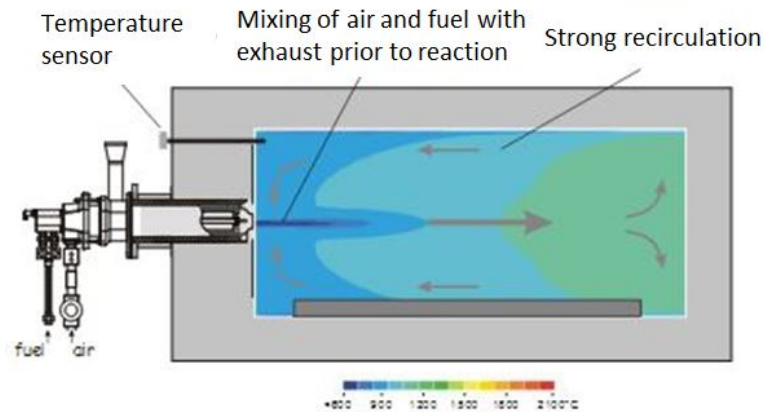


Figure 2.15: Schematic representation of a FLOX combustor [20]

The emission output of FLOX combustor is currently unbeaten [34]. However, currently FLOX combustors are prone to instabilities and lack the capability to cope with transient behaviour.

2.2.4 Emissions

Last decades emissions show a downward trend imposed by legislation. New combustion technologies have been developed to be able to comply with the legislation. Most combustion technologies aim to reduce NO_x emissions as the legislation of these emissions is the most challenging to meet.

Exhaust gas consists mainly of carbon monoxide(CO), carbon dioxide(CO_2), water vapor(H_2O), unburnt hydrocarbons (HC), particulate matter(mainly carbon), NO_x and excess oxygen and nitrogen [20]. CO_2 and H_2O are considered as the natural consequence of complete combustion of hydrocarbon bases fuels. These emissions can only reduced by burning less fuel, by increasing the thermodynamic efficiency. The other emissions levels are mainly dependant on temperature, time and concentration history of the combustion process [20]. Figure 2.16 shows the relation between NO_x emissions, flame temperature and equivalence ratio. Around an equivalence ratio $\phi = 1$ and slightly lower, the flame temperature reaches a maximum. The high flame temperature produces a high amount of thermal NO_x produced by the 'Zeldovich mechanism' [20]. The majority of the NO_x emissions generated can be lowered by leaning the fuel-air mixture. Figure 2.16 shows the area where lean premixed combustors operate compared to a conventional(rich) combustor.

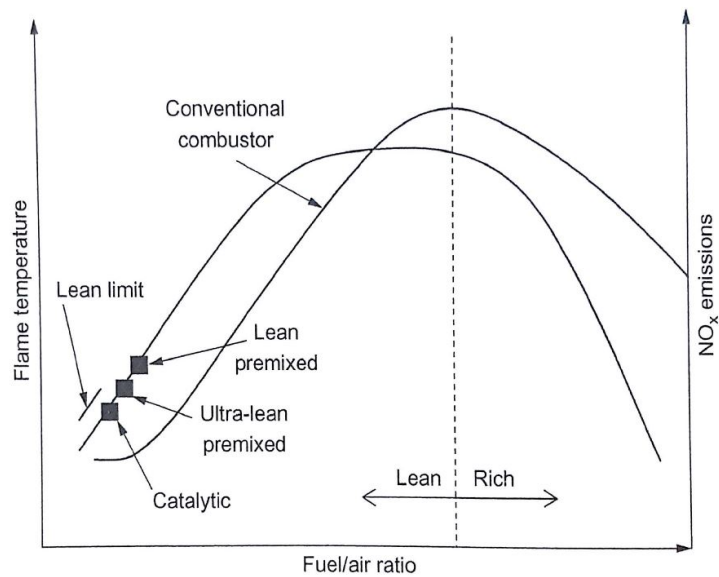


Figure 2.16: NO_x and flame temperature plotted against equivalency ratio [4]

As explained earlier, lean combustion chambers typically suffer from combustion instabilities. Therefore it might be interesting to reduce NO_x by enriching the fuel-air mixture. However a rich flame produces a large amount of CO and HC which is considered undesirable. A low emission combustion chamber should thus be designed to operate in the lean-area.

An RQL combustor has a rich front section that has a relatively low flame temperature and thus low NO_x formation rate [19]. To prevent the mixture from combustion at stoichiometric ratio, it is rapidly quenched to cool the flame and dilute the mixture. An RQL combustor takes the 'low NO_x route' which can be seen in Figure 2.17. The unburnt HC combusts in the lean combustion stage. The overall emissions of an RQL combustor are therefore typically low and still offer stability due to a stable rich flame.

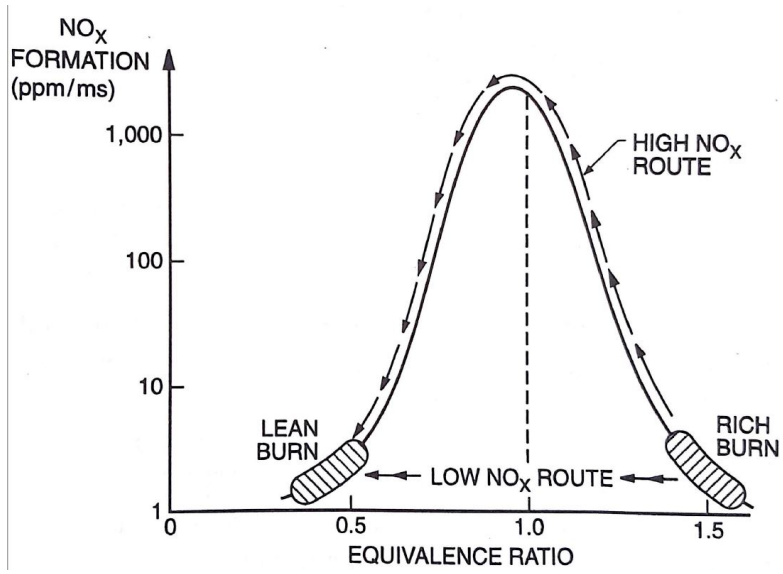


Figure 2.17: Low and high NO_x route [4]

2.2.4.1 Fuel

A gas turbine engine can in theory run on a wide variety of fuels, ranging from gaseous or liquid to solid fuels. Currently diesel and gasoline are the most popular and best available fuels for cars. In the future emission goals and availability of fuel types can play a decisive role in the fuel choice. Trends show that alternative fuels, i.e. bio-ethanol or compressed natural gas, are gaining in popularity due to their potential to lower emissions [15]. Future worldwide availability of alternative fuels is yet uncertain. The gas turbine's multi-fuel capability is beneficial because it can adapt to future fuel trends.

When a fuel is chosen the following factors should be taken into consideration;

- **Fuel consumption**
Different fuels can have a large difference in net caloric value. The gas turbine needs a certain amount of energy independent on the caloric value of the fuel, this means that a fuel with a low caloric value would have a higher specific fuel consumption(in L/km).
- **Combustor size**
Besides the fuel consumption being dependant of net caloric value. The dimensions of the combustor are dependant on the amount and behaviour of the fuel that needs to be burnt.
- **Start-up behaviour**
Fuels come with a wide variety of flammability limits, flash points and auto ignition temperatures. These parameters have a decisive influence on the ignition and start-up behaviour. Typically fuels with a low flashpoint and autoignition temperature reduce the start-up and ignition power consumption [20].
- **Adiabatic flame temperature**
The adiabatic flame temperature of the fuel is an important property of the fuel. A higher flame temperature can create high temperatures within the combustion chamber which would increase the NO_x emission.
- **Emissions**
Fuels can influence the type and amount of emissions. The fuel specific emission is expressed in the 'cleanliness' of the fuel. Fuel with a low level of cleanliness often has bound nitrogen and sulphur which increase the amount of toxic emissions [4].
- **Corrosivity**
Some fuels have highly corrosive properties which could affect the fuel system, combustion chamber and the turbine section. When a corrosive fuel is used, the price of the combustion chamber and turbine could increase the cost.
- **Ways of storage**
Liquid fuels are easily stored in a fuel tank. Gaseous fuels are often stored in a liquid state which requires a pressurized tank. The pressure where gaseous fuels are stored

depends on the vapor pressure of the fuel, which has a high impacts on the cost of the fuel storage tank.

- Availability

Future trends of fuel availability are to be predicted. The gas turbine should run on a fuel that is widely available in the targeted market area.

For the gas turbine range-extender only liquid fuels are considered due to the ease of storage. Currently gasoline, diesel and bio-ethanol are currently commercially available, for the first prototype the fuel choice is restricted to these fuel types.

- Gasoline

Gasoline could be a good candidate to fuel the gas turbine engine as the ignition and start-up behaviour is exceptionally good. The net caloric value is relatively high compared to ethanol. Yet the low flashpoint makes it relatively unsafe for test set-up usage.

- Diesel

Diesel is harder to vaporize and ignite, the ignition and start-up behaviour is therefore compromised. The net caloric value is the highest of the considered fuels, thus it should ensure the highest mileage.

- Bio-ethanol

Bio-ethanol is a fuel that has the potential to lower emissions significantly. Lower grades of ethanol typically have higher water content. Conventional cars only use the more expensive higher grade of ethanol(100%). For a gas turbine engine it is also possible to run on lower grades. These lower grades can reduce the emissions even further as the combustion becomes 'partially-wet'. The water content will cool the flame which reduces the NO_x emissions.

Fuel injection

Prior to the combustion process the fuel needs to be injected and mixed with air. The fuel then becomes atomized into a large number of small droplets. These small droplets evaporate before they combust. The distribution of the fuel and the droplet diameter is critical for achieving an efficient combustion process and reducing low emissions.

The main goal of the fuel nozzle is to produce a droplet size which ensures that the evaporation process is not rate-controlled.

Fuel can be injected using various devices. The most frequently used injectors are [23]:

- Pressure injector

A pressure injector uses high fuel pressure to force it through an orifice. Often the fuel enters the orifice with a swirling motion. The fluid exits the orifice with high velocity which disintegrates the formed fluid-sheet [23]. This type of injector can be easily scaled to be able to handle low fuel flows.

- Twin fluid injector

With in a twin fluid injector air flows tangentially over a surface of fuel. The induced

shear stresses break away the fluid film, disintegrating it [23]. The advantage of this system is that the fuel can be accurately distributed but, the system is relatively complex.

- Rotary injector
A rotary injector uses centrifugal forces to inject the fuel into the combustion chamber. Often a shaft or disc is used where fuel exits forming a liquid sheet or jets. This technique has in the past been applied to large gas turbine engines and is difficult to adapt for small scale applications.
- Vaporizer tubes
Micro gas turbines often use vaporizer tubes for atomizing the fuel. Vaporizer tubes use the heat generated by combustion to evaporate the fuel. The tubes run through the combustion chamber as shown in Figure 2.18. The disadvantage of this system is that locally rich combustion occurs which can cause high NO_x , CO and HC emissions. Another disadvantage is the start-up difficulty, when the combustion chamber is cold it should be pre-heated in order to initiate the vaporization.

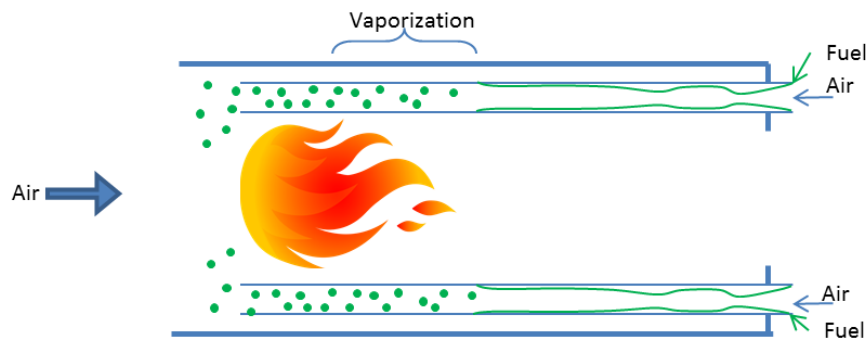


Figure 2.18: Schematic representation of vaporizer tubes with in the combustion chamber

2.2.4.2 Stabilisation

Discharge velocities of compressors are relatively high. Often these velocities are well above the flame speed. Diffusers are used to decrease the airspeed, yet it remains higher than the flame speed [23] [4]. If the fuel would be injected and ignited, the flame would be carried downstream and a flame-out would follow. Stabilisers are used to ensure an anchoring point for the flame. The types of stabiliser commonly used can be divided into two groups: bluff-body stabilisers and swirl-stabilisers. The bluff-body stabilisers consist of a baffle, placed in the combustor, which generates an eddy region [4]. Within this eddy region the recirculating flow combusts. A bluff-body is the simplest type of stabilizer. The pressure loss of bluff-body stabilisers is significant, yet they are still widely used in afterburners.

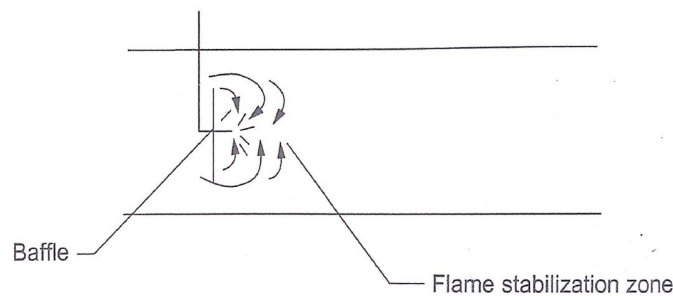


Figure 2.19: Bluff-body stabilizer with eddy region [4]

A flame can also be stabilised by generating a highly swirling flow around the fuel nozzle. This swirling flow generates toroidal flow recirculation which captures a portion of the hot combusting gasses and mixes it with incoming fresh air and fuel. This stabilising process can be enhanced by installing the swirler in the centre of a diverging cone. Vortex breakdown would not only occur inside the core of the swirl but a toroidal recirculating flow will also form at the surface of the cone. Often single swirler set-ups are used but on some occasions two counter-rotating swirlers are placed concentrically to increase the mixing behaviour.

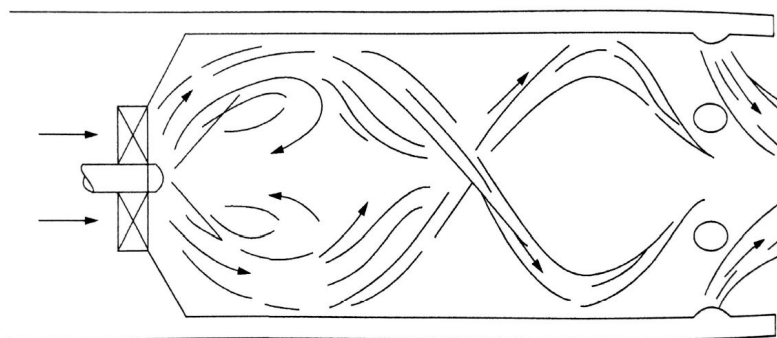


Figure 2.20: Axial swirler and its flow pattern [4]

Swirlers exist in various types, the three most frequently used are: axial vane swirlers, radial vaned swirlers and discrete jets. The discrete jet can be either axial, semi-axial or fully-radial.

The pressure losses generated by the axial are relatively low compared to the radial swirler. Yet the radial swirler can generate a larger recirculation due to increased angular momentum. The pressure drop of the discrete jet swirler can be categorized between the axial-vaned and radial-vaned swirler. Discrete jet swirlers typically have lower swirl numbers than vaned swirlers. The swirl number is defined by Lefebvre [20] as:

$$S_n = \frac{2G_m}{D_{sw}G_t} \tag{2.2}$$

Where G_m represents the angular momentum while G_t represents axial thrust. When the swirl number is lower than 0.4 the swirl is described as weak and insufficient [20].

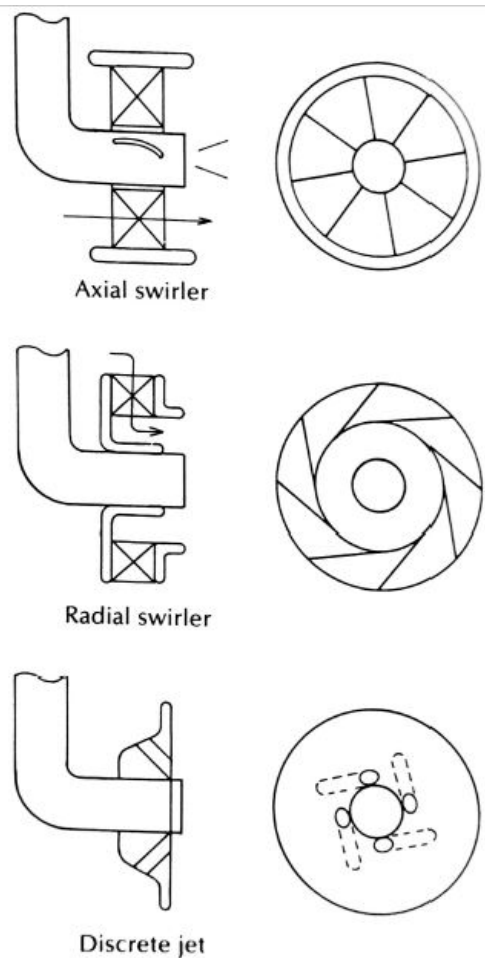


Figure 2.21: Type of swirlers [4]

2.2.4.3 Configuration

The combustion chamber can be shaped and configured almost fully independent of the type of combustion, fuel or pre-mixer used. The three most widely used combustion chamber configurations are; can, can-annular and annular. A cross-sectional view of these configurations can be seen in Figure 2.22, where the blue area represents the area where combustion takes place.

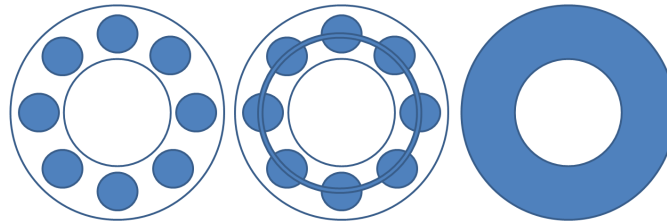


Figure 2.22: Graphical representation of the cross section of combustors. From left to right: can, can-annular and annular [4]

Can

The can combustion chamber, also known as 'tubular' chamber, is a configuration that uses single or multiple cylindrically shaped combustors (Figure 2.22) [4] [14]. When multiple can combustors are used, they are often placed in an annular configuration. Each combustor is enclosed by its own casing and is not inter-connected to the others. Each can combustor operates on its own, the entire assembly is often called a multi-combustor set-up [23]. Their case length and weight prohibit the engine from being used in aircraft engines, therefore their use is restricted to ground applications. The main advantage of a can combustor is the accessibility and ease of maintenance [20]. A multi-combustor set-up has a relatively high surface to volume ratio, this ratio will increase even more when it is scaled down. For this reason a multi-combustor set-up is not suitable for micro gas turbines. However a single can has a relatively low surface to volume ratio which makes it suitable for micro gas turbines. Micro gas turbines based on turbochargers often use single-can combustors as they are easily integrated with standard turbine housings. Gas turbine engines that use a radial compressor often use can combustors, when the air exits the diffuser, it separates the air flows and divides it evenly [3].

Can-annular

Can-annular combustion chambers consist of several can combustors placed in an annulus configuration which can be seen in Figure 2.22. The cans are connected with cross-over tubes that let the flame travel between cans and reduce pressure differences [20]. Can-annular combustion chambers are easy to maintain as they can be removed and worked on individually. Besides the weight and size, the light-around³ is a problem that a can-annular combustor often faces [4]. The development of a can-annular design requires experiments with a single can, whereas an annular combustor would need a complete disassembly [14]. When

³A problem where fuel does not ignite along the entire circumference of the combustor

applied on small scale the surface/volume ratio will increase, this makes the can-annular design unsuitable for micro gas turbines.

Annular

s The annular combustor consist of an annulus shaped single combustor. Within an annular combustor light-around problems are minimal [23]. In most designs the shaft of the turbine to the compressor runs through the centre of the annulus. An annular configuration makes the most efficient use of the available volume, the length of the combustor can therefore be reduced. The combustion process is evenly distributed along the annulus, creating an evenly distributed TIT. Compared to a can or can-annular design, the annular combustor experiences fewer hot-spots. For applications where high TIT's are required annular combustors are often used [4]. Naturally annular combustors have a lower structural integrity, at high TIT's these effects can become more pronounced [23]. Annular combustors gain popularity due to a trend of increasing TIT's and lower allowable emissions. This is possible due to the relatively low surface area of an annular design, which reduces the amount of cooling air needed [4]. Annular combustor are widely used for large scale applications as well as small scale turbines.

Flow direction

In addition to the combustion chamber configuration, the flow direction can also be chosen. The flow through the combustion chamber is most often straight or reversed. When a straight flow configuration is used, the air flows from the compressor in a straight line towards the turbine. Within the reverse flow combustor the air flow is reversed one or multiple times. Figure 2.23 shows a graphical representation of the straight can combustor. The pressure losses of a straight flow combustor are typically lower compared to a reversed flow combustor.

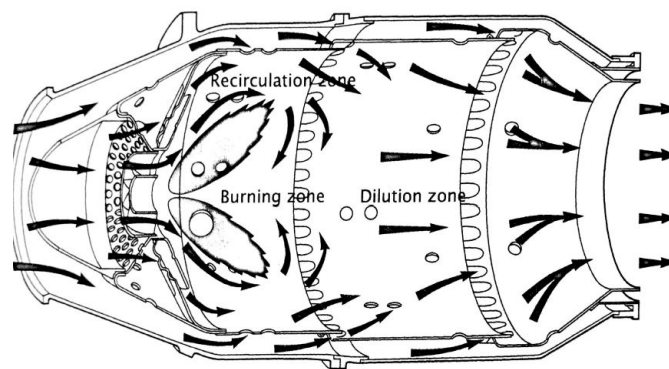


Figure 2.23: Straight flow combustor [4]

Figure 2.24 shows a reverse flow annular combustion chamber. When the length of the gasturbine plays an important role, i.e. for turboprops, reversed flow combustion chambers are often used.

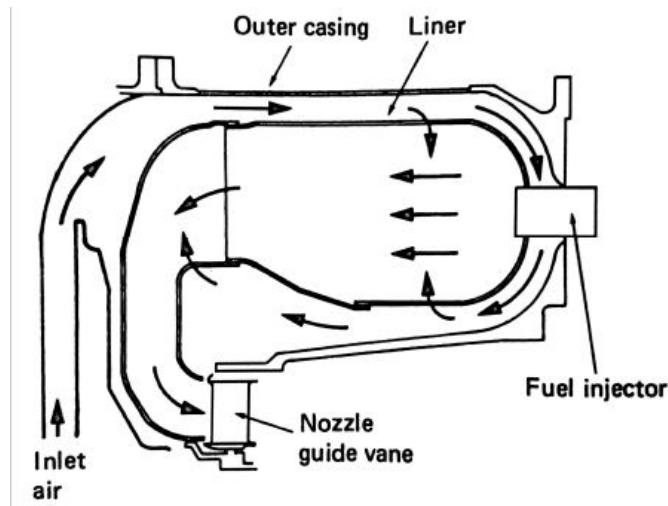


Figure 2.24: Reversed flow combustor [20]

2.2.5 Turbine

The last step within the Brayton cycle is the turbine stage. In a direct drive, or shaft-power, configuration the turbine stage generates power to drive the compressor and generator. When a free-power configuration is used a separate turbine drives the generator. Just like the compressors discussed earlier, turbines can be divided into two main groups; axial and radial turbines.

2.2.5.1 Axial

Most industrial and aviation gas turbines use axial turbines. Usually axial turbines are built up from several stages. Often the front stages are impulse-turbine and the later stages 50% reaction turbines.

The axial turbines have a relatively low expansion ratio compared to radial turbines, therefore several turbine stages are needed when axial turbines are used. Even though the cost of an axial turbine is typically higher than a radial turbine, axial turbines are still widely used due to their high efficiency.

Modern micro gas turbines often use axial turbines. When a single turbine stage can be used the turbine section could be even more compact than a radial turbine depending on its combustor shape. If these engines output shaft power, a free-power set-up is often used which voids the compactness.

2.2.5.2 Radial

Radial turbine's can be divided into two groups: fully radial turbine and radial turbine (or mixed flow). Within the fully radial turbine, the fluid not only enters radially but also exits radially [4]. A cantilever turbine is an example of a fully radial turbine, which can be seen in figure 2.25. This type of turbine is today only used in nano turbines due to its compactness.

On larger applications radial turbines are used that have an axial outlet which can be seen in figure 2.26. The efficiency is much higher at the cost of compactness.

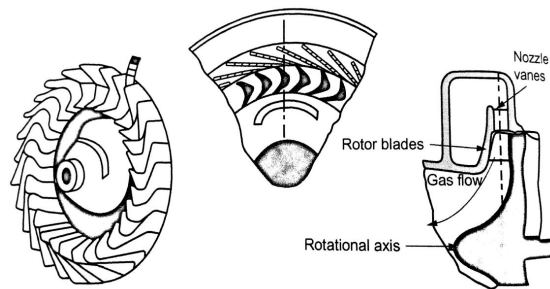


Figure 2.25: Fully radial cantilever turbine [4]

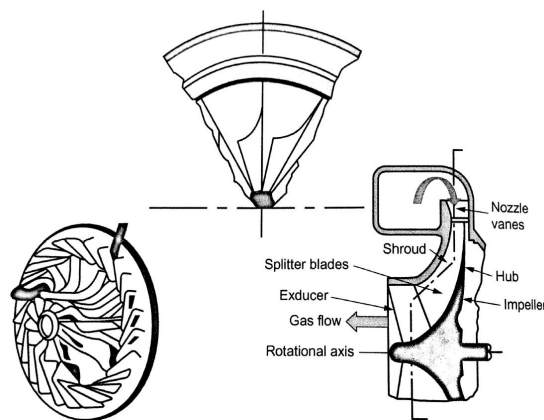


Figure 2.26: Mixed flow or Radial turbine [4]

Radial turbines' main advantage over axial turbines is that the performance of a single radial stage is equivalent to two or more axial stages [4]. This is caused by the fact that radial turbine wheels often have a slightly higher allowable tip-speed. As the power output of a turbine is quadratically proportional to the tip-speed this has a large impact on compactness.

Besides the difference in performance, radial turbines are often less expensive than axial turbines. For these reasons automotive turbochargers primarily make use of radial turbines. To summarize, the compactness and low cost character of a radial turbine make it suitable for range-extender use.

Low cost micro gas turbines typically use radial turbines from automotive turbochargers as the turbine is a significant cost factor.

2.2.6 Recuperator

A recuperator is a device that transfers heat from the exhaust gas to the compressor discharge air. By transferring this heat, less heat needs to be added by means of combustion which reduces the fuel consumption. The thermodynamic cycle of the recuperator cycle can be seen

in figure 2.5. The temperature change from 2'-3 is caused by the heat recuperated from 5'to 6.

The total recuperated heat is dependent on the design and difference between the turbine discharge and compressor discharge temperatures. The larger this temperature difference, the more attractive the use of a recuperator. For this reason larger gas turbines (>1MW) do not use recuperators as the pressure ratio's and thus compressor discharge temperatures are typically high. These large gas turbines often use boilers to extract heat from the exhaust and produce steam.

The recuperator types most used and that are taken into consideration are [22];

- Plate
The plate heat-exchanger consists of plates that divide the cold and hot airflow. The efficiency can be enhanced by dividing the air flows and using multiple stacked plates. Picture 2.27 shows the set-up of a stacked plate recuperator.
- Plate fin
The plate fin recuperator, as shown in Figure 2.28, shows large similarity with the plate recuperator. While a plate recuperator uses flat or stamped plates, a plate fin recuperator has fins or pins attached to the plates to guide the flow and increase its surface area.
- Swiss roll
The swiss roll recuperator is the most often used recuperator design for micro gas turbine engines. Its compact design allows it to be easily incorporated with in the gas turbine itself. Figure 2.29 shows the flow direction within the swiss roll.
- Thermal wheel
The thermal wheel consists of a circular mesh that is partially placed within the cold flow and partially in the hot flow. The thermal wheel slowly rotates so that the hot section moves to the cold section where it releases its heat. The thermal wheel recuperator is a compact construction that was widely used for the early gas turbine powered cars(Fig. 2.30). Despite the high efficiency of a thermal wheel the overall cost of the system kept it from being applied to micro gas turbines.

The most important feature of the range-extender should be cost, the efficiency is of less importance. Therefore the chosen recuperator concept is primarily based on cost, compactness and ease of production. The biggest challenge in recuperator design is to generate a large surface area while maintain a low volume, low weight and low pressure drop. Within a gas turbine application the size of the recuperator and its pressure drop can be slightly reduced when the recuperator is integrated within the design, instead of a stand-alone design.

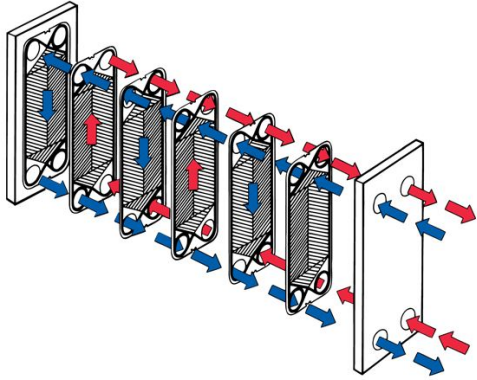


Figure 2.27: Parallel plate recuperator [11]

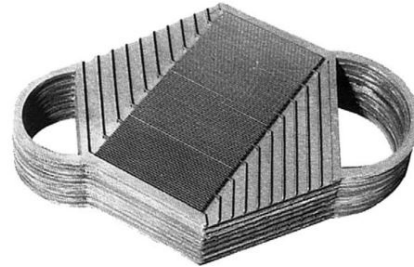


Figure 2.28: Plate fin recuperator [22]

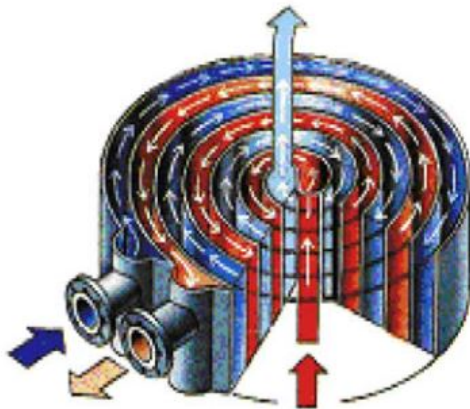


Figure 2.29: Swiss roll type recuperator [33]

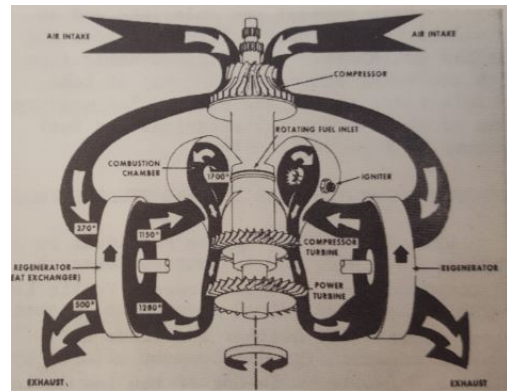


Figure 2.30: Layout of Chrysler 6th gen gas turbine with two heat wheels [26]

Chapter 3

Modelling

3.1 Goals / requirements

Before the modelling/design process starts, the requirements of the range-extender need to be specified. Based on the results of the market research the requirements of the range-extender have been defined. Most of the requirements are not specified to an exact number. This is caused by the fact this project can be seen as a feasibility study and thus it is not known yet to which extent a certain goal is feasible.

Below the requirements/goals are summarized in order of importance:

- **Low emissions**
Future trends show that emission legislation is likely to become more stringent. The range-extender should comply with future emission-legislation.
- **Cost**
According to the market research the cost of the final product may not exceed 1.000 euro. The design should be cost-effective and show the potential for a low cost final product.
- **Power output: 10-30 kWe**
With a power output of 10 kWe a car could drive continuously with a speed of 80 km/h. 30 kWe would allow a continuous velocity of 130 km/h.
- **Small packaging**
The range-extender should only be used in emergency situations. Therefore it is important that the size of the range-extender is minimized.
- **Low weight**
The weight of the range-extender should be as low as possible because of the emergency only usage.

- Fuel: Bio-ethanol
The fuel used to power the range-extender is bio-ethanol. This fuel not only lowers the emissions but also has a marketing-strategic advantage.
- Max. 105 kRPM
This limit is set by the generator that is going to be used.
- Off-the-shelf components
In order to reduce cost and construction time, many off-the-shelf components need to be used.

The goals for the first prototype differ from the long-term goals. The long-term goals are shown in Figure 3.1 with respect to the prototype goals.

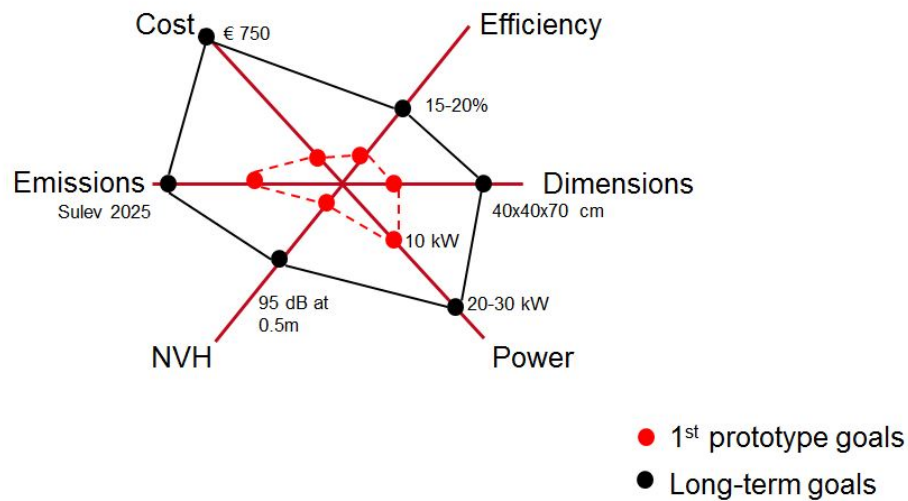


Figure 3.1: Spider diagram with prototype goals in relation to long-term goals

3.2 Basic design

Based on the literature research and the market research the range-extender concept can be shaped to suit the requirements. The configuration of the gas turbine engine can be defined using a morphological overview. This overview summarizes the main characteristics of the engine. For each characteristic several options are available. Usually morphological overviews are grades quantitatively like in Appendix A, but for determining the configuration this is not satisfactory. Therefore the following morphological is judged qualitative instead of quantitatively.

Figure 3.2 shows the morphological overview that is used to determine the general layout of the gas turbine engine. The design starts with determining the generated electric power output. From an efficiency point of view a high power output is preferable as smaller engines are typically less efficient due to scaling effects. For the first prototype and off-the-shelf generator should be used, due to RPM and power limitations of available generators only one option is feasible. Therefore 10 kWe configuration with a TD06 compressor should be used so that standard generator and turbocharger parts can be used.

When the generator's output and thus the build-size of the turbocharger is defined, a fuel type can be chosen. Diesel is widely available and has a high energy density content which is beneficial for mileage. However the emissions are typically higher when diesel is being used. Gaseous fuel like CNG or LPG show great potential to reduce the emissions significantly, yet they require large and costly pressure tanks to store fuel. Bio-ethanol also shows potential to lower emissions and is suitable for partially wet combustion, hence for this prototype bio-ethanol is the most suitable fuel. Note that gasoline is not included within the morphological overview. Due to safety precautions gasoline cannot be used for the first prototype.

Each fuel can combust using different combustion principles. Due to the low-emission goal of the project a rich combustion is ruled out due to high NO_x formation rates. A lean-premixed combustion process would lower the combustion temperature and thus the NO_x formation rate significantly, yet it is prone to instabilities. Because bio-ethanol is chosen a fuel, a partial wet combustion process could be used as lower qualities of bio-ethanol have a certain water content. This would reduce emissions while keeping the cost low.

The combustion process takes place within the liner, the shape and configuration of this liner can be can, annular or can-annular. An annular combustion liner could reduce the overall dimensions of the engine but does require multiple fuel injection points which impacts the costs negatively. A can-annular design is unsuitable due to the high surface to volume ratio, which would cause significant losses. A can combustor would suit our needs best as it is cheap and can be easily integrated with an off the shelf turbocharger.

The efficiency of the recuperator has a large influence on the eventual fuel consumption but is often costly. A trade-off must be made between cost and efficiency. Due to the affordable nature of the range-extender, a basic recuperator should be integrated into the design. This

way recuperator efficiency can be obtained without adding much cost.

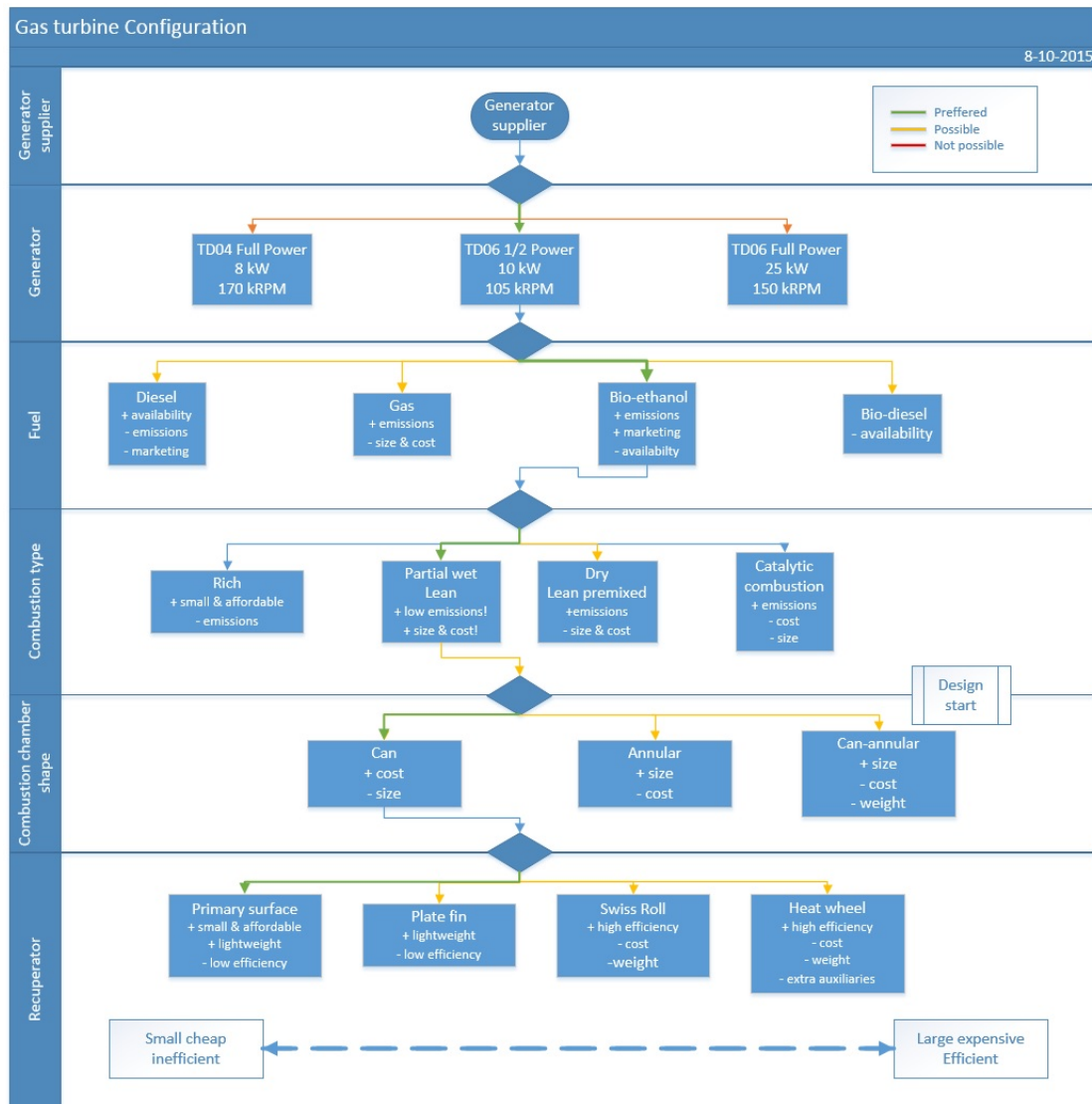


Figure 3.2: Mophological overview

By using the morphological overview a rough design of each individual component has been made. Basically the individual building blocks are known, yet the building blocks can be assembled in various ways. When a can combustor is used, it can be placed in a straight or silo configuration. Within the straight configuration, shown in Figure 3.3, the can combustor is placed parallel with respect to the shaft of the turbomachinery. This configuration is very compact, even when a long generator is attached to the compressor side. However due to the bends, pressure losses are typically higher than the losses from within a silo configuration.

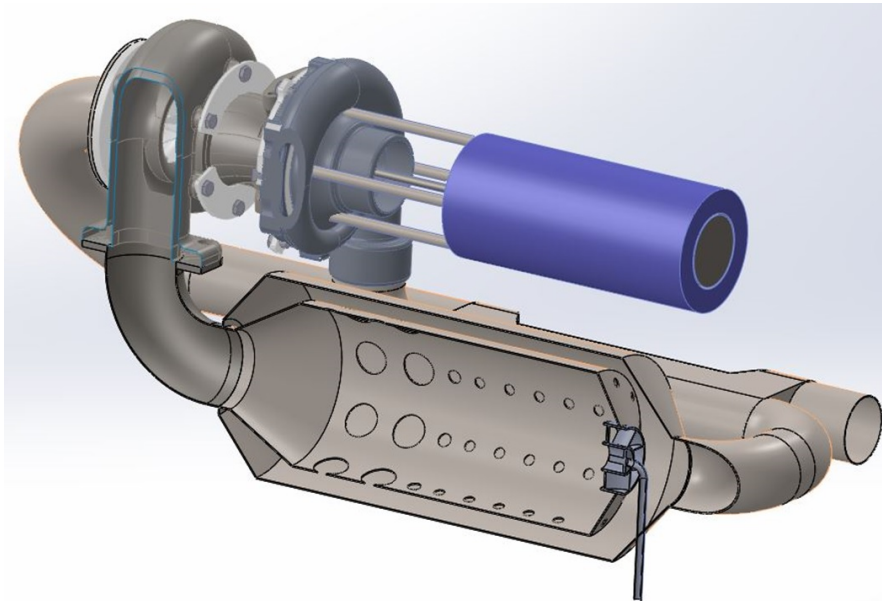


Figure 3.3: Straight configuration of a can combustor

To reduce the pressure losses a silo configuration can be used which can be seen in Figure 3.3. Within the silo configuration the can combustor is placed perpendicular with respect to the turbomachinery shaft. While the silo configuration is beneficial for reducing pressure losses, the overall dimensions of the engine increase. The generator protrudes creating an L-shaped engine, the length of the bottom cord is primarily dependent on the length of the generator when placed in front of the compressor. The L-shaped engine could be disadvantageous when it is integrated within a vehicle, but it could also offer room to place auxiliary systems.

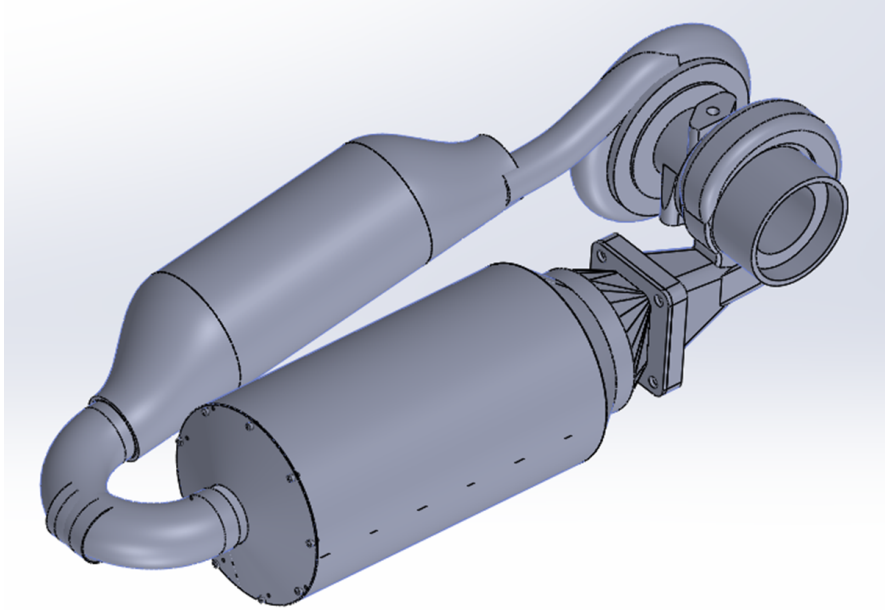


Figure 3.4: Silo configuration of a can combustor

To reduce the size of the engine and enhance the recuperator efficiency, the recuperator can be integrated within the combustor as shown in Figure 3.5. The efficiency of the recuperator is improved due to an increase in surface area while maintaining an equal engine volume.

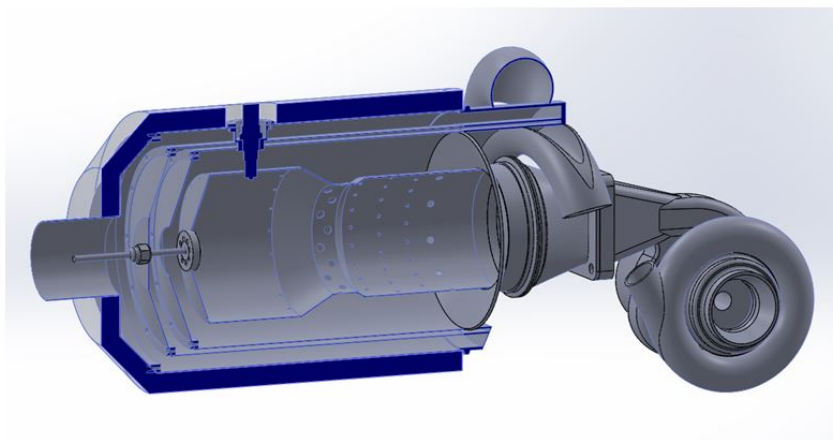


Figure 3.5: Silo configuration of a can combustor with integrated recuperator

3.3 Matlab thermodynamic cycle model

Prior to the design process itself, the thermodynamic cycle should be defined. The thermodynamic cycle is modelled to predict the behaviour of the gas turbine engine. Besides extracting the engine's performance it can also be used for optimizing certain parameters, i.e. pressure ratio, mass flow or TIT. The final configuration was found using an iterative approach where different configurations, parameters and/or designs were tested.

While gas turbine engines exist in a wide variety of configurations, the workings are based on the thermodynamic Brayton cycle. Figure 3.6 shows the TS diagram of the recuperated Brayton cycle. The components and their configuration can be seen in Figure 3.7.

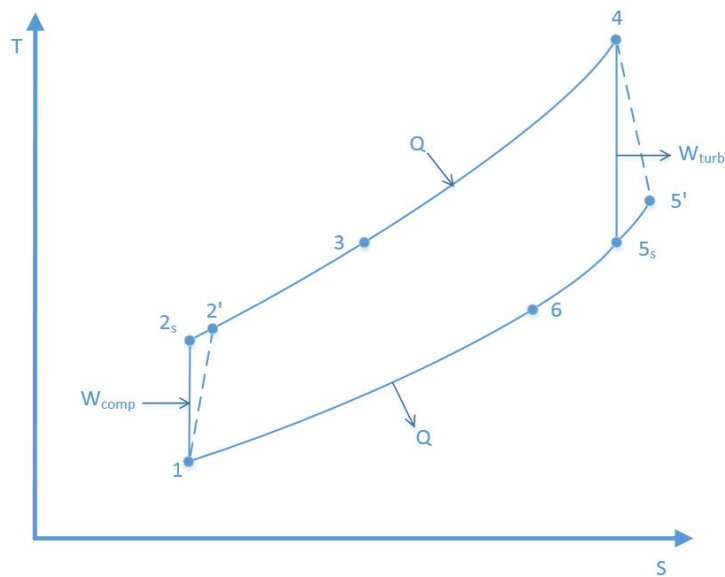


Figure 3.6: TS diagram of recuperated Brayton cycle

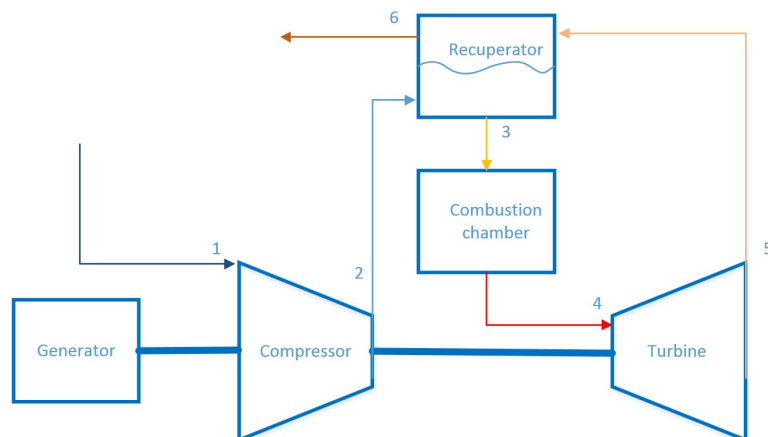


Figure 3.7: Schematic representation of recuperated Brayton cycle

The model describes the behaviour of the gas turbine engine at a fixed RPM of 105 kRPM as no transient behaviour is required.

Compressor

The Brayton cycle starts by compressing air with a compressor. In our case we make use of an single stage radial compressor. The following assumption are made;

- Constant RPM, 105 kRPM
- Constant κ and C_p
- Adiabatic process

The isentropic compressor discharge temperature can be computed with the following relation.

$$T_{2s} = T_1 \left(\frac{P_2}{P_1} \right)^{\frac{\kappa-1}{\kappa}} \quad (3.1)$$

The actual compressor out temperature is computed using the following equation.

$$T_2 = \frac{T_{2s} - T_1}{\eta_{comp}} + T_1 \quad (3.2)$$

The total work of the compressor can be defined as;

$$W_{comp} = \dot{m}(C_p T_2 - h_1) \quad (3.3)$$

Combustor

The heating of the compressed air takes place inside the combustor. The exiting temperature of the combustor is equal to the maximum allowable TIT for maximum system efficiency. The following assumption are made;

- Pressure loss, 10% over complete combustor, recuperator and piping
- Heatlosses are estimated by applying a constant combustion efficiency
- Constant κ and C_p
- Ethanol fuel without any contaminations, added water content is pure H₂O

The enthalpy of the combustor out is computed using equation 3.4.

$$h_4 = T_4 C_p \quad (3.4)$$

A certain amount of fuel needs to added to heat up the air to the TIT by means of combustion. The amount of energy needed for this heating process is computed with the following equations.

$$Q_{in} = \dot{m} C_p (T_4 - T_3) \quad (3.5)$$

$$\dot{v}_{fuel} = \frac{Q_{in}}{\eta_{combustion} * C_{fuel}} \quad (3.6)$$

Recuperator

The recuperator's contribution to T_3 (combustor inlet temperature) is modelled using a fixed efficiency determined by using the heat transfer equations for parallel flow heat-exchangers [24]. The following assumptions are made;

- No heatloss
- Constant κ and C_p
- Mass flow of hot and cold flow are equal
- Fixed end pressure
- Fixed pressure drop of 200 mbar over the hotside
- The pressure on the cold side of the recuperator is combined with the pressure loss from the combustor and is assumed at 200 mbar

The combustion chamber inlet temperature T_3 is computed using equation 3.7.

$$T_3 = T_2 + \eta_{\text{recup}}(T_5 - T_2) \quad (3.7)$$

The recuperator efficiency is determined by using the following equations [24].

$$h_c = \frac{k}{D_h} \text{Nu} \quad (3.8)$$

$$\text{where} \quad (3.9)$$

$$\text{Nu} = 0.023 \text{Re}^{0.8} \text{Pr}^{0.4} \quad (3.10)$$

$$T_3 = T_{\text{recup}} - (T_{\text{recup}} - T_1) e^{\left(\frac{-h_c A_{\text{transfer}}}{\dot{m} * C_p}\right)} \quad (3.11)$$

$$\text{Finally this leads to:} \quad (3.12)$$

$$\eta_{\text{recup}} = \frac{T_3 - T_2}{T_5 - T_2} \quad (3.13)$$

When the geometry shown in Chapter 4 is used the recuperator efficiency will be 20%. The applied boundary conditions and assumptions can be found in Appendix D2.

Turbine

The turbine wheel not only drives the compressor but also powers the generator. Within the turbine model the following assumptions are made:

- Constant RPM, 105KRPM
- Constant κ and C_p
- Adiabatic process
- Heatloss is incorporated into the turbine map

The temperature of the turbine discharge gas is computed using the following equation.

$$T_{5s} = T_4 \left(\frac{1}{ER} \right)^{\frac{\kappa-1}{\kappa}} \quad (3.14)$$

$$T_5 = T_4 - \eta_{turb}(T_4 - T_{5s}) \quad (3.15)$$

The work of the turbine can be computed using equation 3.16.

$$W_{turb} = (\dot{m} + \dot{m}_{fuel})(h_4 - h_5) \quad (3.16)$$

Note that within the model \dot{m}_{fuel} is added symbolically. The exact value can be solved when the T_3 is defined. This can be done at the end of each iteration step.

Generator

The generator generates electric power to charge the batteries. The power output of the generator is defined the following way.

$$W_{gen} = \eta_{bearings} * \eta_{gen} * W_{turb} - W_{comp} \quad (3.17)$$

Note that the bearing losses and electrical losses are estimated to 2% and 5% respectively, based on Smith [32], [16] and experience.

The overall efficiency of the engine is computed by dividing the output energy over the input energy.

$$\eta_{overall} = \frac{W_{gen}}{Q_{in}} \quad (3.18)$$

3.4 Matlab matching model

The turbine drives the compressor and generator, in order to get a steady-state their behaviour should match. In order to keep the costs of the range-extender low an off-the-shelf compressor has to match an off-the-shelf turbine.

In an automotive turbocharger application, the turbine generates enough torque to overcome bearing losses and drive the compressor. For a shaft-power gas turbine an automotive turbocharger match is thus not sufficient (but it could be used for a free-power set-up).

The generator has an operating RPM of 105 kRPM and a limiting RPM of 110 kRPM, this limiting RPM may not be exceeded. Because a single-rotor set-up is being used this automatically defines the rotational velocity of the compressor and turbine on its point of operation.

Small sized rotors typically used for turbochargers have an operating speed well above the limiting speed. Thus only larger compressor wheels are suitable for this application. The thermodynamic cycle model clearly showed that a high pressure ratio is beneficial for the system's efficiency. This means a compressor wheel is needed which has a high pressure ratio at the operational RPM of 105 kRPM. A TD06H compressor wheel was chosen for its performance on our point of operation. Figure 3.8 shows the compressor map of the chosen TD06H. Note that we have to operate on the 105 kRPM line due to the generator's properties. To maximize the system's efficiency we operate on this line at the highest pressure ratio possible, with an air flow that is sufficient to generate the power output that is needed.

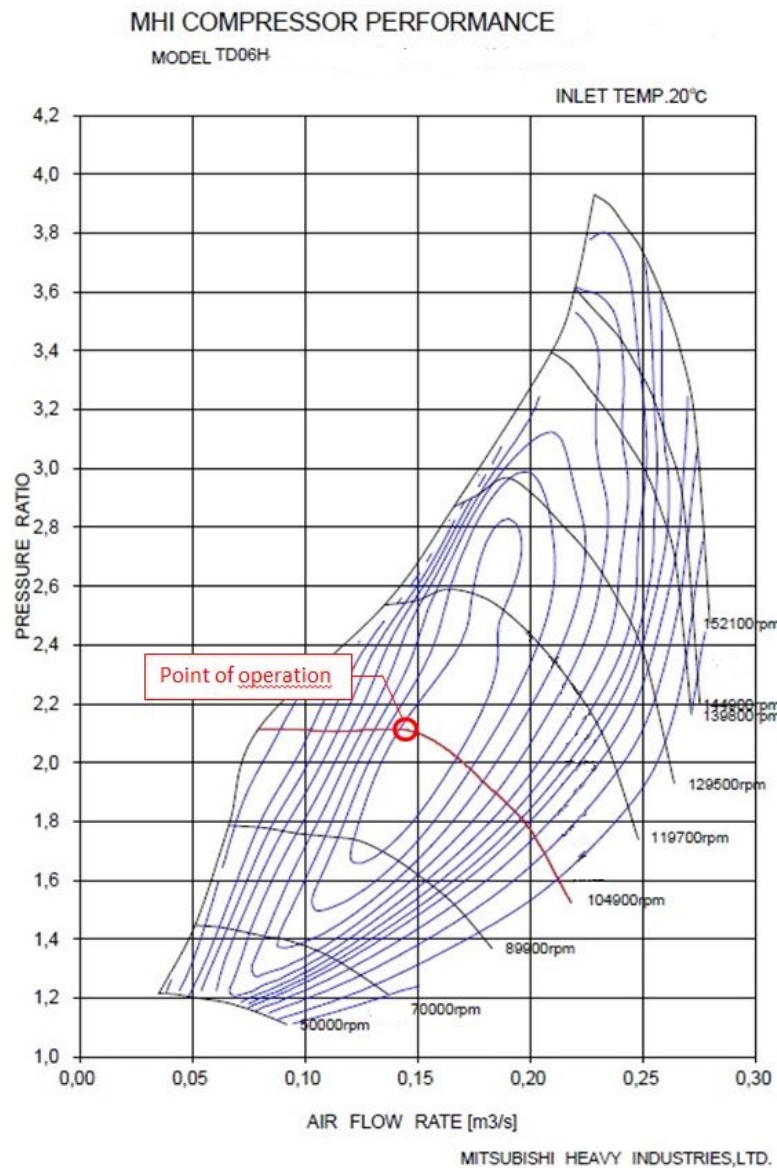


Figure 3.8: Compressor map of the TD06H with POI indicated

When a TD06H compressor is used for a turbocharger application it is driven by a TD05H turbine. The point of operation plotted in the turbine map can be seen in Figure 3.9. This turbine map is a 'Hot-map' as it is measured at 600°C.

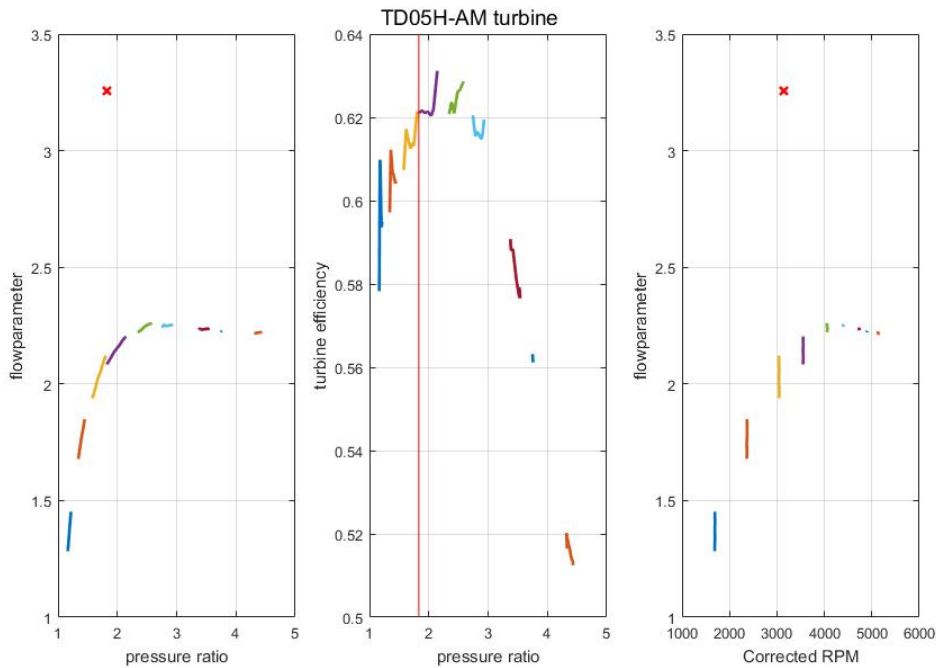


Figure 3.9: TD05H turbine map with POI indicated

It can be clearly seen that the flow parameter of the POI is too high for this turbine. This is caused by the fact that automotive turbochargers are equipped with a waste-gate¹. At the chosen POI, the waste-gate is opened and lets through approximately 30% of the mass flow. For a shaft power configuration a waste-gate is not preferred. This means that a turbine wheel should be used which can handle the high flow-parameter with a closed waste-gate.

The flow parameter and corrected RPM can be computed using the following equations.

$$\text{Flow parameter} = \frac{\dot{m}\sqrt{(TIT)}}{PR} \tag{3.19}$$

$$\text{RPM}_{\text{corrected}} = \frac{\text{RPM}}{\sqrt{(TIT)}} \tag{3.20}$$

Figure 3.10 shows the turbine map of a TD07S, when the POI is plotted it fits the behaviour of the turbine. Besides the matching flow parameter the RPM should also match, which is the case for a TD06H-TD07S combination. The turbine efficiency can be read from the middle-plot. The found compressor- and turbine-efficiency values can now be incorporated into the Matlab cycle model to improve its accuracy.

¹A waste-gate is a turbine bypass valve that regulates the speed of the turbocharger, another advantage is that a waste-gated turbine can use smaller A/R housing which lowers the spool-up time

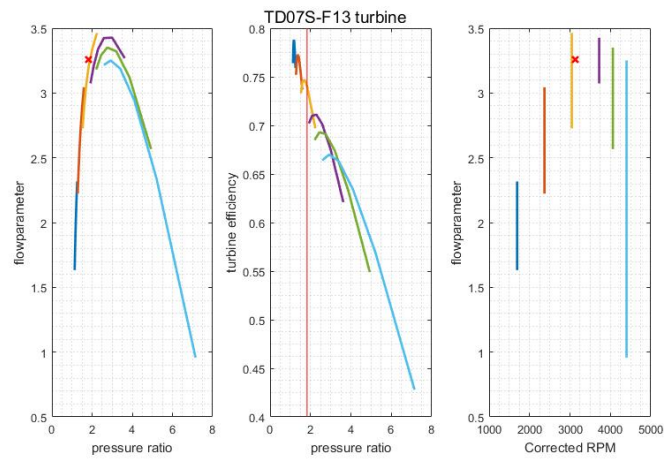


Figure 3.10: TD07S turbine map with POI indicated

When the results of the cycle model and matching model are combined, it can be concluded that a compressor/turbine match has been found which would have the following properties.

Power output	10.1 kWe
Efficiency	7.5 %
Fuel consumption	25.5 L/hr (E100)

Table 3.1: Engine properties derived from Matlab modelling

3.5 Cycle-Tempo model

The results of the Matlab cycle model is validated using a Cycle-tempo model. The model is constructed using [10]. Figure 3.11 shows the cycle modelled.

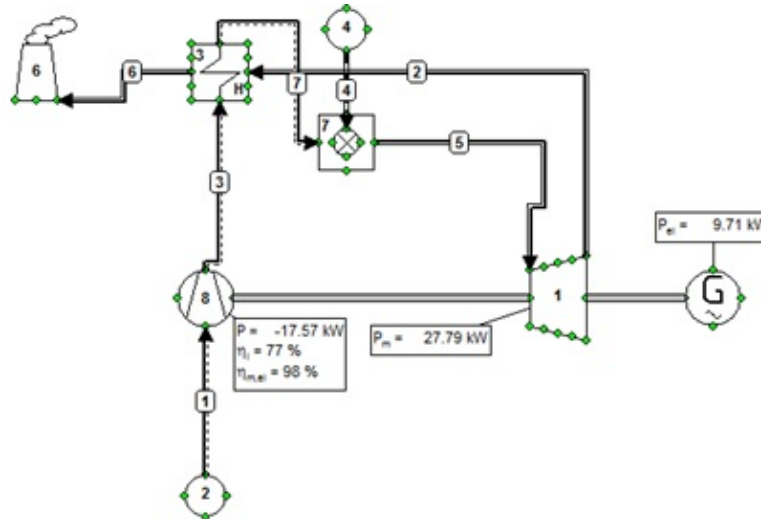


Figure 3.11: The Cycle-tempo model

The results of the Cycle-tempo model match the results of the Matlab model with an error within 3%. This error is caused by the fact that the fuels from Cycle-tempo differ from the fuels used in the Matlab model. Cycle-tempo does not offer 100% ethanol as a fuel and uses coal instead. While this has no impact on the TIT it changes the total mass flow going through the turbine changing the turbine work slightly.

3.6 Fluent combustion simulation

In order to check the behaviour of the combustion chamber, primarily focussing on flame length and wall-cooling, a CFD combustion simulation is made using Ansys Fluent. The results of a stepped RQL liner can then be compared with a SRQL liner. An additional study can be conducted to investigate the impact of 90% bio-ethanol compared to 100% bio-ethanol. The simulation is based on the work of Sallevelt [30], making use of the non-premixed combustion model within Fluent.

3.6.1 Combustion model

The combustion process is modelled as non-premixed combustion because the fuel and oxidizer enter the reaction zone in separate streams. The turbulent flame is modelled using an ensemble of laminar flame jet [25] [17]. The chemical reaction rate is expressed with the Damköhler number², when the Damköhler number is unity or above the reaction is limited by turbulent mixing which is the case for combustion reactions. The thermo-chemistry can be reduced to a single parameter; the mixture fraction [25]. By using this approach the species transportation does not have to be solved. The thermochemical calculations are solved during the preprocessing of the simulation. The results are tabulated for look-up which is done in the processing itself. This approach requires the combustion problem to meet the following criteria [2];

- Deflagrational combustion with discrete fuel and oxidizer inlets
- Fast chemical reaction, limited by turbulent mixing
- Lewis number³ is equal or around 1, which is true for turbulent flows
- Only one type of fuel can be used
- Only one type of oxidizer can be used

The mixture fraction, defined by equation 3.21, is a conserved quantity and therefore its governing transport equation does not have a source term [2]. By using this approach combustion is simplified to a mixing problem and the need for solving non-linear mean reaction rates is avoided. The local mass fraction consists of unburnt fuel elements(C, H) and the other elements(CO_2, H_2O, O_2). Once the fuel mixture is mixed with air, the thermochemical behaviour is looked-up in the previously made tables, which are modelled with the equilibrium model [2]. The chemical reaction modelled is restricted to equation 3.22. The formation of nitrogen-oxides or sulphuric oxides is therefore not present.

$$f_i = \frac{m_i}{m_{tot}} \quad (3.21)$$

²Ratio of the reaction rate and mass transport rate

³Ratio of thermal diffusivity to mass diffusivity

Where m_{fuel} represents the amount of fuel in moles while m_{ox} represents the quantity of air in moles.



The mixture fraction is modelled using the Favre mean mixture fraction [2] which is expressed the following way;

$$\frac{\partial}{\partial t}(\rho \bar{f}) + \nabla \cdot (\rho \bar{v} \bar{f}) = \nabla \cdot \left(\frac{\mu_t}{\sigma_t} \nabla \bar{f} \right) + S_m + S_{user} \quad (3.23)$$

Where S_m is the source term⁴ describing the transfer of mass in liquid form into gas phase while f represents the fraction. Note that this equation is only valid when the Lewis number is unity, which is the case for turbulent flows.

Besides solving for the Favre mean mixture fraction, the conservation of the mixture fraction variance needs to be solved for. The conservation of the mixture fraction variance (f') is needed to describe the turbulence-chemistry interactions. The mixture fraction variance is expressed the following way [2];

$$\frac{\partial}{\partial t}(\rho \overline{f'^2}) + \nabla \cdot (\rho \bar{v} \overline{f'^2}) = \nabla \cdot \left(\frac{\mu_t}{\sigma_t} \nabla \overline{f'^2} \right) + C_g \mu_t (\nabla \bar{f})^2 - C_d \rho \frac{\epsilon}{\kappa} \overline{f'^2} + S_{user} \quad (3.24)$$

Where 0.85, 2.86 and 2 are used for σ_t , C_g and C_d respectively, again S_{user} is an added source term.

3.6.2 Geometry & Boundary conditions

The Fluent combustion simulation focusses on the behaviour of the combustion chamber. Therefore only the geometry of the combustion chamber is used. The combustion chamber has rotational symmetry and thus a 2D geometry is sufficient for studying the flame-pattern and effectiveness of wall-cooling. The shape of the stepped RQL combustion chamber and its hole pattern are based on the design of Samuelsen [31].

The first step of the defining the combustion chambers geometry is to study the amount of fuel and air needed to carry out the complete combustion. When the molar masses are computed and equation 3.22 is taken into account, it appears that 100% bio-ethanol would have a stoichiometric ratio of about 9. By using these values in combination with the recommended equivalence ratio's, from [31] seen in Figure 3.12, the air distribution over the liner can be defined. 13% of the total mass flow of air should go through the swirler and mix with the fuel. The design of the swirler is based on the mass-flow and swirl number. For this application a swirl number of 5 is recommended, see equation 2.2.

Within the first combustion zone two rows of cooling air are present, each taking 10% of total air mass flow. The quenching zone requires 40% air while the remaining 27% is used for the lean combustion and dilution.

⁴The source term is a scalar function and are added to describe the addition of fuel

The diameter of the combustion chamber impacts the airspeed which, in turn, influences the combustion process and overall stability. The initial airspeed within the combustion chamber should be relatively low, but still higher than the flame-speed. When the average airspeed is higher than the flame-speed, recirculation area's should occur to maintain an anchor point for the flame. According to Lefebvre [20] the turbulent flame speed of ethanol can be computed using equation 3.25. The turbulent flame is based on the laminar flame speed which is 0.3m/s for the rich section and speeds up to 0.45m/s once quenched according to [1].

$$S_t = \left(\frac{D^2}{\alpha \lambda} + \frac{1}{S_L^2} \right)^{-0.5} \tag{3.25}$$

Where D represents the droplet diameter which in our case is 30 micron based on the chosen injector, α represents the thermal diffusivity and λ the evaporative constant.

When the turbulent flame speed is evaluated it appears that it is close to the laminar flame speed which is between 0.3 and 0.45 m/s. If the airspeed within the combustion chamber needs to be slowed down to such a low value the diameter would become excessively large. To avoid a large combustion chamber, recirculation area's need to be added.

Further down the combustion liner airspeed will increase due to a temperature rise and decreasing liner diameter. The diameter of the quenching section influences the quenching depth and thus its effectiveness. If the diameter of the quenching zone is chosen too large, the quenching air-jets will not penetrate to the core of the flame, thus maintaining a high core temperature. When the diameter of the quenching zone is too small, the quenching effect could become too strong creating a partial or even full blow-off. To enhance mixing and dilution, the air speed of the lean combustion and dilution section should be higher than the initial rich combustion section. The conical shape between the quenching zone and lean combustion zone offers another anchor point for the flame. After the combustion liner the airspeed will increase further until the flow reaches choke-point.

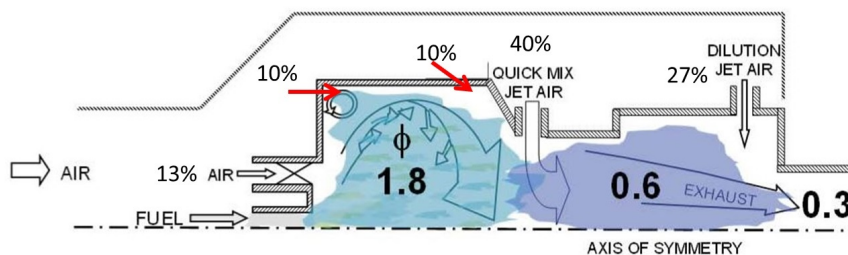


Figure 3.12: Equivalence ratio's along the length of the RQL combustor

To ensure the right airspeed along the combustion chamber the dimensions seen in figure 3.13 are used. The overall length of the combustion chamber should be sufficient to be able to house the complete flame and partially its mixing zone. The last mixing/dilution phase can also occur in the turbine inlet and scroll.

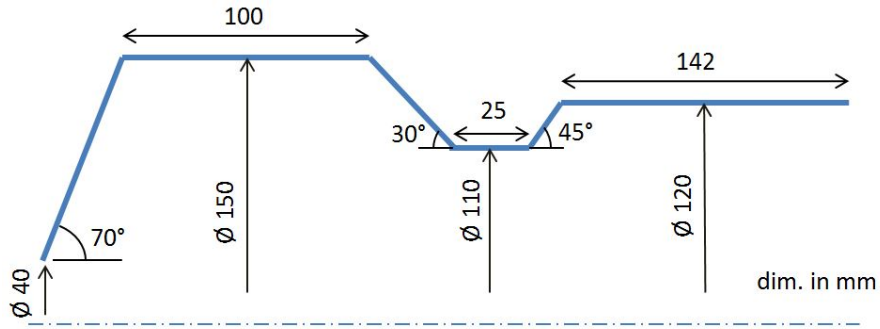


Figure 3.13: Outer dimensions of the combustion liner

Figure 3.14 shows the geometry and boundary conditions used. A mass flow rate is specified at the air-inlet and fuel inlet, which are $0.1993 \frac{\text{kg}}{\text{s}}$ and $0.0068 \frac{\text{kg}}{\text{s}}$ respectively, which were derived from the Matlab cycle model. The temperature of the air-inlet is equal to the recuperator discharge temperature obtained from the Matlab cycle model. The inlet air consists of 21% O_2 where the fuel consists of 100% $\text{C}_2\text{H}_5\text{OH}$. The turbulence intensity is assumed to be 5% based on [30]. The turbulence intensity parameter is used to compute the κ and ω . The back-pressure caused by the turbine is set at 1.85 bar.

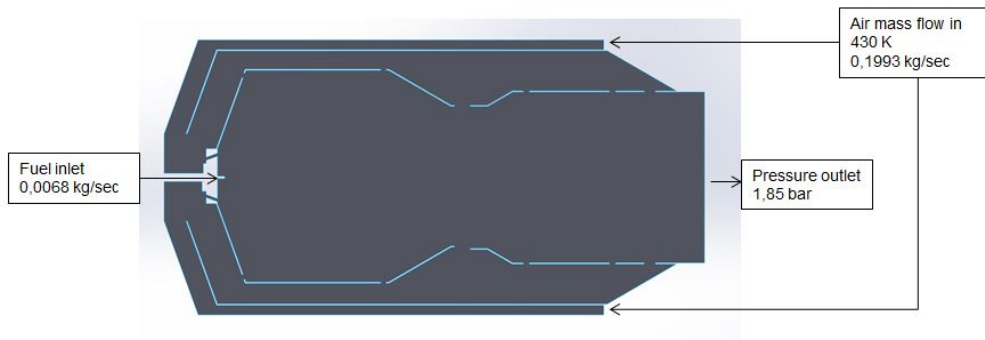


Figure 3.14: Boundary conditions used for the Fluent combustion simulation

Note that the CFD-simulation only models the fluid-domain. The influence of the sheet-metal on the flame shape can be neglected.

The fuel is injected in the form of droplets with a Sauter mean diameter of $30 \mu\text{m}$. The non-uniformity of the droplets is described using the Rosin-Rammler distribution which is described in [20]. The distribution is described with the following function;

$$1 - F = \exp\left(-\left(\frac{d_p}{d}\right)^q\right) \quad (3.26)$$

3.6.3 Mesh

Figure 3.18 shows the meshed geometry. The mesh consists of 30.391 quadrilateral elements. Quadrilateral elements are used as the geometry can be considered structured, which reduces the computational time. The mesh is refined around the hole pattern of the combustion liner so it can handle the large gradients (i.e. velocity and temperature).

3.6.4 Solver set-up

Fluent provides several different solvers that can be used, for a combustion problem a 'Coupled Pressure-based' solver is preferred due to its stability and convergence behaviour [2]. Within the Coupled Pressure-based solver the mass conservation and momentum equations are solved. The velocity field can be obtained from the momentum equations. All energy and species equations are solved sequentially.

Combustion simulations typically struggle to converge. The convergence can be eased by using the pseudo transient method. While a steady-state solution is being computed a pseudo time-step can be used to evolve the initial condition to the final steady-state. The length of this pseudo time step is automatically computed based on the velocity field.

The turbulence is modelled using the $\kappa - \omega$ model. Within the $\kappa - \omega$ model wall functions are being used [9].

Choosing a good initial condition is essential to get the combustion simulation to converge. The initial condition used by the solver is based on a 'cold' flow simulation. The solution contains information about the flow-field but neglects species and energy equations.

When solving actual combustion simulation several higher order under-relaxation factors were used. By increasing the relaxation factors the convergence can be accelerated, yet when excessive high values are used the solution becomes unstable. Figure 3.16 shows the relaxation factors used. The magnitude of the relaxation factors are determined experimentally.

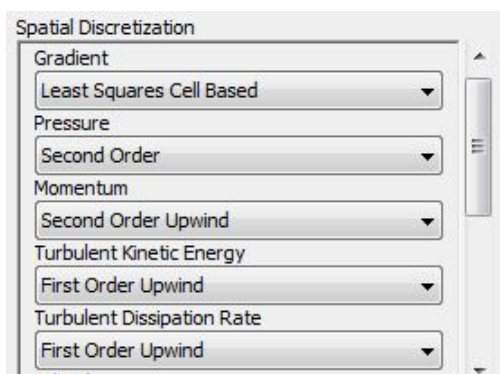


Figure 3.15: Discretization models used

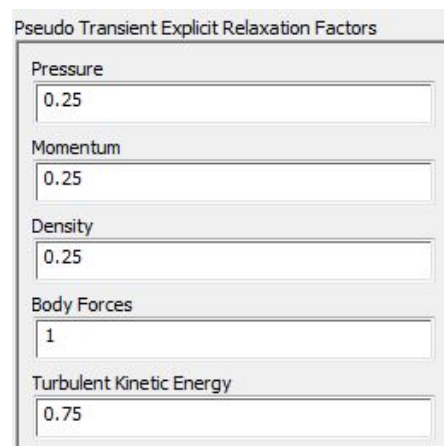


Figure 3.16: Relaxation factors used

3.6.5 Validation

To investigate the validity of the results several validation checks can be conducted. The first validation check is conservation of mass, the mass inlets should equal the mass outlet. Figure 3.17 shows the conservation of mass flow. The error present is in the order of 10^{-8} which is a numerical error. This error is small enough to be neglected.

Mass Flow Rate	(kg/s)
air_velocity_inlet	0.20004633
fuel_velocity_inlet	0.0068014428
pressure_outlet	-0.20684774
Net	3.5518608e-08

Figure 3.17: Mass flow calculation

When the conservation of energy is investigated, it appears that the error is exactly zero. This is caused by the fact that the energy equations are based on an energy equilibrium. This means that the solution can only converge when the energy equilibrium equations holds.

During solving the simulation Fluent can plot the convergence residuals. Besides conservation of mass and energy, the magnitude of the residuals is used as a criterion to determine if the computation can be stopped. The following figure shows the convergence of different parameters. It can be clearly seen that species typically have a larger error than other variables. This is caused by the fact that species have a relatively larger relaxation-factor.

The grid dependency is studied by refining the mesh up to a point that the grid dependence is negligible. Table 3.2 and Figure 3.19 show the number of elements versus the residuals. Initially the accuracy of the computation increases with an increasing element number. After a certain point the problem has converged enough and there is no extra benefit in increasing the element number. Therefore the mesh with 30391 elements has been used.

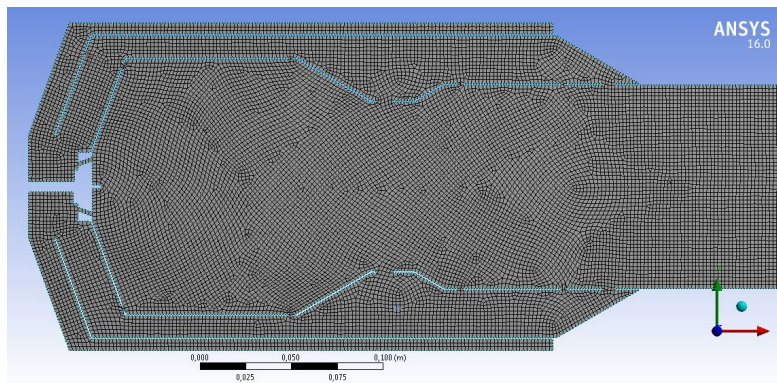


Figure 3.18: Combustion chamber meshed

number of elements	Continuity
5791	Not converged
7791	Not converged
8926	Not converged
14427	1.6698×10^{-3}
17074	9.5969×10^{-4}
30391	6.9048×10^{-4}
46832	3.7738×10^{-4}
55848	5.4695×10^{-4}
66864	4.5796×10^{-4}
104595	9.5422×10^{-4}

Table 3.2: Grid dependency check

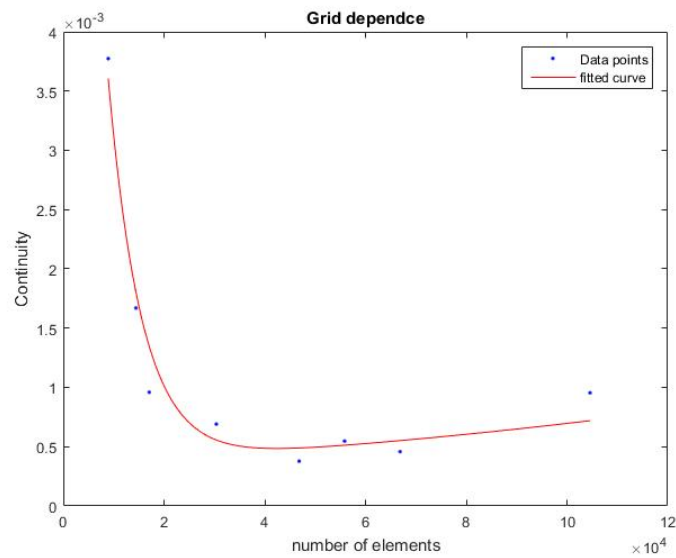


Figure 3.19: Residual with respect to the number of elements

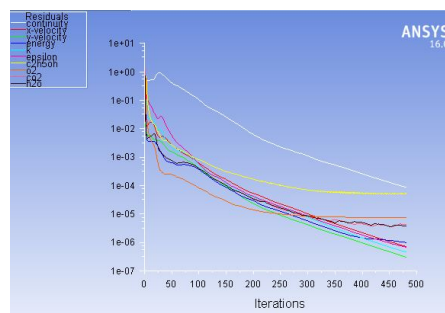


Figure 3.20: Convergence plot

3.6.6 Results

Figure 3.21 and 3.22 show the velocity distribution along the combustion chamber. The magnitude of the velocity within the liner is relatively low which could emphasize the buoyancy effect, meanwhile it offers robustness. The flame is anchored by three anchor points which are clearly visible in the velocity distribution figures. The anchor points are created by the recirculation area generated by the axial swirler and the toroidal recirculation caused by the front cone. The SRQL combustion liner has a larger swirler recirculation area, this can offer more robustness against flame-out but is likely to increase NO_x emissions due to increased residence time.

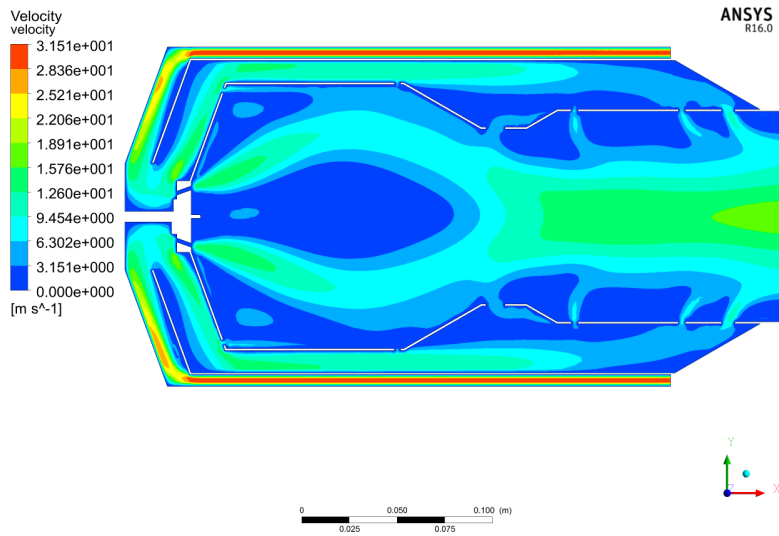


Figure 3.21: Velocity distribution of the SRQL liner

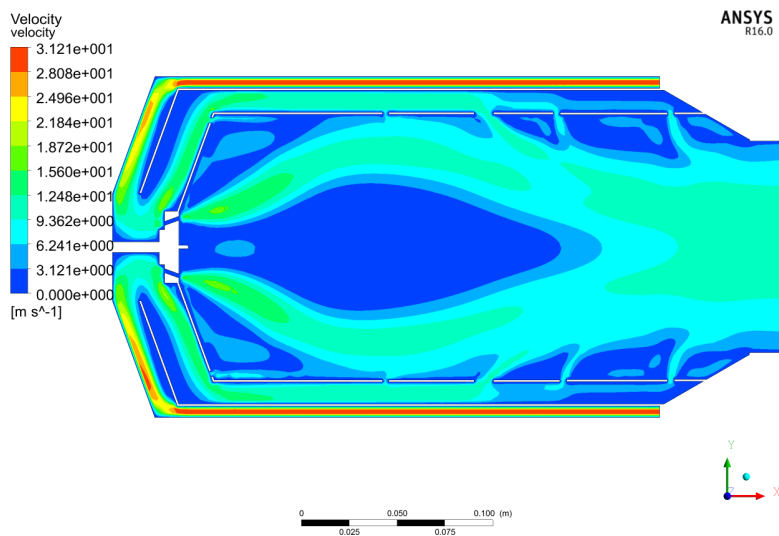


Figure 3.22: Velocity distribution of the SRQL liner

The temperature distribution of the RQL and SRQL combustion chamber is shown in Figure 3.21 and 3.22.

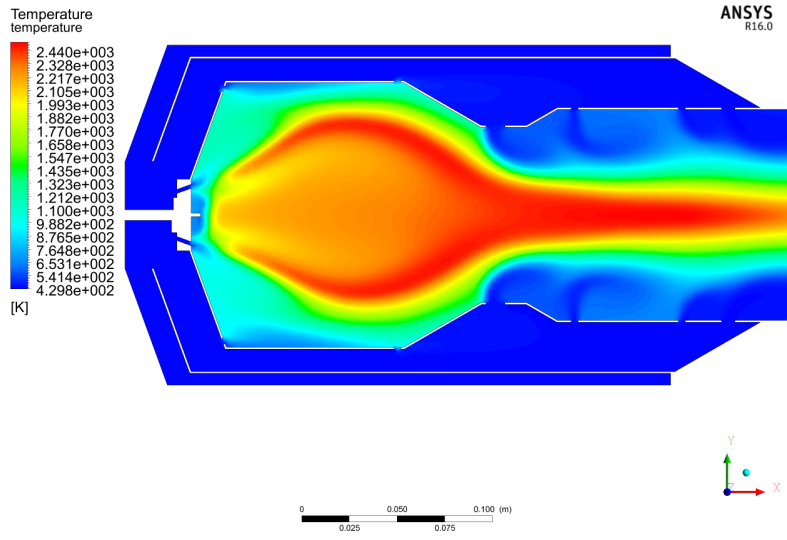


Figure 3.23: Temperature distribution of the SRQL liner

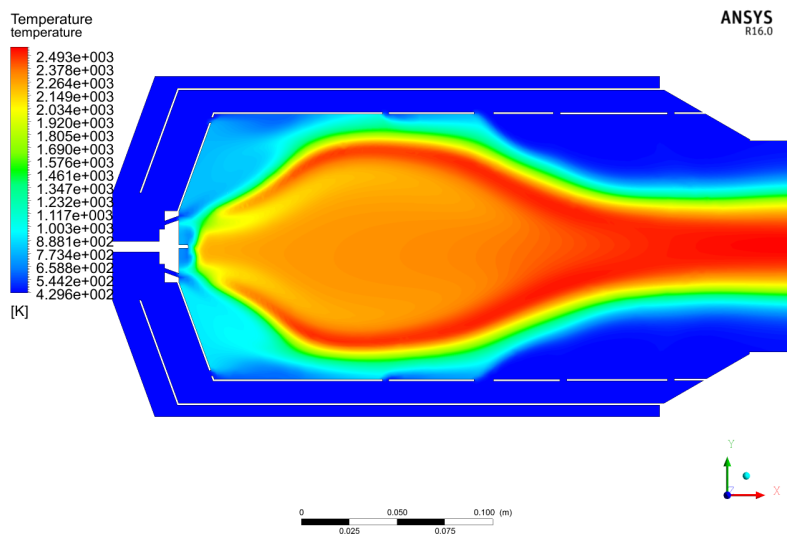


Figure 3.24: Temperature distribution of the SRQL liner

The temperature distribution of the RQL combustion chamber clearly shows the quenching effect of the middle section. While the peak temperatures are comparable the hot zone in

the quenching zone is significantly narrower than the hot zone of the SRQL liner. This means that the quenching zone in the RQL liner is more efficient at cooling and diluting the flame than the SRQL quenching zone. The jets of cold air penetrate the hot-section deeper while the quenching effect of the SRQL liner only affects the surface of the flame. Although the RQL quenching zone is more efficient at cooling and diluting the flame it also increases the risk of blow-off or partial incomplete combustion lowering combustion efficiency.

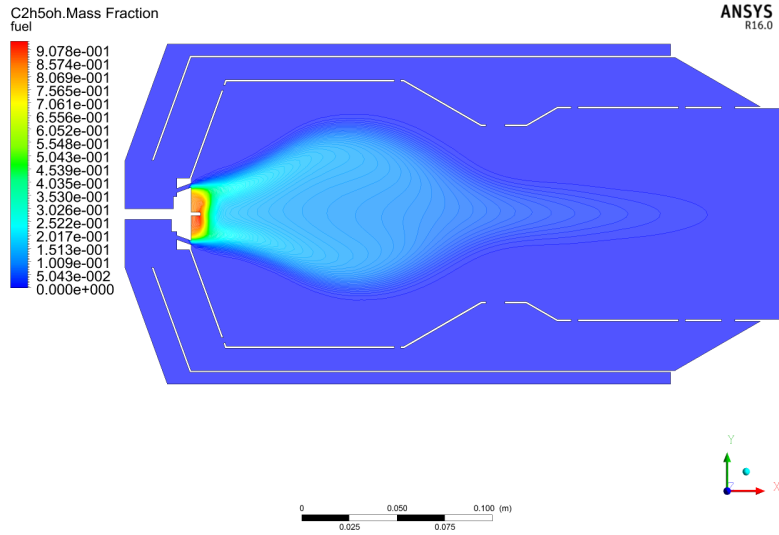


Figure 3.25: fuel fraction of the stepped RQL liner

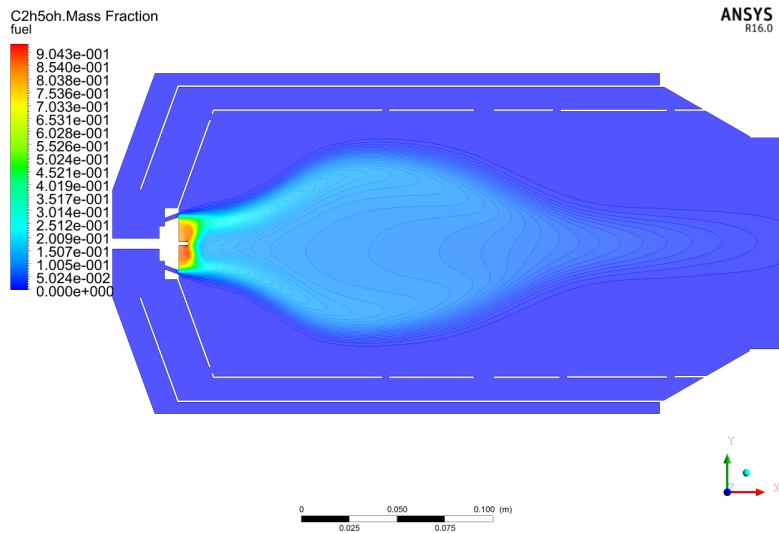


Figure 3.26: Fuel fraction of the straight RQL liner

A clear difference can be noticed when the temperature distributions of the liners are compared. The difference can be explained with the results of the fuel fraction distribution that can be seen in Figure 3.25 and 3.26. At the quenching zone of the RQL liner the fuel fraction gets diluted with air and extra oxygen is added to quench the flame from rich to lean. When a straight can is used the dilution effect is reduced, which means in the core the flame is not well mixed. The rich burning flame retains a lack of oxygen in its core. This causes the flame to grow longer and might cause (locally) a higher measured TIT. The length of the flame, which can be derived from the fuel fraction figures, shows that the length of the combustion chamber is sufficient for both the RQL and SRQL liner.

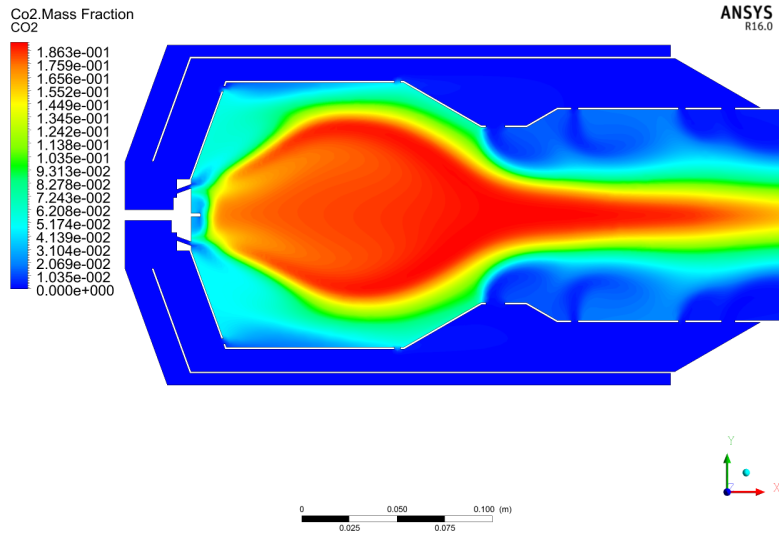


Figure 3.27: CO₂ mass fraction of the stepped RQL liner

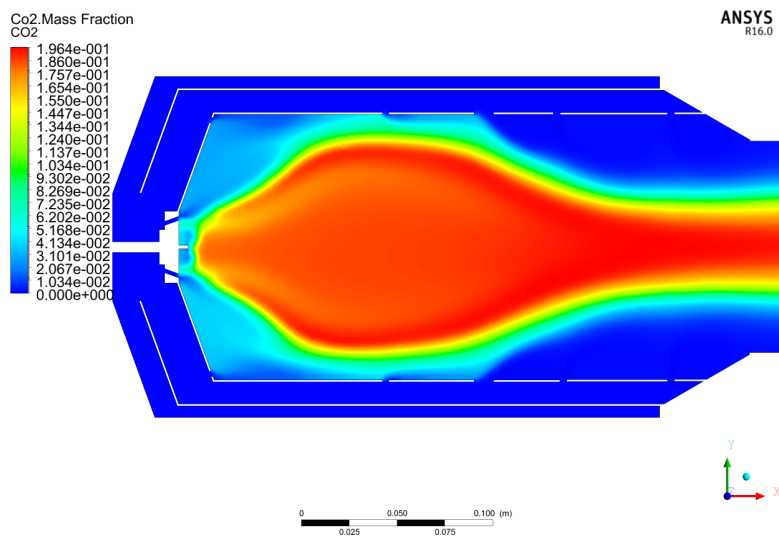


Figure 3.28: CO₂ mass fraction of the straight SRQL liner

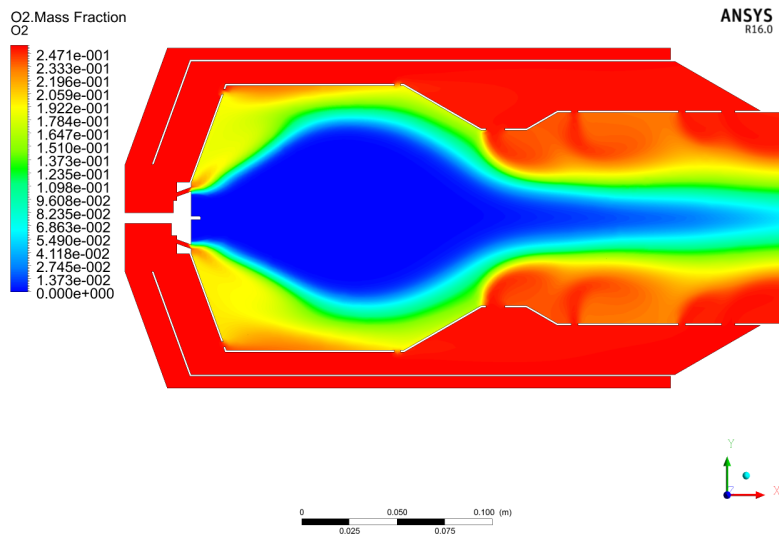


Figure 3.29: O₂ mass fraction of the stepped RQL liner

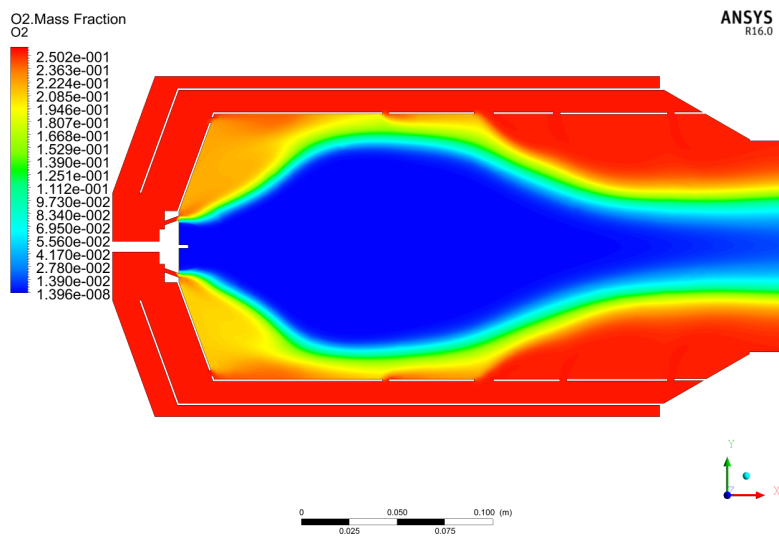


Figure 3.30: O₂ mass fraction of the straight RQL liner

From the CO₂ and O₂ mass fraction distribution it can be derived whether the flame is rich or lean. The front sections of both liners are identical, therefore the behaviour is comparable. The first combustion section should be rich, which is confirmed by the lack of O₂. When the flame is quenched the mixture is diluted which reduces the lack of O₂. This can

be clearly seen in Figure 3.29. When the SRQL liner is used, the diluting effect is less pronounced, this causes a rich core to remain. The effect of this rich core can also be seen in the temperature distribution, as the temperature increases.

Besides the change in liner shape, an experiment with different fuels can be conducted. To lower emissions a wet combustion process can be applied. The following simulations are conducted using bio-ethanol with 10% water content.

When the results shown in Figure 3.31 are compared with figure 3.23 it can be noticed that the peak temperatures are lower due to the cooling effect of the water content. The reduced peak temperature means that the NO_x emission is lower. The SRQL can shows a similar result when 90% bio-ethanol is used, which can be seen in Figure 3.24 and 3.32 .

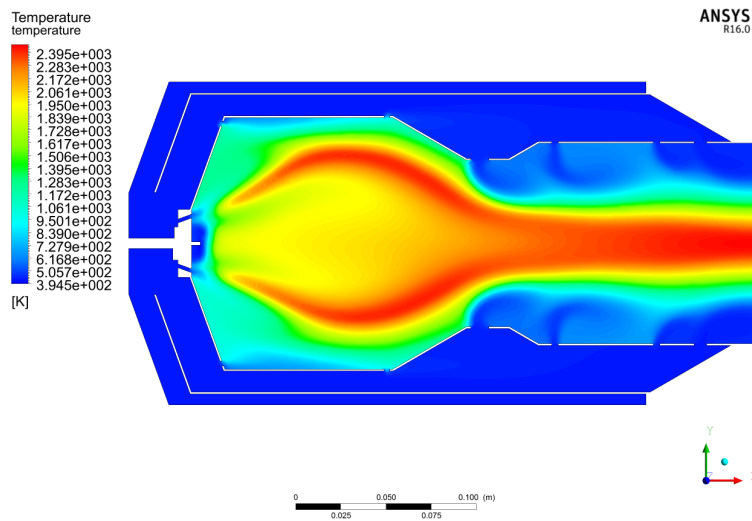


Figure 3.31: Temperature distribution of the RQL liner with 90% ethanol

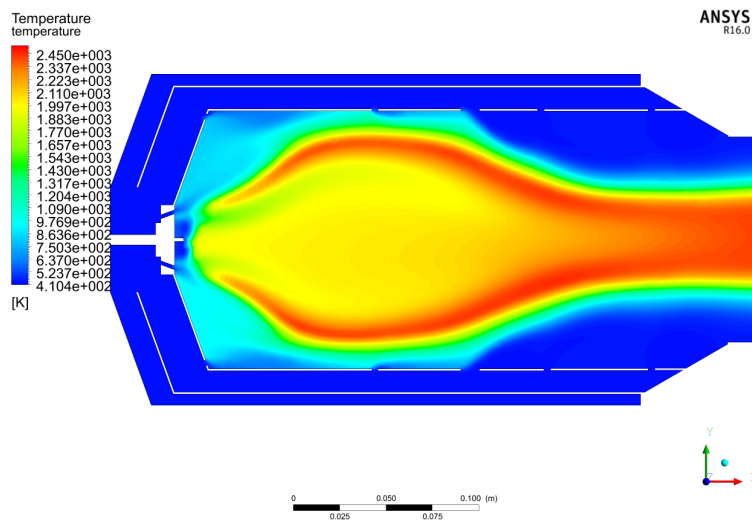


Figure 3.32: Temperature distribution of the SRQL liner with 90% ethanol

The length of the flame increases in size due to the water content as the evaporation rate is slowed down. The result of this effect can be seen when Figure 3.33 is compared to Figure 3.25. The same effect occurs within the SRQL liner: the flame length is increased and is not fully combusted at the end of the combustion liner. A small section of the flame will enter the turbine inlet manifold. The length of the turbine inlet is sufficient to cope with this flame-tip. The fuel fraction distribution of both liners also shows that due to the water content less fuel combusts within the rich combustion zone. This means that more fuel is burnt within the lean combustion section, lowering the NO_x emissions even further.

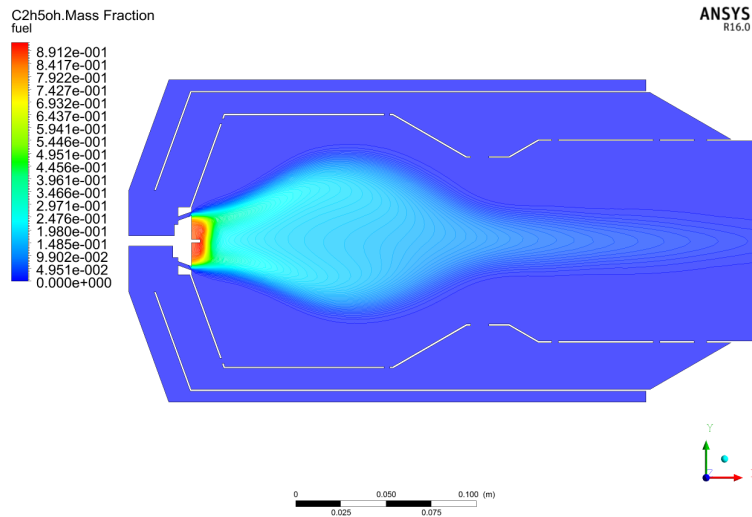


Figure 3.33: Fuel fraction along the RQL liner with 90% ethanol

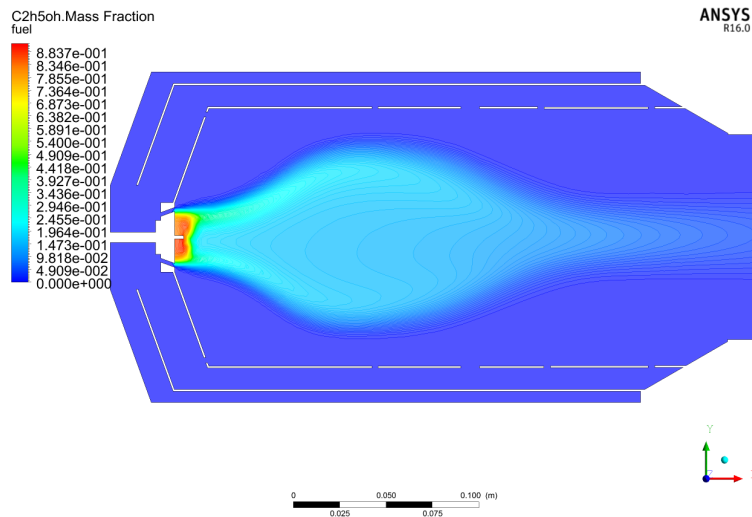


Figure 3.34: Fuel fraction along the SRQL liner with 90% ethanol

The results of other parameters, i.e. CO₂ and O₂, are similar to their original results as the same amount of combustible fuel is used. Equivalence ratio's are therefore independent of the water content.

3.6.7 Conclusion

From the results obtained from the Fluent combustion simulation it can be derived that the dimensions and hole pattern of the combustion liner are satisfactory but not yet optimized. The behaviour and the robustness of the combustion chamber can be fine-tuned with the test-results from engine tests.

The main questions answered by the Fluent combustion simulation is that it appears that the main dimensions(length and diameter) of the combustion chamber ensure a sufficient mixing, stabilising and combustion behaviour. The wall-cooling seems sufficient to prevent the liner from over-heating.

From the combustion simulation it can also be concluded that the 90% bio-ethanol is not only cost-wise an interesting fuel, but that it has the potential to lower the NO_x emission due to lower peak temperatures. Besides the lower NO_x emissions the CO₂ emission could be slightly reduced due to an increase in turbine mass flow.

The simulation showed that the shape of the quenching zone plays a decisive role for the quenching effectiveness. The RQL showed the strongest quenching behaviour but it risks partial blow-off while the SRQL quenching zone might be ineffective. The influence of the phenomenon on combustion efficiency and stability should be studied in practice.

Chapter 4

Final Design

The geometry of the gas turbine range extender can be finalized when the model iterations loops are finished. The 3D CAD design has been made using Solidworks.

The layout of the engine is primarily focused on reducing packaging-size and enhancing mass-production capability.

The engine consists of a turbocharger with a generator mounted on the compressor-side and a horizontal can shaped combustion chamber with integrated recuperator. Figure 4.1 shows a section view of the complete engine.

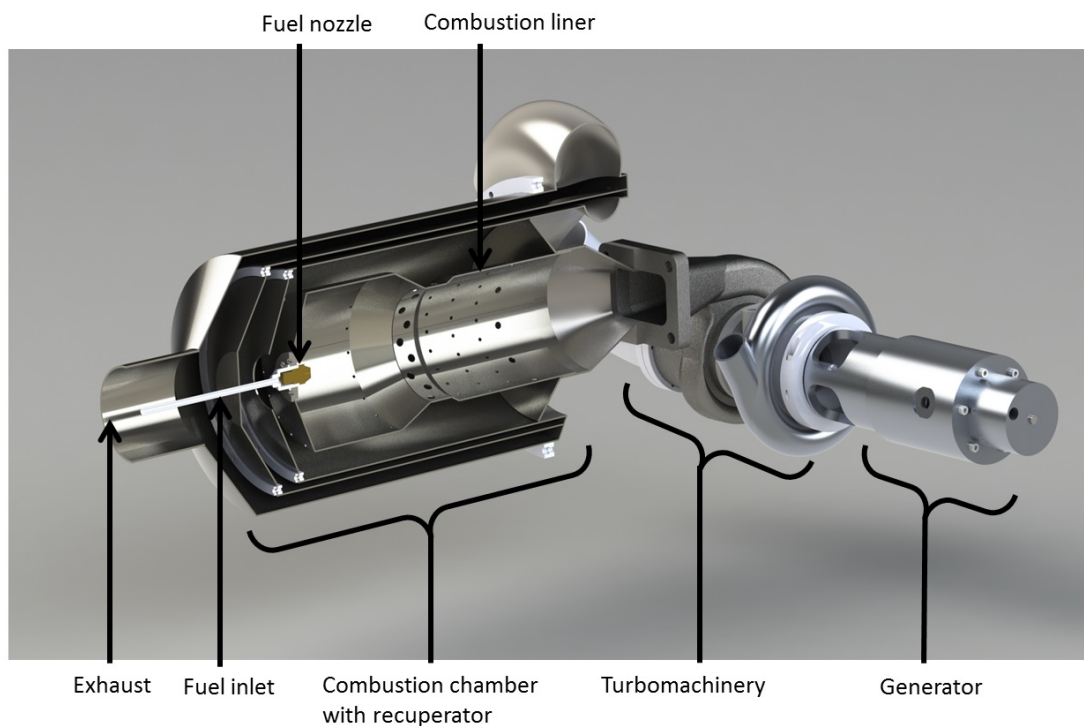


Figure 4.1: Overview of gas turbine engine with section view of the combustion chamber and recuperator

The combustion chamber consists of several concentric stainless steel tubes that can be seen in Figure 4.2. These concentric tubes not only house the combustion liner but also act as an recuperator. The outer tube holds the exhaust gas while it heats up the middle tube holding the compressed air. In the centre the combustion liner is placed. At the end of the middle tube the air is redirected to flow into the centre tube.

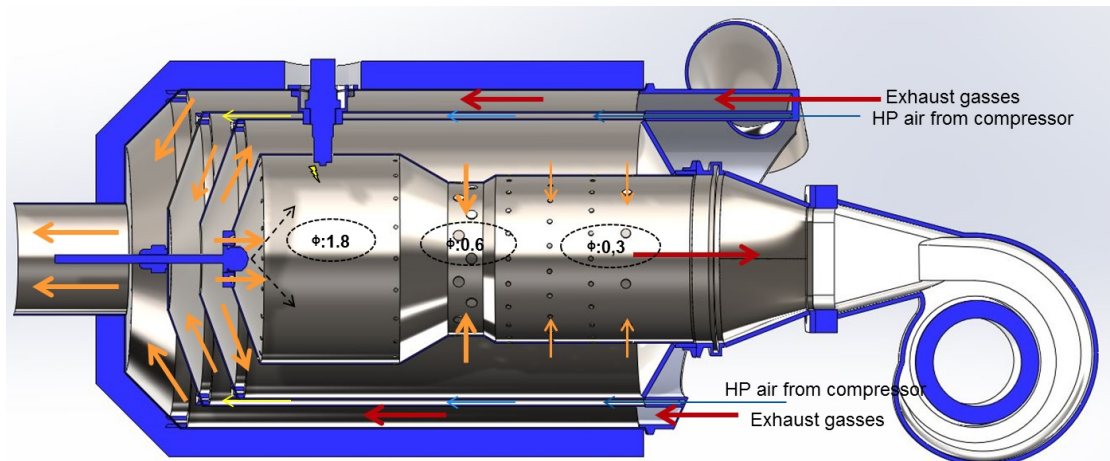


Figure 4.2: Section view of the combustion chamber with incorporated recuperator

All tubes are made of stainless steel(304L) sheets that are rolled and welded. The design is made so that these parts could be stamped and deep drawn for mass-production, minimizing the cost. The inlet and outlet manifold could be manufactured using die-casting or investment-casting methods.

4.1 Turbomachinery

The results of the matching model made clear that a standard automotive compressor/turbine combination cannot be used. A combination of a TD06H compressor driven by a TD07S turbine did match and thus a custom turbocharger assembly is needed. The turbine-housing, turbine rotor and bearing-housing from the TD07S turbocharger are used. In order to fit the compressor compressor-cover, the TD07S bearing-housing is trimmed-down.

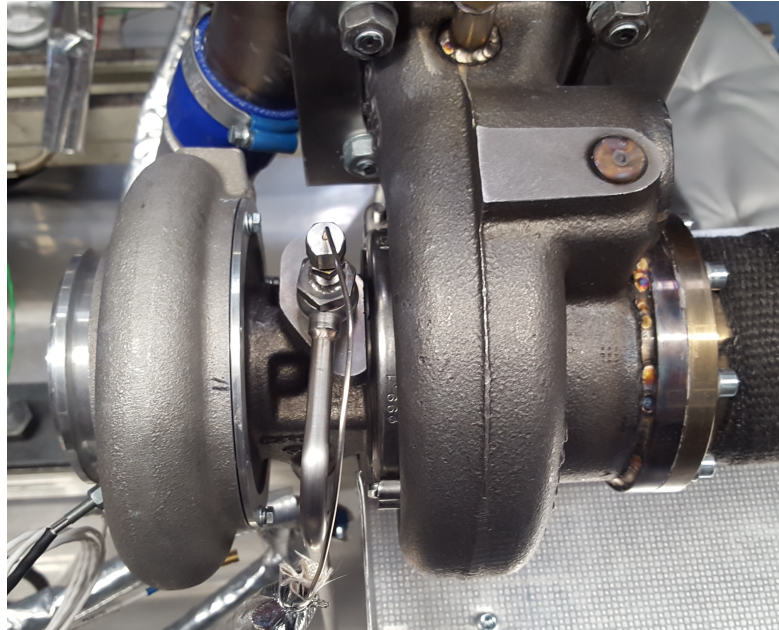


Figure 4.3: TD07 Cartridge modified to fit a TD06H compressorwheel and compressor cover

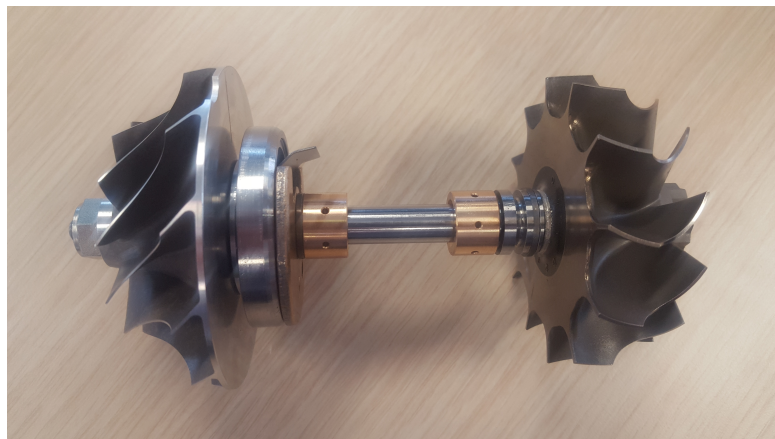


Figure 4.4: Turbocharger rotor, with 2 radial floating ring bearings and one axial bearing

4.2 Combustion Chamber

The final design uses a can shaped combustion chamber. In order to be able to experiment with different liners the design of the combustion chamber is modular. The liners can be interchanged while other parameters, i.e. nozzle, swirler, remain the same.

Three combustion liners have been made, a stepped RQL liner, a straight RQL liner and a rich combustion liner. Both RQL liners use the same equivalence ratio along the liner which is specified in Figure 4.2.

The rich liner is a more conventional design that makes use of rich flame [23] [4]. While a full rich combustion chamber is not beneficial for the emissions, it is known for its stability. The rich liner can be used to test the engine's rotor/generator without the risk of instabilities.

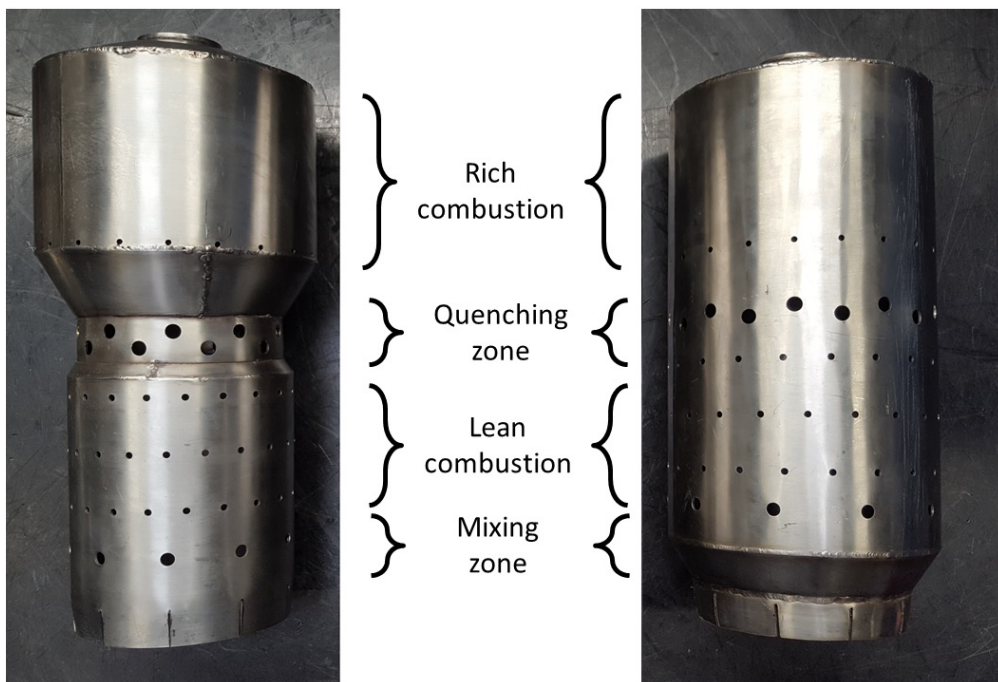


Figure 4.5: RQL and SRQL liner

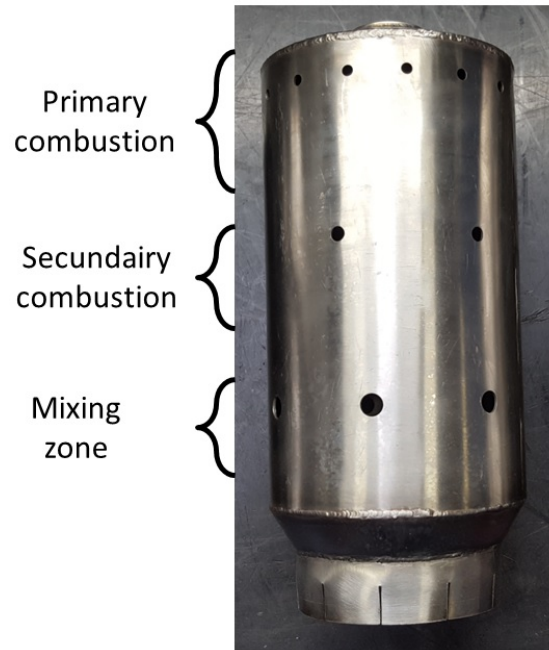


Figure 4.6: Rich Liner

The front cone of the combustion chamber houses the swirler, this swirler stabilises the flame. An axial hole swirler is used to minimize the losses and focusses on manufacturability [4] [23]. On the edge of the front cone holes provide wall-cooling for the first section of the combustion liner. The dimensions of the swirler and wall-cooling holes are chosen so that an equivalence ratio of 1.8 is obtained [23] [4].

After the front cone, the rich combustion starts. To reduce the temperature of the flame, which reduces NO_x emissions, a quenching zone is used in the RQL liners. This quenching zone reduces the equivalence ratio from $\phi = 1.8$ to $\phi = 0.6$. This rapidly cools down the flame lowering the NO_x production. After the quenching zone the mixture is further diluted by the lean combustion zone. Within the lean-zone the mixture is diluted to an equivalence ratio of $\phi = 0.3$.

The rich can has an identical front cone and swirler that generates a rich flame. Along the liner there are three section, primary combustion, secondary combustion and a mixing zone. The rich can offers stable behaviour with the disadvantage of a higher NO_x emission.



Figure 4.7: Axial hole swirler

In the centre of the axial swirler a fuel nozzle is placed which can be seen in Figure 4.11. Fuel nozzles provided by Hago and Danfoss are used which have a wide variety of cone angles, mass flows and flow patterns.

Table 4.1 shows the properties of the available fuel nozzles.



Figure 4.8: Insides of the pressure swirl atomizer used

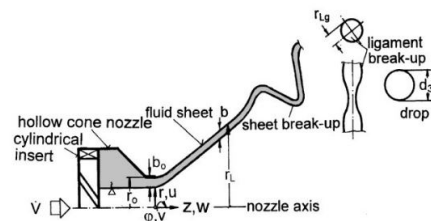


Figure 4.9: Schematic section view of the injector

Table 4.1: Nozzels and their properties

Nozzle, #	Flow (7 bar), LPH	Flow pattern	Cone angle [°]	Manufacturer
1	24	Full cone	80	Hago
2	19	Full cone	80	Hago
3	19	Hollow Cone	160	Hago
4	27	Hollow Cone	160	Hago



Figure 4.10: Fuel nozzle with its nozzle holder



Figure 4.11: Fuel nozzle mounted in the centre of the swirler

4.3 Recuperator

The requirements of the range-extender puts more focus on the outer dimensions than on overall efficiency. Therefore a compact recuperator design has been chosen to boost the efficiency with minimum added cost and volume. The recuperator is a 'wrap-around' design that is placed around the combustion chamber. This makes the recuperator small and relatively cost-effective. The initial recuperator design is a hollow space which the exhaust gas flows through. In a later stadium of the development guide/heat transfer fins can be added to increase the gas path length to boost the efficiency. The flow direction can be seen in Figure 4.2. The characteristics of the recuperator on the point of operation can be seen in Table 4.2.

Parameter	Value
η_{recup}	20 %
ΔT_{cold}	123 °C
ΔT_{hot}	94 °C

Table 4.2: Recuperator characteristics on the point of operation (105 kRPM)

The behaviour of the recuperator is not optimized yet. Within this project the rough shape and configuration is determined, further improvements can be made within future research.

4.4 Generator

A high-speed permanent magnet motor is used as a generator. This motor is built by e+a Elektromaschinen und Antriebe AG. The motor arrives as a separate rotor and stator. The stator consists of permanent magnets that create a two-pole field. A two pole stator has been chosen to lower the frequency, which is preferable when the generator would be used as a starter motor. The stator contains the coils that generate the electric power. Due relatively high losses and high power density, the generator should be water cooled. Table 4.3 and Figure 4.12 show the properties of the generator. More detailed specifications can be found in the Appendix.

Power	10 kW
Voltage	280 Vac
Frequency	1750 Hz
Current	22 A

Table 4.3: Generator properties

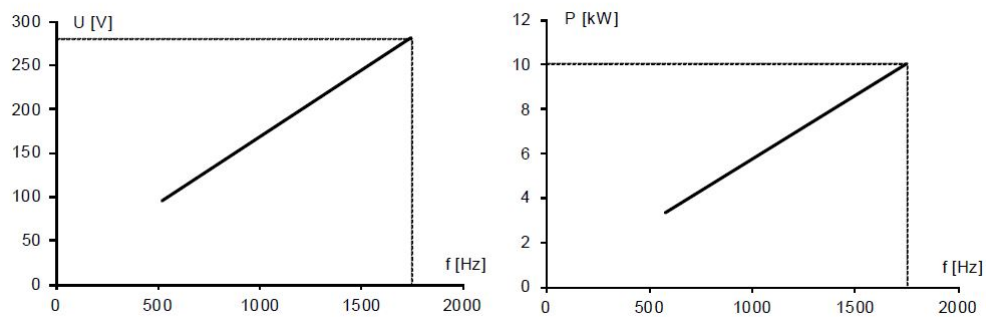


Figure 4.12: Voltage and power plotted against frequency

The generator is mounted on the compressor side. The generator stator and rotor are mounted inside the generator housing that can be seen in figure 4.13. To ensure that the generator can be easily removed it is mounted in front of the compressor. The shaft of the generator is coupled to the shaft of the turbocharger by a coupling-shaft. This coupling shaft replaces the standard compressor nut.

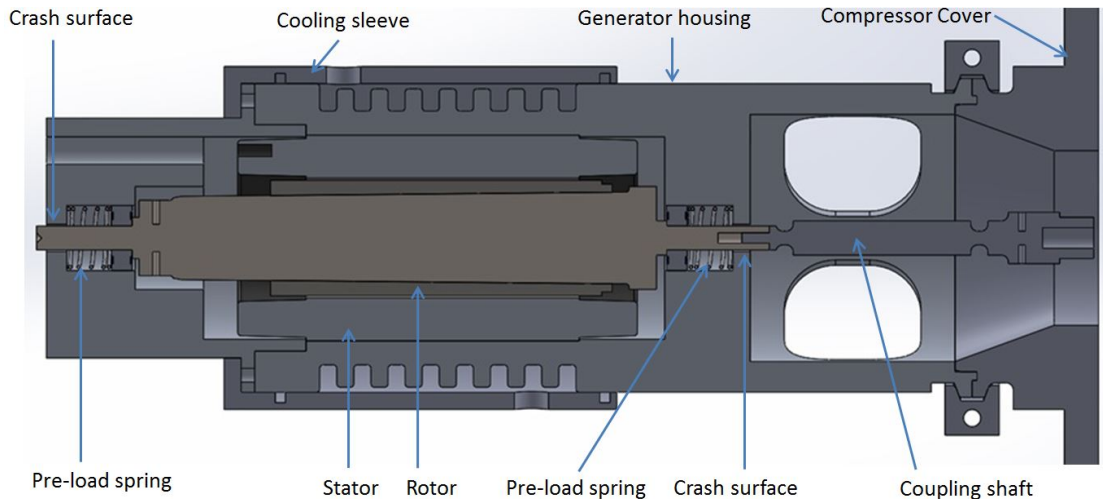


Figure 4.13: Generator section view

The coupling shaft has two indents making it compliant to compensate for small alignment errors. These indents also act as a break-away safety feature. If in any case the generator or turbocharger seizes, the coupling shaft will break.

The shaft of the generator houses the permanent magnet rotor that is press-fitted on a conical surface. While the turbocharger uses floating-ring bearings, the generator uses full complement hybrid angular contact bearings. These bearings are preloaded with two springs. These springs give the rotor the ability to move horizontally direction for short distances. This is needed to not over-define the axial-thrust bearing inside the turbocharger. Finally the shaft has two crash surfaces. In case of a bearing failure, the shaft crashes onto these surfaces while preserving a clearance between the rotor and stator. The bearings are lubricated with high-speed LGLT grease supplied by SKF.

The stator should be water-cooled as forced-air cooling would not be sufficient. The generator housing has cooling fins that are wrapped in an sleeve. Water flowing between the cooling fins and the sleeve cools the stator as well as the bearings.

An eigenfrequency analysis has been conducted in order to check the first bending mode of the rotor. A conventional turbocharger passes the rigid body modes during normal operation, however the bending modes should be avoided by creating a stiff enough shaft to lift the first bending mode above the operation range. In this case this is not possible as the compliant coupling should have a low stiffness. Luckily the gas turbine engine has a single point of operation with a constant RPM. The coupling shaft can be dimensioned in such a way that the operational RPM lies between the eigenfrequencies so that the eigenfrequencies are not excited during operation. During start-up the engine does cross these frequencies while accelerating, but because of the acceleration the duration of the excitation is minimized. The operational RPM of the engine is 105 kRPM which corresponds to 1750Hz. By altering the stiffness of the coupling shaft the bending modes are placed at 1496 Hz and 1912 Hz.

Table 4.4: My caption

Frequency Hz	corresponding RPM
237.47	14248
237.54	14252
1494.8	89688
1496.5	89790
1912.5	144750
3294.1	197646

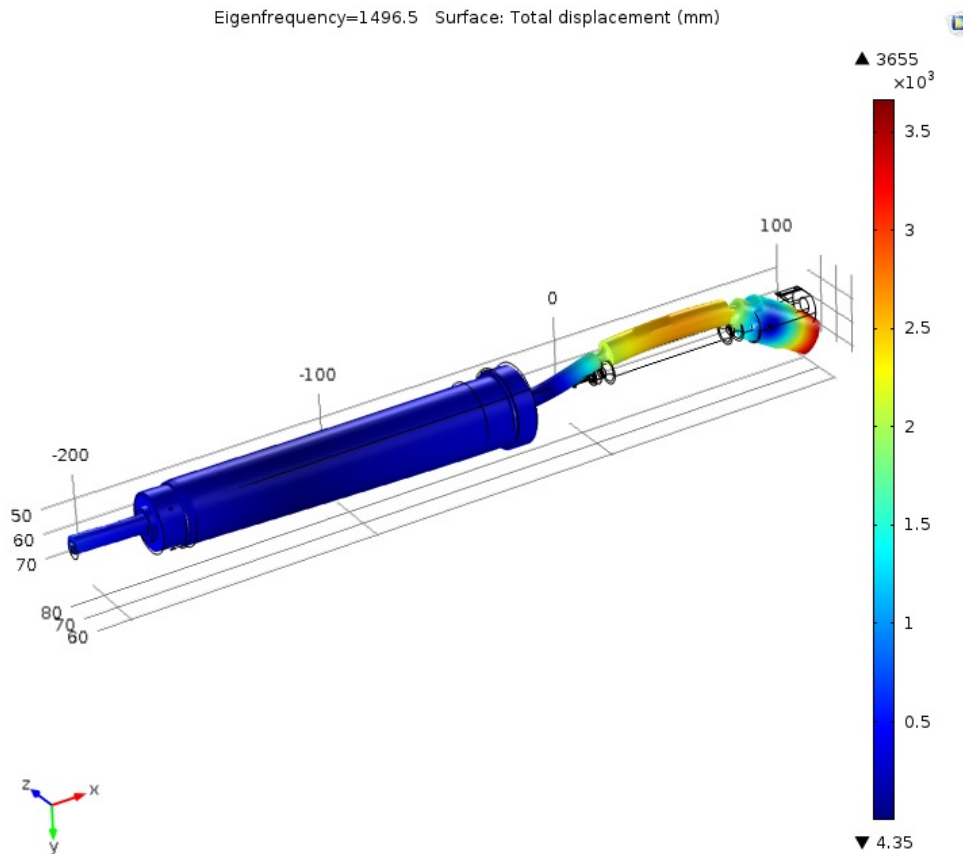


Figure 4.14: Bending mode of the generator and coupling shaft

As mentioned before, the generator uses angular contact ball bearings. The choice of bearings to use depends of the limiting-, reference-speed and the dynamic- and static-load rating, fatigue load limits are not taken into account for this prototype . The maximum allowable speed which the bearing can take is determined by the limiting speed or the reference speed. The limiting speed expresses the mechanical load on the rollers, races and lubricants. The reference speed only takes into account the thermal load on the bearing. Due to the construction of the generator the limiting-speed is typically lower than the reference-speed,

therefore the limiting-speed is the parameter used for selecting a bearing. The limiting-speed is closely related to the centripetal force caused by the rolling-elements, the limiting-speed can thus be increased by choosing a bearing with a smaller outer shoulder diameter¹ or by the reducing ball-weight. For the generator both measures are needed to increase the limiting speed above our operating speed. The ball-mass is reduced by using Si_3N_4 ceramic for the ball, the dimensions of the ball bearing are reduced to 8x22x7 mm. The exact specifications of the chosen bearing can be found in Appendix E.

¹Inner diameter of the outer race

Chapter 5

Test Set-up

5.1 Engine test-stand

The gas turbine engine is mounted on an engine pallet shown in Figure 5.1 & 5.2. The test set-up is made such that all auxiliary systems are mounted onto the pallet.

The engine is supported by three posts mounted on an engine pallet¹. The support of the turbine-housing is fully fixed meaning all degrees of freedom are restrained. The combustion chamber and the generator are both supported by a sliding support. These sliding supports will restrain only 4 degrees of freedom. This ensures that all parts can expand during heating and cooling without adding extra stresses on the engine parts.

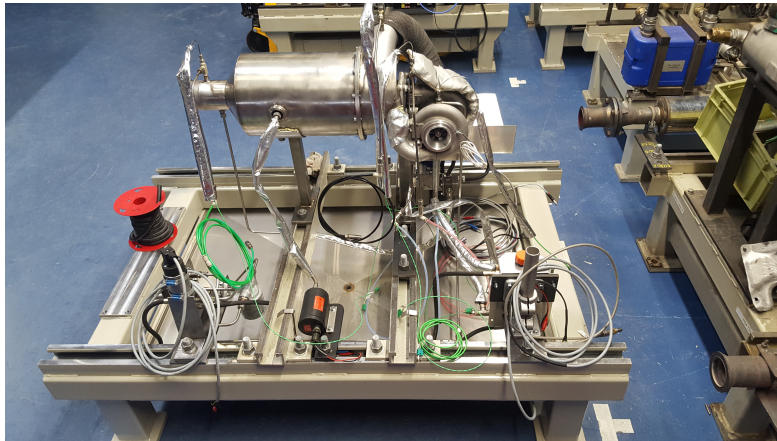


Figure 5.1: Engine mounted on engine-pallet

¹Standardized engine support frame used in engine test-cells

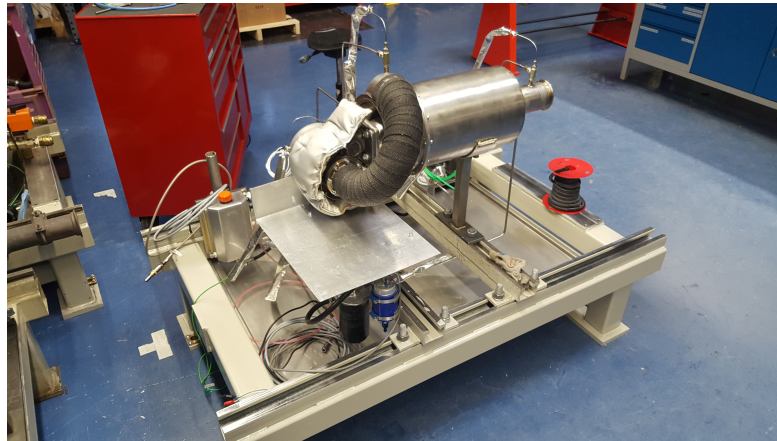


Figure 5.2: Engine mounted on engine-pallet

5.1.1 Oil circuit

The turbocharger has oil pressure-fed journal bearings. An oil system with pump, storage-tank, cooler, and filter is needed to supply the oil to the turbocharger. The oil-cooler is connected to the cooling system of the test-cell via a heat-exchanger.

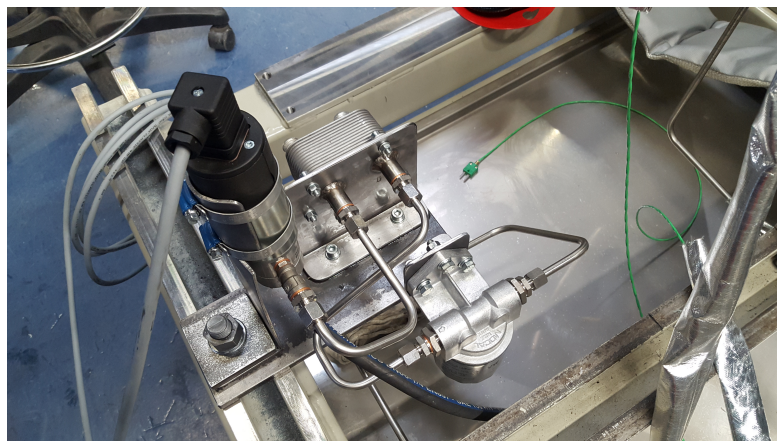


Figure 5.3: Oil pump, cooler and filter

5.1.2 Fuel-system

Three types of fuel can be used for the engine tests: diesel, 100% bio-ethanol and 90% bio-ethanol(10 % water). Diesel is supplied by the test-cell with a pressure of 5 bar. A Bosch 044 fuel pump that is capable of reaching a fuel pressure of 5 bar is used. Between the fuel nozzle and the fuel pump a fuel filter and a mass flow meter have been placed.

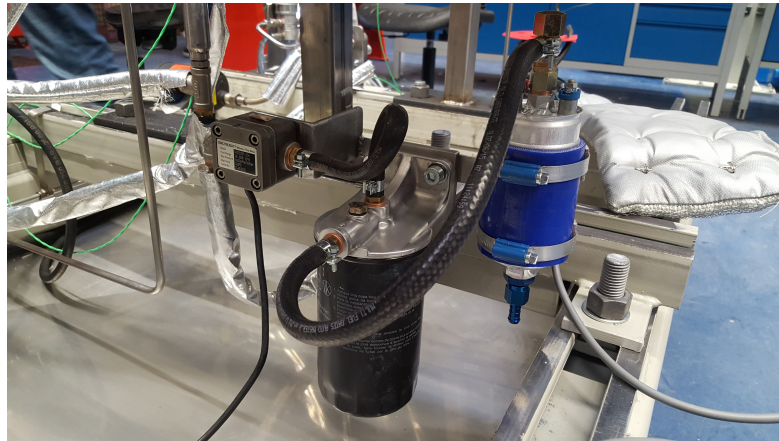


Figure 5.4: Fuel system including; pump, filter and mass flow sensor

The corrosive effects of bio-ethanol make it unsuitable for the existing fuel-supply system. Therefore a separate fuel-tank containing bio-ethanol is placed on the engine-pallet.

5.1.3 Sensor layout

Measurements are carried out by different sensors placed at the point specified in Figure 5.5. The total temperature measurements are conducted using K-type thermocouples. The thermocouples are placed directly in the flow at 1/3 of the tubes diameter to get the most accurate reading. The static pressure is measured at the same spot as the temperature using the sensor mountings that can be seen in Figure 5.6. Due to the lack of room it was not feasible to install multiple thermocouples or dynamic pressure measurements.

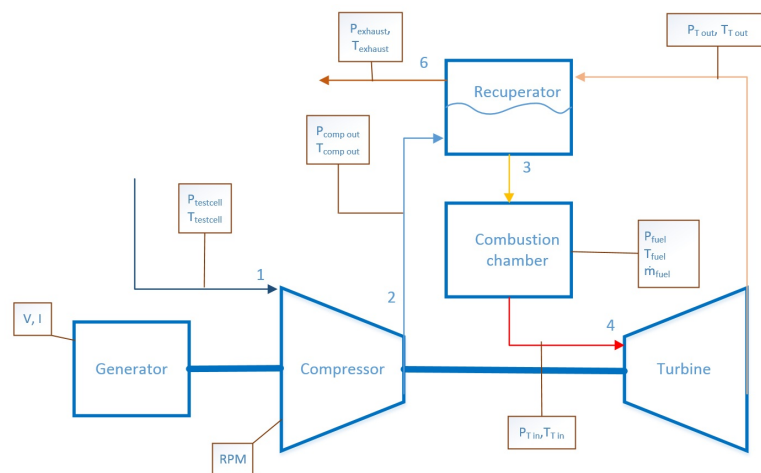


Figure 5.5: Sensor layout

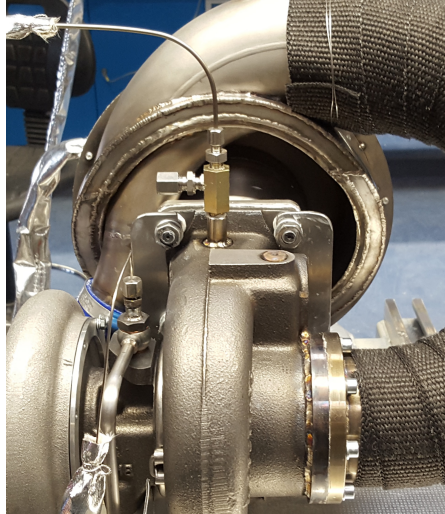


Figure 5.6: Thermocouple and static pressure connections on the turbine inlet

5.2 Preliminary test

5.2.1 Vaporizing nozzle test

The amount of fuel supplied by the fuel nozzle is controlled by pressure. At low pressures the fuel nozzle does not generate a proper spray. For this reason the minimum fuel flow needs to be determined. This is done using a stationary test where the fuel pressure is increased till the nozzle begins to spray. The minimum fuel setting needed for decent spray behaviour appeared to be 25% of the maximum fuel flow(Fig. 5.7). The flow pattern and cone angle remain constant beyond this point which can be seen in Figure 5.8.

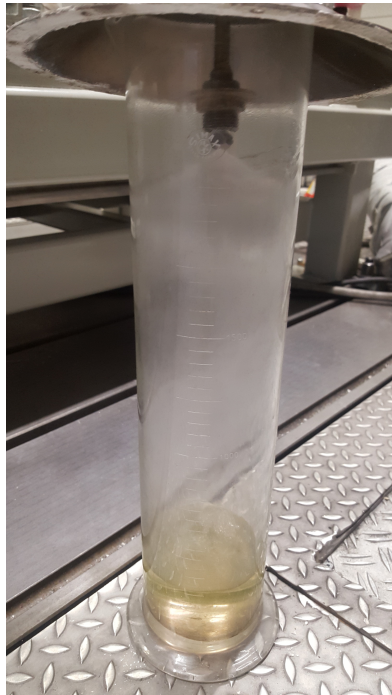


Figure 5.7: Fuel nozzle spraying bio-ethanol at 25% throttle



Figure 5.8: Fuel nozzle spraying bio-ethanol at 75% throttle

5.3 Engine test

5.3.1 Testing goals

The goals of the engine tests are defined as follows;

1. Start up & Stabilise

The engine should be started and run at a constant RPM. Instabilities in the combustion chamber could cause RPM fluctuations. By optimizing the combustion chamber design these instabilities should be reduced.

2. Power measurements

The gas turbine should drive the generator that can be loaded using an electrical DC-load. By varying the electrical load, the mechanical load on the gas turbine engine can be controlled. The engine should be able to reach an electrical power output of 10kW_e

Chapter 6

Test Results

6.1 Stability tests

Before and during the start-up tests the effects of using different nozzles were observed. Table 4.1 shows the nozzles that are being tested. Nozzle #1 and #2 are full cone nozzles while #3 and #4 are hollow cone nozzles. Besides the difference in spray pattern, both types of nozzles have different spray patterns. Nozzle #1 and #2 have a hollow cone spray pattern while #3 and #4 offer a full cone spray pattern. When a small cone angle is used (nozzle #1 and #2) the flame narrows but increases in length. Due to placement of the spark ignitor, the small cone is more difficult to ignite as the fuel is sprayed past the cone. To resolve this issue a lower ignition speed needs to be used. A wide cone ignites more easily as it sprays in front of the spark ignitor. The disadvantage of a wide cone spray is that a wider and shorter flame is more sensitive to instabilities.

The spray pattern has a large influence on stabilities and emissions. The hollow cone nozzle sprays more fuel on the circumference of the cone where the air velocity is higher due to the axial swirler. A hollow cone generates a more constant equivalence ratio which prevents temperature peaks, and thus lowering NO_x emissions.

The fuel flow is controlled by the fuel pressure. A smaller nozzle needs a higher pressure to achieve an equal fuel flow. Therefore a smaller nozzle suffers less from pressure fluctuations within the combustion chamber. The mechanism creating this instability is shown in Figure 6.3.

6.1.1 Rich can

The first start-up tests were conducted using the rich can with nozzle #3. The first start-up was not successful due to large combustion instabilities.

From the discolouration (see Table 6.1) of the combustion liner the position and length of the flame can be derived. Figure 6.1 and 6.2 show the discolouration patterns of the combustion liner. The liner clearly shows that the flame starts after the first row of holes, this means that the primary combustion section is not functioning as it should.



Figure 6.1: Discolouration pattern on the rich can

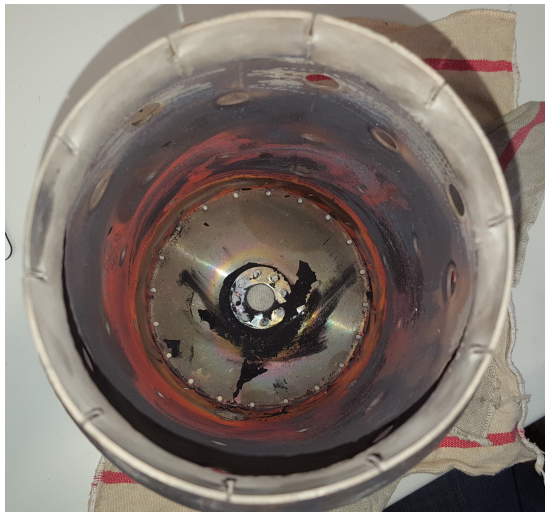


Figure 6.2: Inside of the rich can

Colour	Temperature [°C]
Pale yellow	290
Straw yellow	340
Dark yellow	370
Brown	390
Dark purple	450
Blue	540
Dark blue	600
Carbide separation	680
Light red	750
Dark Red	830

Table 6.1: Tempering colours for 304 stainless steel [6]

Apart from the late combustion the flame is too short. It is likely that this is caused by incomplete combustion due to large instabilities as the fuel flow was relatively high.

The combustion instabilities have two major causes. The first cause is the relatively low fuel pressure. The fuel flow is dependent on the pressure difference over the nozzle and dependant on the combustion liner pressure. When the combustion chamber pressure fluctuates the fuel flow becomes lower due to a lower fuel nozzle pressure. This makes the engine lower its rotation speed, which lowers the combustion chamber pressure. A lower combustion chamber pressure increases the fuel nozzle pressure which increases the fuel flow. This loop makes, as can be seen in Figure 6.3, makes the engine unstable. At a point the fluctua-

tions had a sufficient magnitude to turn the combustion chamber on and off which thermo-shocked the turbine wheel.

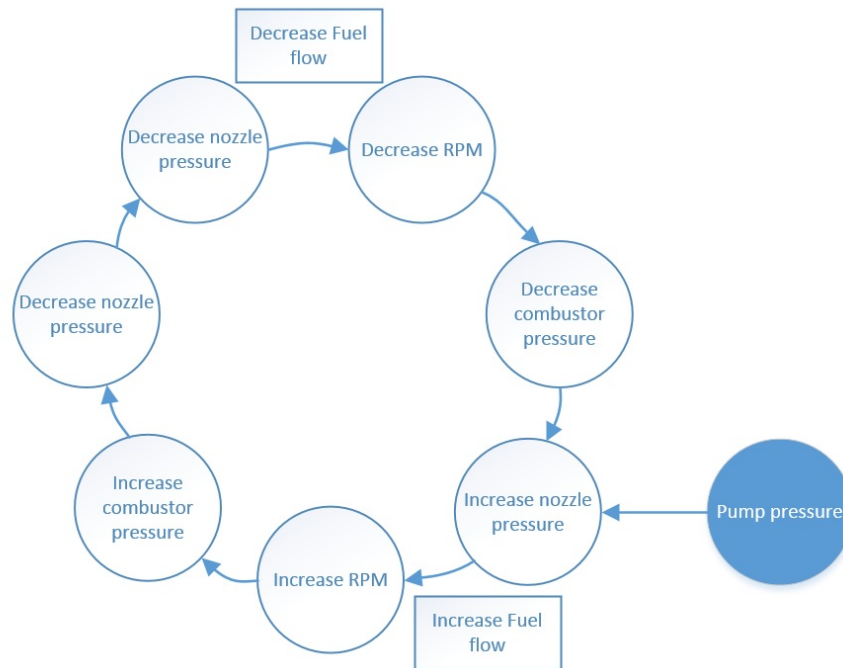


Figure 6.3: Instability mechanism causing a fluctuating RPM

These instabilities can be reduced when a higher fuel pressure is used. With a higher fuel pressure, the fluctuation of the combustion chamber pressure has much less effect on the nozzle pressure.

Another cause of the instabilities is that the fuel is not combusting behind the front cone. The front cone causes a toroidal vortex that stabilises the flame. This instability can be resolved by moving the flame more in front of the combustion liner. The position of the flame is determined by the hole-pattern. The area of all holes combined is relatively small, as shown in Figure 6.1. Due to the small hole area, the pressure drop is relatively high which causes higher air velocity in the holes. This velocity can become high enough to form 'jets' that can partially or fully extinguish the flame. The air velocity can be lowered by making the holes bigger or by drilling extra holes.

6.1.1.1 Modifications

In order to stabilise the flame an extra fuel pump is added which is placed in series with the existing pump. When the dual fuel pump set-up is used, a maximum fuel pressure of 15 bar can be achieved. The nozzle pressure fluctuations dropped from 25% to 6.7%. The high pressure fuel system supplies a more stable fuel flow to the combustion chamber.

To move the flame more towards the front of the combustion liner, the hole pattern has been adjusted. Extra holes have been drilled within the secondary zone as well as the mixing zone. To enhance mixing and stability in the primary combustion zone the holes have been bent into a swirler.

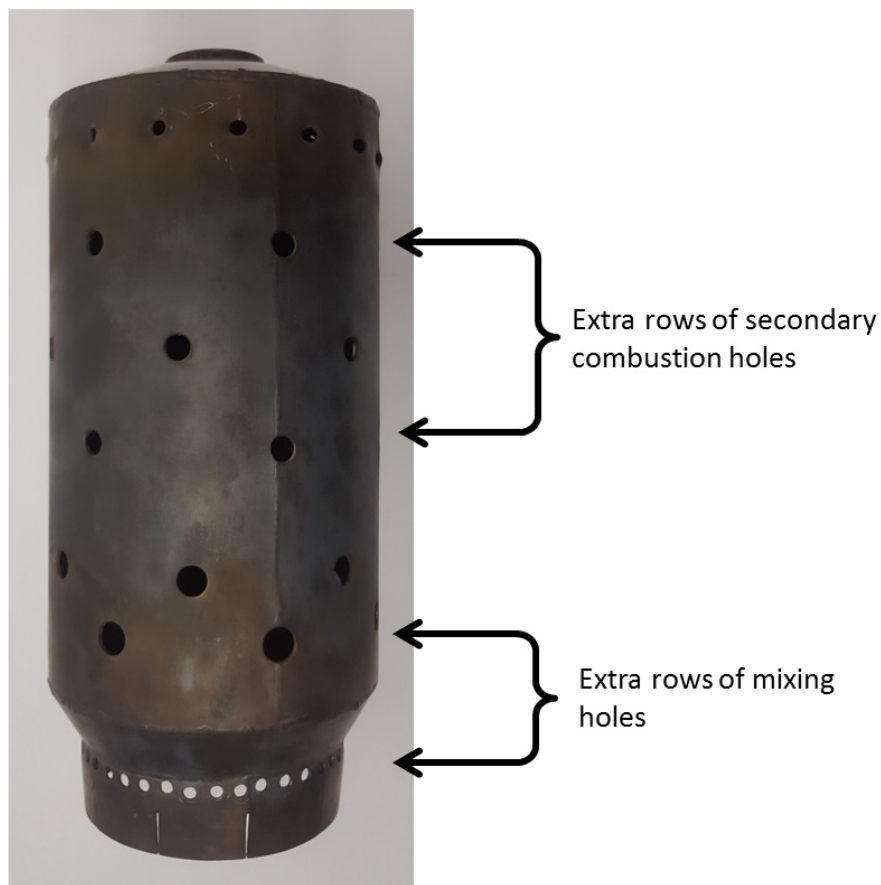


Figure 6.4: Modified rich liner, with modified secondary and mixing zone

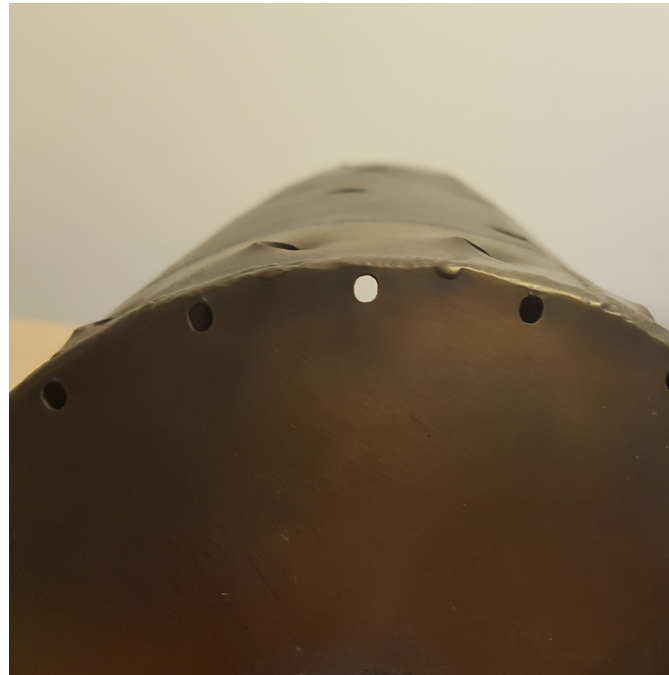


Figure 6.5: Modified primary combustion zone holes, tilted to enforce the swirl

The modifications described above increased the swirl number and stabilised the combustion process which made the engine run self-sustained.

6.1.2 RQL can

The stepped RQL liner is tested using nozzle #3. When the discolouration pattern on the outside of the liner is examined, it becomes clear that the principle of Rich-Quench-Lean is effective. A soot build-up on the front cone and around the swirler indicates that the flame is indeed burning rich in the first section. This section stayed relatively cool but became hotter once it entered the quench section due to the extra oxygen supplied by the holes. When the equivalence ratio drops the temperature increases at around $\phi = 1$, after this point the temperature drops again. The Quench section cooled the flame which initiated the lean combustion. The lean combustion zone heats up again, which is to be expected. The combustion process is finished at the last row of holes. These holes provide mixing air which cools the liner.



Figure 6.6: Discolouration pattern on the RQL liner



Figure 6.7: Inside of the RQL liner

Figure 6.7 shows the discolouration of the inside of the RQL liner. The discolouration is not symmetric, meaning the flame is not centred in the liner. This is caused by a swirling effect of the inlet air. Due to the design of the inflow of compressed air into the recuperator, the air becomes axially swirled. This swirl is dampened by the bends it takes when entering the combustion chamber, yet the swirl is not eliminated. Figure 6.8 shows the swirling motion of the air flowing around the combustion liner imprinted on the wall. This swirl creates an uneven velocity (and thus pressure) distribution which can 'push' the flame towards the wall of the combustion liner. This causes a hot-spot from 2 to 6 o'clock.

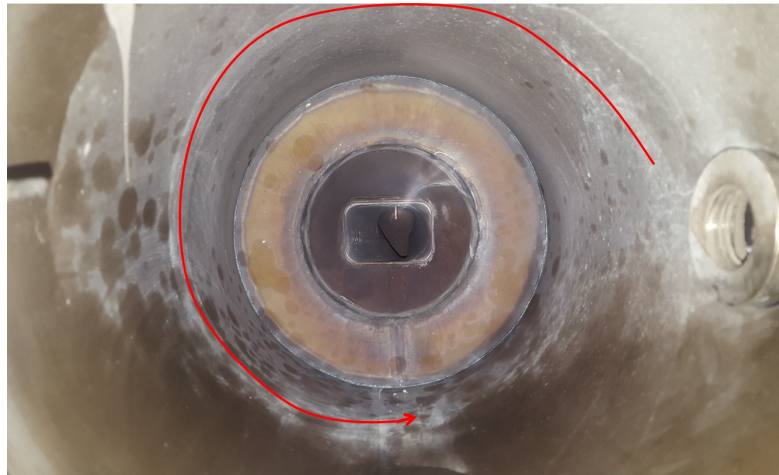


Figure 6.8: Inside the combustion chamber the flow of the inlet-swirl can be seen

6.1.3 SRQL can

The SRQL can is tested using nozzle #3 as this nozzle gave the best results. The discolouration on the inside of the combustion liner shows that the flame length and position are in accordance with the simulation conducted using Fluent. The initial combustion is rich which can be seen from the soot build up on the front cone. As expected the lean combustion is not clearly visible when the discolouration pattern is examined. This is caused by the lack of mixing. The air flowing through the lean combustion zone holes acts more as wall-cooling. The core of the flame is therefore not well mixed and remains at relatively high temperatures, which is confirmed by the TIT measurement.

Figure 6.10 shows a similar asymmetry as the RQL liner, this is likely to be caused by a swirling inlet flow which can be seen in Figure 6.8. The general behaviour of both the RQL and the SRQL liner is according to expectations, based on the results of the Fluent combustion simulation.



Figure 6.9: Discolouration pattern on the RQL liner

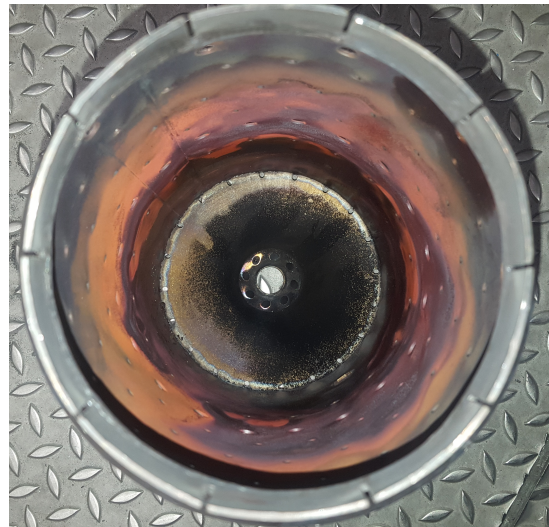


Figure 6.10: Inside of the SRQL liner

When Figure 6.11 is compared to Figure 6.7 the difference in quenching effectiveness becomes clear. The RQL rapidly cools down the flame where the SRQL liner needs several cm's for a comparable effect.

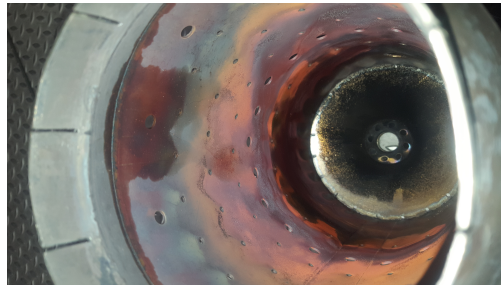


Figure 6.11: Inside of SRQL liner

6.1.4 Fuel nozzles

Each liner has been tested with nozzle #1, #2, #3, #4, #7 and #8. The flow of each nozzle has an impact on the fuel pressure that needs to be used. A higher fuel pressure is beneficial on the stability of the fuel flow and thus on the stability of the combustion chamber. The angle of cone influences the width and length of the flame. A larger cone angle generates a wider and shorter flame which lowers the TIT. However a wide cone fuel nozzle was prone to combustion instabilities. The effect of these increased instabilities can be reduced by altering the hole pattern of the liner. Small cone fuel nozzles are more stable but their narrow and long flames travel much further into the liner which increases the TIT. The hollow cone fuel nozzle generates a low velocity area in the centre of the liner. This low velocity area stabilises the flame as the axial swirler swirls air around it. A full cone lacks this low velocity area and is thus more sensitive for instabilities.

Parameter	Characteristic
Low flow	Higher fuel pressure needed, less instabilities
High Flow	Lower fuel pressure, more instabilities
Large cone	Improved ignition behaviour, shorter flame that lowers TIT, can cause instabilities
Small cone	Impairs ignition behaviour, Longer flame which increases TIT, Stabilises the combustor

Table 6.2: The influence of the nozzle parameters on the behaviour of the combustion chamber

6.1.5 Generator test

Once combustion instabilities are removed the generator can be attached. When the cartridge is removed, the generator can be mounted on the compressor cover.

During the first start-up with the generator connected, a bearing pre-load spring shot into the bearing itself. This happened when the generator was running at 70 kRPM which caused

the generator to seize. The seizing bearings made the coupling shaft break away, separating the running turbocharger from the (seized) generator. Besides the damaged coupling-shaft, the bearing failed which made the generator crash into its cash-surfaces. This impact caused the generator shaft to bend beyond repair.

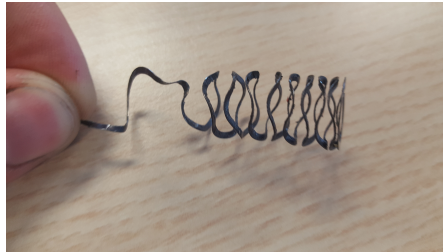


Figure 6.12: Pre-load spring which went into the bearing

Figure 6.12 shows the damaged spring which shot into the bearing. On the left side of the spring indentations can be seen which are caused by the ceramic balls from the bearing. The inertia of the ceramic balls is relatively low so this damage cannot have been caused by flying debris. This damage can only occur when the spring is pulled through the bearing when it is running at high speed.

6.2 Measurements

6.2.1 Engine behaviour

Measurement data were gathered using the available data-acquisition equipment from the test-cells. The data is sampled using a sampling frequency of 10Hz. This is sufficient for extracting low frequency instabilities. The gathered data were processed using Matlab in order to compare them with the results derived from modelling. The following table shows the boundary conditions used for the testing.

Parameter	Setting
Liners	RQL, SRQL and Rich
Fuel nozzle	# 3
Fuel pressure	8-12 bar
RPM	80 kRPM
Fuel	100% and 90% bio-ethanol
Generator	0 kWe, detached
TIT max.	850°C

Table 6.3: Settings used during testing

In order to compare the results of each liner all tests were conducted using nozzle #3. The engine was run at an RPM of 80.000 as this is a stable self-sustaining RPM when no generator is attached. When a higher RPM is chosen, the engine has the tendency to accelerate due

to the unbalance in the power output/consumption. Each liner was tested using 100% bio-ethanol and 90% bio-ethanol(10% water).

Figure 6.13 shows the rotational velocity of the engine, within the plot the mean value is represented by a red line. It can clearly be seen that the RPM fluctuates, which indicates that an instability is present. The instability is most noticeable when the RQL and SRQL are run on 90% bio-ethanol.

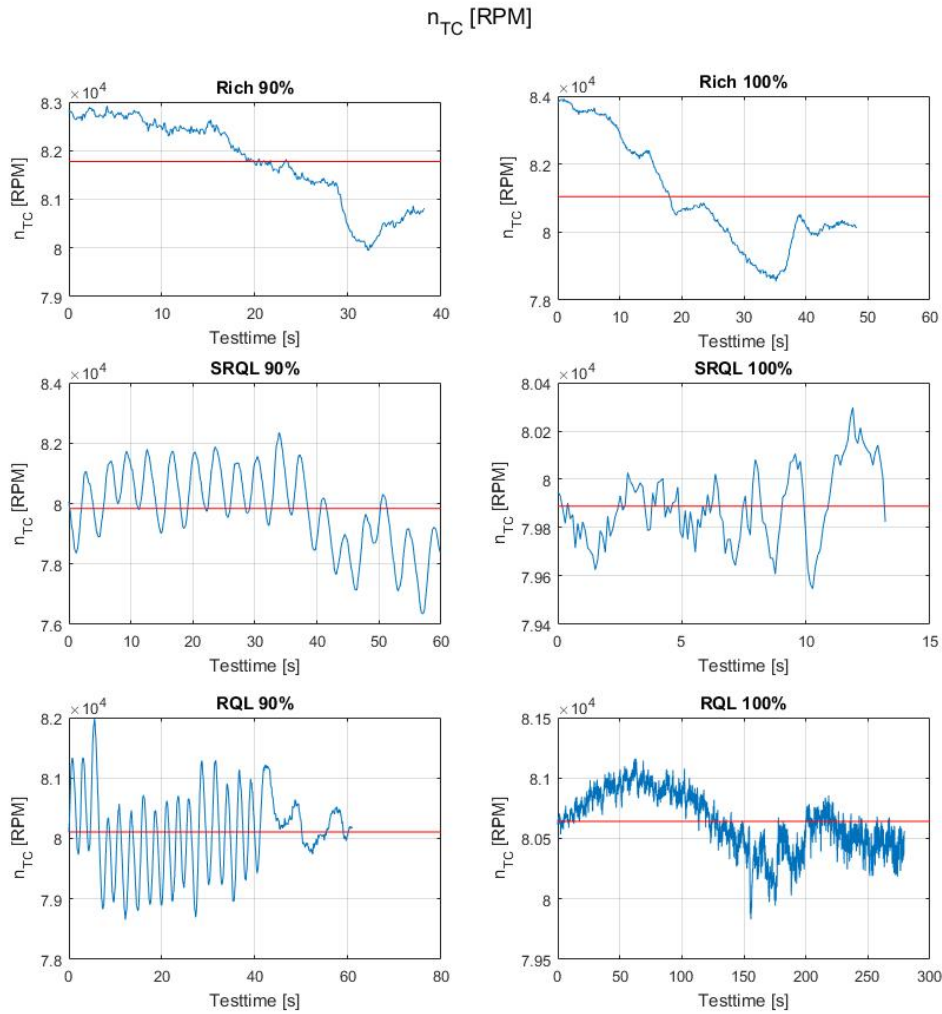


Figure 6.13: RPM of the engine with different fuels and liners

Figure 6.14 shows the turbine inlet temperature of each test. The fluctuations that are visible in the RPM plots are also visible in the TIT. When the mean values of the TIT from the RQL and SRQL liner are investigated it becomes clear that increasing the water content of the

fuel lowers the TIT. This is caused by the increased mass flow through the turbine and the cooling effect of the evaporating water.

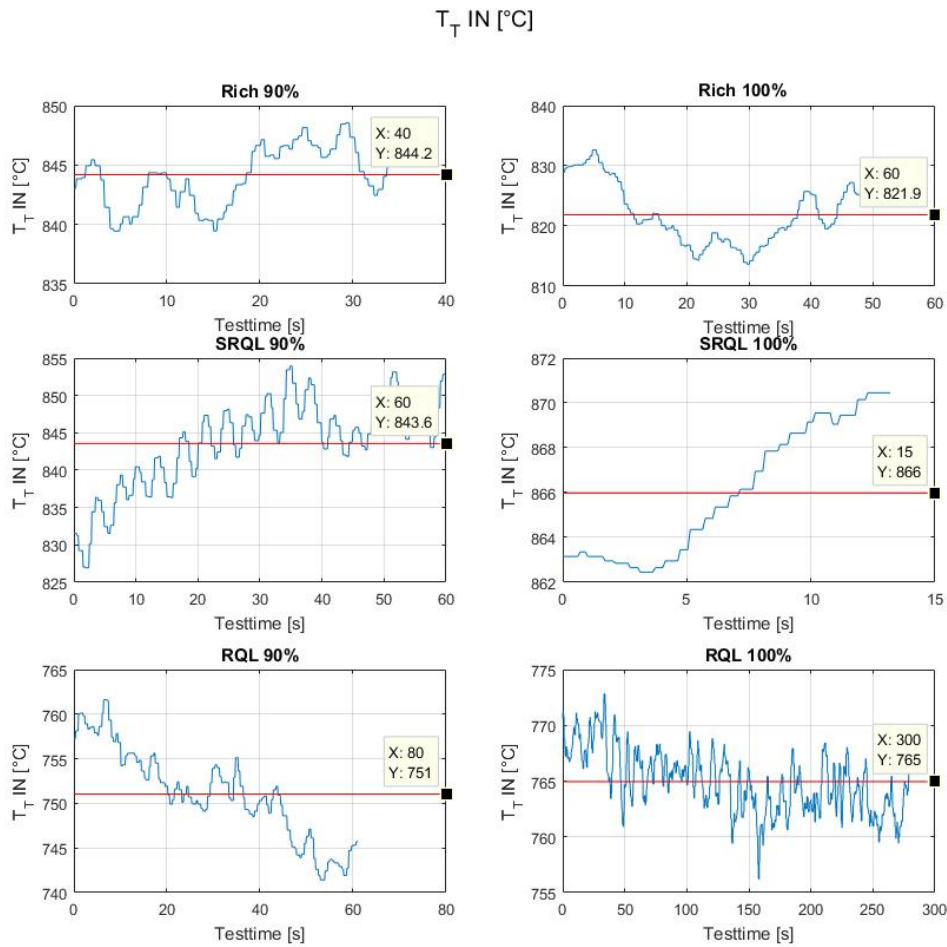


Figure 6.14: RPM of the engine with different fuels and liners

There is a significant difference in average TIT between the liner types. The TIT caused by the RQL liner is lower than the SRQL and the rich liner. This indicates that the quenching effect of the quenching zone is effective. The TIT caused by the SRQL combustion chamber is similar to the rich TIT. This means that the SRQL quenching zone is not effective. The shape of the SRQL flame is probably comparable to the flame within the rich can, which would mean that the flame remains rich along the combustion chamber.

Figure 6.15 shows the fuel consumption of the engine. The signal of the fuel flow sensor shows the same instabilities as the RPM measurement. Besides the occurring instabilities, the signal is also affected by interference caused by the PWM-signal driving the fuelpumps. The small differences in fuel consumption between 100% and 90% are likely to be affected by noise. A

clear conclusion of the effect of adding water to the fuel cannot be drawn. However between the liners, a large difference in fuel consumption is present. This is mainly caused by the combustion efficiency of each liner. It appears that the Rich and SRQL have relatively high combustion efficiency. When the RQL combustor is used the fuel consumption increases which is likely to be caused by the quenching section. The quenching section within the RQL liner provides a much stronger quenching behaviour than the SRQL quenching zone. Probably the RQL quenching zone causes partial blow-off of the flame.

Fuel flow [LPH]

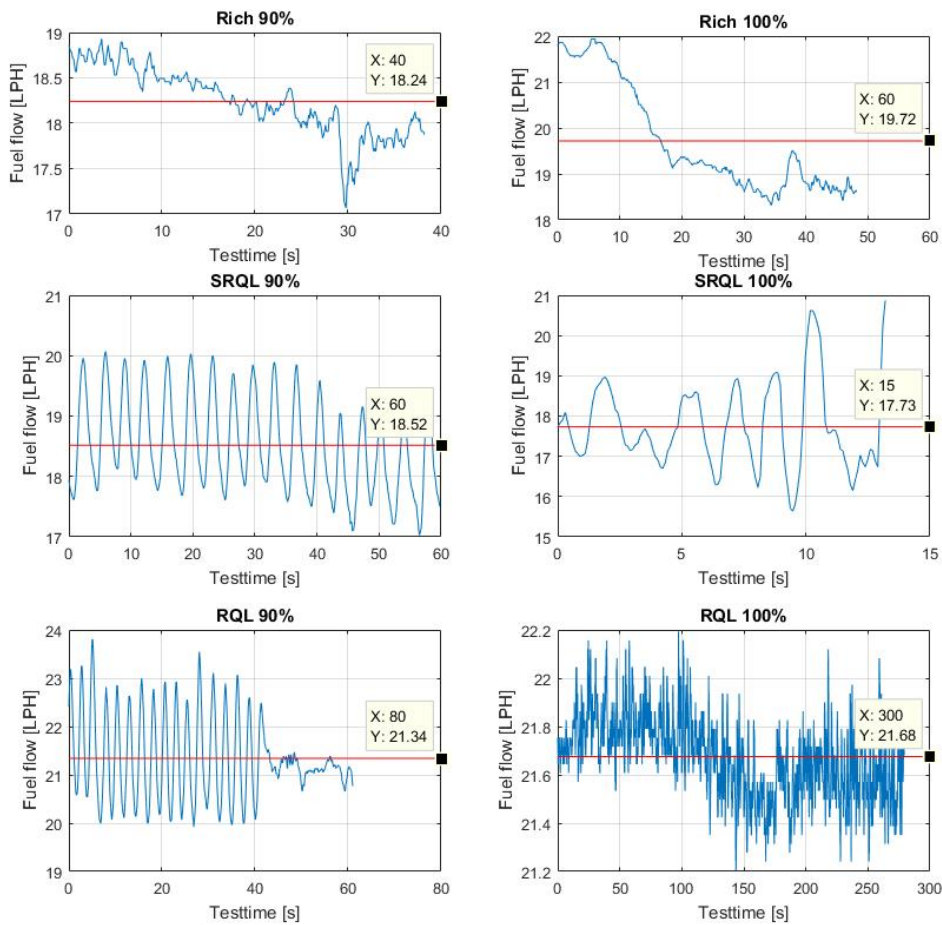


Figure 6.15: Fuel consumption of the engine with different fuels and liners

Figure 6.16 shows the static compressor discharge pressure in Pascal. In almost all cases the compressor discharge pressure is around 540 Pascal, which is to be expected. The small deviations in compressor discharge pressure are likely to be caused a small difference in RPM.

The compressor operates at a point where a small fluctuation in RPM or flow has a large impact on the pressure build up. The exact values of the compressor discharge pressure and RPM can be seen in Table 6.4.

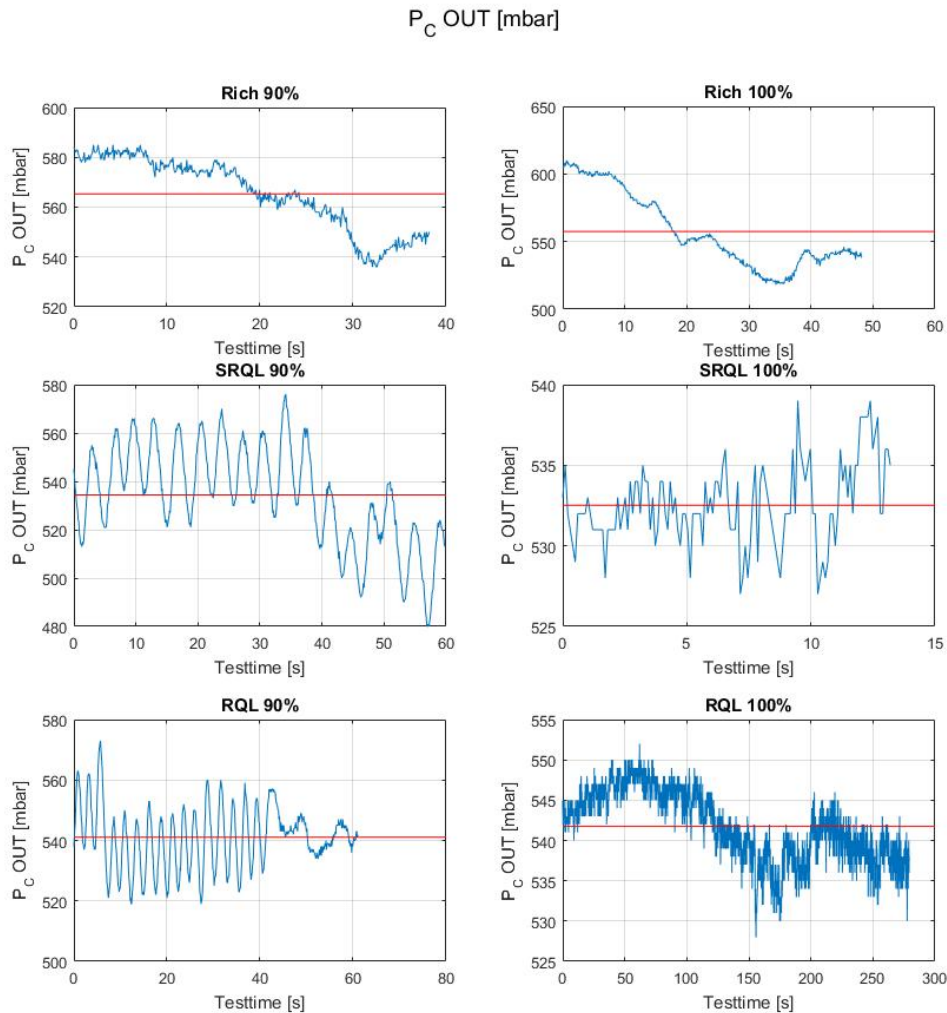


Figure 6.16: Compressor discharge pressure

Figure 6.17 shows the pressure drop in percentage of the inlet manifold, recuperator and combustion chamber. Both the RQL and SRQ have a pressure drop of around 19. %. The rich combustion chamber has a pressure loss of approximately 18.5%. The rich combustion liner has a much more 'open' construction while the difference in pressure loss is small. We can conclude from this that the pressure loss over the inlet manifold and recuperator are much larger than the pressure drop over the combustion liner.

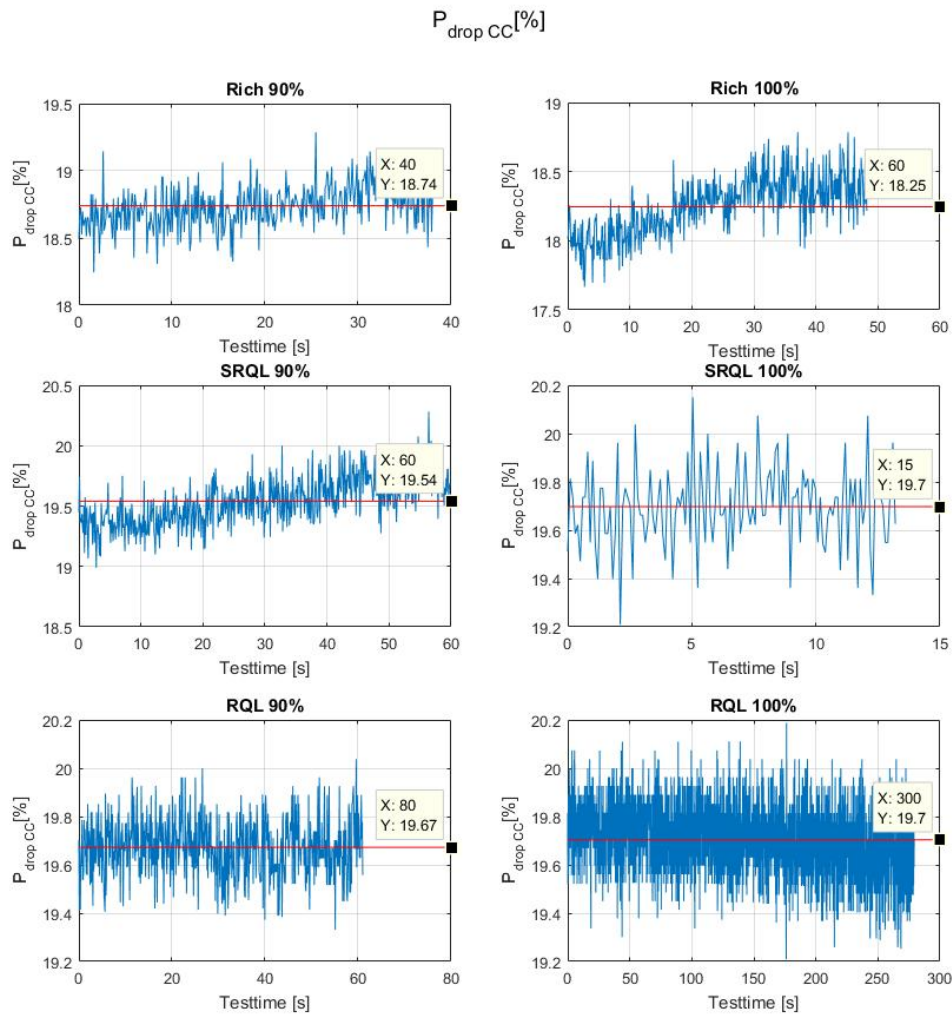


Figure 6.17: Pressure drop between compressor discharge and turbine inlet

An important parameter for the complete system is the corrected turbine RPM. Figure 6.18 shows the burner power ¹ plotted against the corrected turbine RPM. The corrected turbine RPM is defined as:

$$RPM_{corrected} = \frac{RPM}{\sqrt{TIT}} \quad (6.1)$$

All data points of a test form an area, each liner has a specific area colour. Through the area a trend line is drawn. The colour of the trend line represents type of fuel used. Figure 6.18 shows that each specific fuel has a different energy input for its corrected RPM. When the figure is studied, it appears that when diesel is used as a fuel a larger energy input is required.

¹Energy input of the combustion chamber

When 100% bio-ethanol is used, the required energy input is reduced. The energy input is even further reduced when 90% bio-ethanol is used. This phenomenon is caused by the difference in net. caloric value of the fuel, which impacts the turbine inlet mass flow. Another factor is the possible change in combustion efficiency for each specific type of fuel.

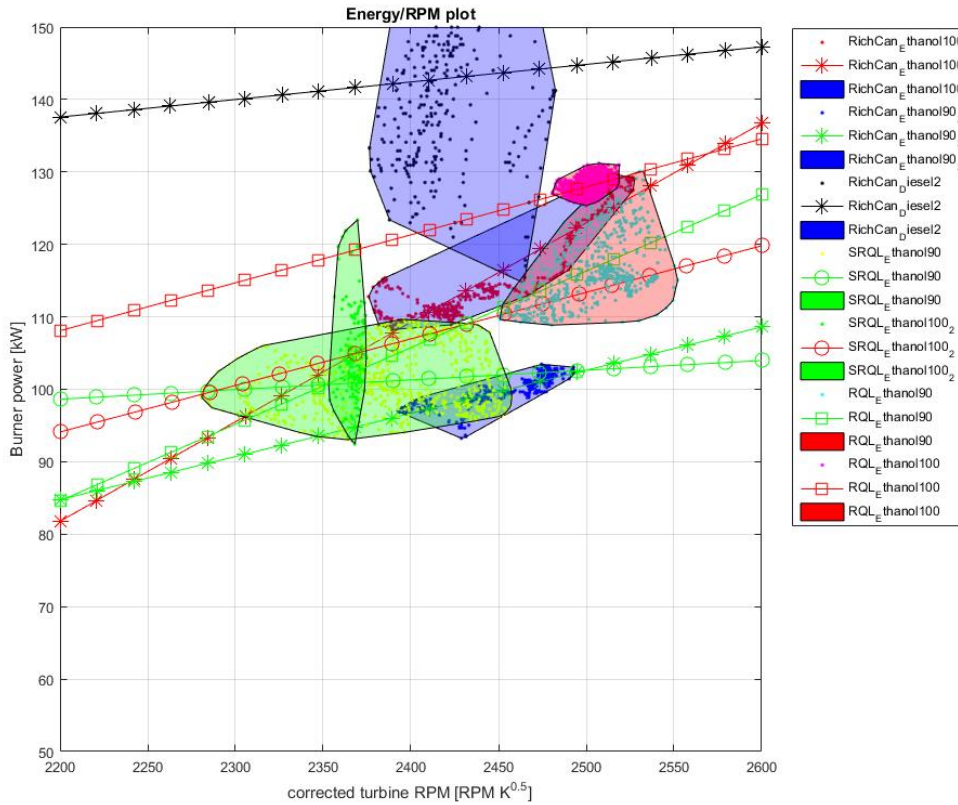


Figure 6.18: Burner capacity plotted against the corrected turbine RPM

The magnitude of the instabilities of the combustion chamber can be quantified using a Fourier transform. Figure 6.19 show the test results in the frequency domain. The instabilities are only present when 90% bio-ethanol is used. The RQL 90% test shows a peak at around 0.4 Hz which is not present when 100% bio-ethanol is used. The instabilities have the highest magnitude when the SRQL liner is used with 90% bio-ethanol. Besides the instabilities in both the RQL and SRQL the rich can also shows a small instability of around 0.35 Hz.

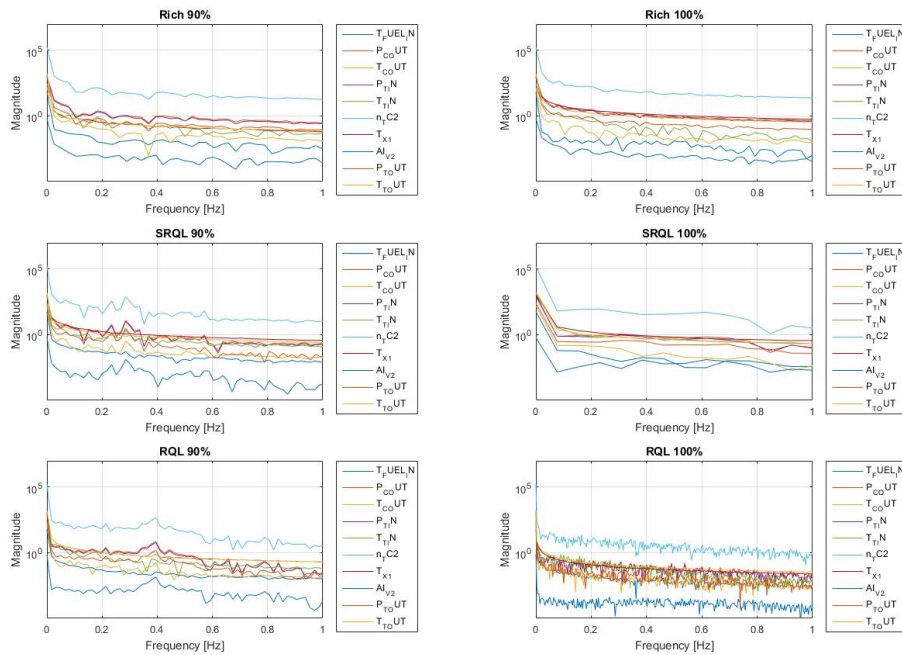


Figure 6.19: Fourier analysis of tests

Table 6.4 shows all averaged parameter values of each test.

Parameter	Rich 90%	Rich 100%	SRQL 90%	SRQL 100%	RQL 90%	RQL 100%
Test time [s]	1901	1299	87046	85091	95586	98535
$T_{fuel_{in}}$ [°C]	31,94	32,99	26,96	28,02	26,52	30,38
$P_{comp_{out}}$ [mbar]	566	547	534	531	541	541
$T_{comp_{out}}$ [°C]	82,8	83,1	77,6	79,5	77,2	82,1
$P_{turb_{in}}$ [mbar]	460	442	430	427	434	434
$T_{turb_{in}}$ [°C]	844	846	842	865	751	764
η_{TC} [RPM]	81835	80961	79846	79874	80108	80640
Fuel flow [LPH]	18,24	19,72	18,52	17,73	21,34	21,68
$P_{turb_{out}}$ [mbar]	144	136	123	123	126	134
$T_{exhaust}$ [°C]	626,2	624,0	523,3	544,9	544,4	608,2
$P_{drop_{CC}}$ [%]	18,7	19,0	19,5	19,7	19,7	19,7

Table 6.4: Averaged values of each measured parameter

From the measured values a power balance can be computed, which can be seen in Table 6.5. The power consumed and generated by the compressor and turbine is what can be expected. The energy added by the fuel is computed by using the measured fuel flow and its heating value, therefore the combustion efficiency is not taken into account. The energy added by the fuel shows large deviations, this is likely to be caused by changes in combus-

tion efficiency. The heat exchanged in the recuperator shows large increases during both the SRQL test and the RQL 100% test. The cause of this increase in exchanged heat is yet unclear and should be studied in future research.

Parameter	Rich 90%	Rich 100%	SRQL 90%	SRQL 100%	RQL 90%	RQL 100%
W_{comp} [kW]	10.2	10.0	9.89	9.86	9.98	9.97
W_{turb} [kW]	-11.6	-11.2	-10.9	-11.0	-10.1	-10.2
E_{fuel} [kW]	91.2	109.6	92.6	98.5	106.7	120.4
$Q_{\text{recuperator}}$ [kW]	22.8	23.8	39.5	39.5	22.4	24.4

Table 6.5: Calculated power balance of the averaged measured values

6.2.2 Recuperator behaviour

To study the behaviour of the recuperator, a test is conducted using the following parameters.

Parameter	Setting
Liners	RQL
Fuel nozzle	# 3
Fuel pressure	8-12 bar
RPM	80 kRPM
Fuel	100%
Generator	0 kWe, detached
TIT max.	850°C

Table 6.6: Settings used during testing

The compressor discharge temperature is increased by the recuperator. The combustion inlet temperature is hard to measure with a thermocouple as this sensor should penetrate several stainless steel shells. However the temperature can be calculated by computing the temperature difference of the hot-side of the recuperator. Unfortunately the turbine discharge temperature measurement is inaccurate and cannot be used for this calculation. Instead the turbine discharge temperature can be computed using the power balance and the turbine's efficiency. Using equation 3.14 the turbine discharge temperature is 688°C. Because the outer shell of the recuperator is insulated, the heatloss to the outside world can be neglected. The enthalpy loss on the hot-side of the recuperator is transferred to the cold-side. This means that the combustor inlet temperature is around 170°C, which would mean that the recuperator efficiency is 16,5% when equation 3.13 is applied. The pressure drop over the hot- and cold-side is higher than anticipated as the swirl of both flows was stronger than initially expected.

Table 6.7 shows the values of all parameters measured during the recuperator test.

While the recuperator extracts heat from the exhaust and increases the combustor inlet temperature, it also generates a pressure drop. The pressure drop lowers the expansion ratio of the turbine which negatively impacts the overall efficiency. The results of the pressure drop

Parameter	RQL 100%
Test time [s]	5279
$T_{fuel_{in}}$ [°C]	34,32
$P_{comp_{out}}$ [mbar]	538
$T_{comp_{out}}$ [°C]	75,2
$P_{turb_{in}}$ [mbar]	438
$T_{turb_{in}}$ [°C]	755
η_{TC} [RPM]	80350
Fuel flow [LPH]	21,82
$P_{turb_{out}}$ [mbar]	138
$T_{exhaust}$ [°C]	610,5
$P_{drop_{CC}}$ [%]	19,3
η_{recup} [%]	16,5

Table 6.7: Averaged values of recuperator test

and thermal effectiveness of the recuperator can be studied in order to check if the recuperator has a positive effect on the overall engine efficiency. This study is conducted by using the Matlab cycle model, initially the fuel consumption is computed using the measured pressure drop and recuperator efficiency. Second, the same calculation is conducted without using the recuperator effect. Both resulting fuel consumptions are compared in table 6.8. For the current test set-up the losses caused by the pressure drop are larger than the gains from the increase of the combustor inlet temperature.

	Fuel consumption
Recuperated	17.39 L/hr
Non-recuperated	16.33 L/hr

Table 6.8: Fuel consumption of both recuperated cycle and non-recuperated cycle

Note that for the non-recuperated cycle a combustor pressure drop of 5% is assumed.

6.2.3 Cycle model

When the point of operation of the conducted test is considered, these parameters can be used as an input for the Matlab cycle model. This way the cycle model can be validated. The point of operation plotted in the compressor map can be seen in Figure 6.20; the turbine map is plotted in Figure 6.21. The output of the Matlab cycle model can be seen in Table 6.10. The compressor operates on a point that is to be expected, yet the turbine operates on a point slightly below the map. While the turbine still operates at this point, the turbine efficiency drops.

The input parameters for the Matlab cycle model are shown in Table 6.9.

Parameter	Value
\dot{V}_{inlet}	0.11 m ³ /sec
PR	1.56
η_{comp}	75%
$T_{exhaust}$	600 °C
$T_{turb_{in}}$	750 °C
η_{turb}	65/%
η_{shaft}	98/%
η_{gen}	95/%
RPM	80 kRPM
C_{fuel}	20 MJ/L
ρ_{fuel}	789 kg/m ³
$T_{air_{inlet}}$	18 °C

Table 6.9: Input parameters for Matlab cycle model

The power output of the gas turbine engine is almost zero as no generator is attached. This means there is a balance between the turbine power, compressor power and losses. This matches the test results as the engine ran on a stable self-sustaining RPM.

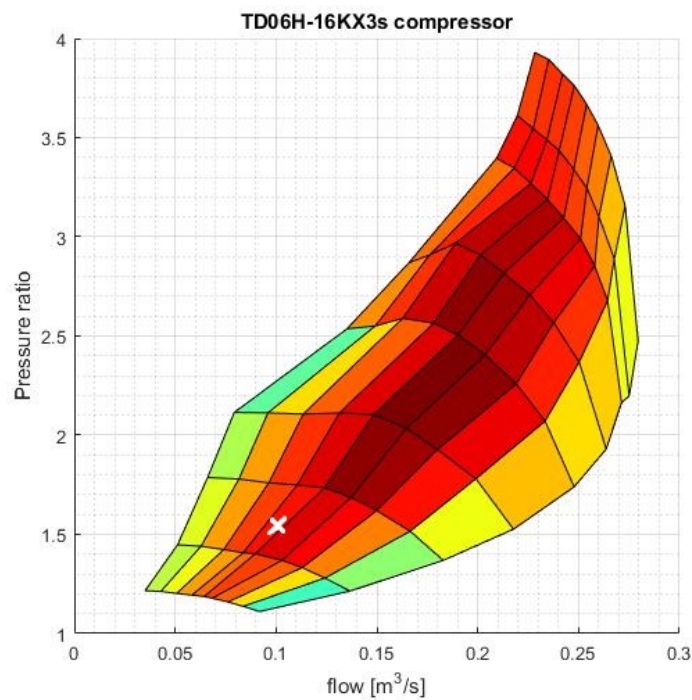


Figure 6.20: Point of operation plotted in the compressor map

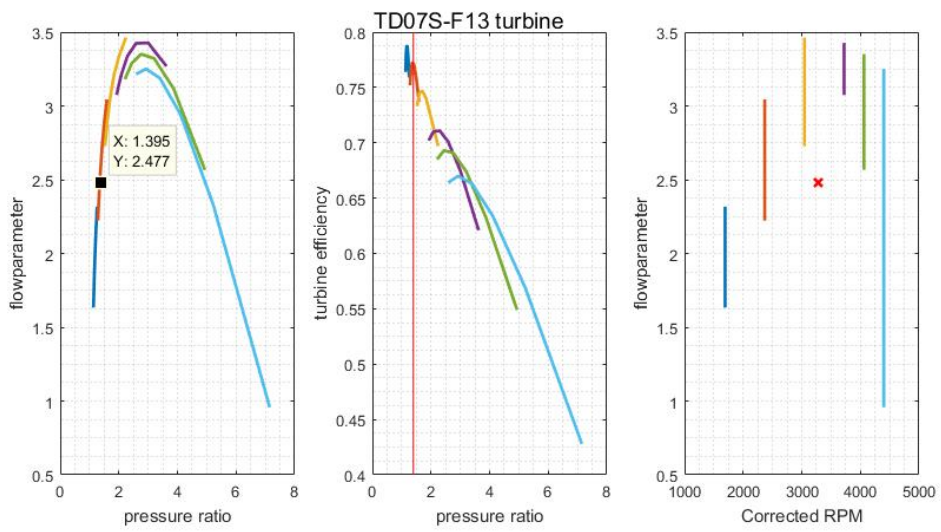


Figure 6.21: Point of operation plotted in the compressor map

Table 6.10: Engine's properties derived from Matlab modelling

Power output	0.1 kWe
Efficiency	- % (generator detached)
Fuel consumption	18 L/hr (E100)

Chapter 7

Conclusions

A micro gas turbine range-extender in combination with an electric vehicle offer a solution to stringent emission legislation with the benefit of creating a virtually unlimited range. The market research showed great potential for range-extendors. While there are other engines with higher efficiency, gas turbines show the potential to be lightweight, compact and affordable. The use of automotive turbochargers as a basis could be one of the key-factors for success. The gas turbine can benefit from turbocharger technology as turbomachinery, mass-production and assembly facilities are already available.

The aim of this project was to build a working prototype to show the feasibility of this project. The project resulted in a stable running engine. The foundations have been laid for further development of all subsystems. The RQL combustion chambers proved to be stable, even with fuels with a relatively high water content(> 3%).

During the project a few setbacks arose. Combustion stabilities appeared to be a major challenge. The integration of a high-speed generator into a turbocharger needs more attention.

Chapter 8

Recommendations

8.1 General project recommendations

- Build a new prototype range-extender that is more similar to the final product.
In the coming years emission-legislation and the general public's thoughts will change at such a rate that they will have a large impact on the automotive industry. Therefore rapid development of new alternatives is needed. While other prototypes are being built, the test set-up described in this thesis can be used to develop new combustion chambers.
- Reduce the number of auxiliary systems.
The most important feature of the range-extender is its cost-effectiveness. Therefore it is important to reduce the number of auxiliary systems as much as possible. The automotive turbochargers use oil pressure-fed bearings, thus an oil condition system is currently needed. Total cost could be reduced by using oil-less bearing alternatives; i.e. foil bearings.
- Parallelize theoretical and practical research. As described in point 1, rapid development is needed. By simultaneously conducting theoretical and practical research the development process can be sped up significantly.

8.2 Engine recommendations

- Redesign generator coupling
During the first tests the generator failed. The coupling should be redesigned so generator test and endurance test can be conducted.
- Redesign generator bearing
During the first tests the generator bearings failed. The bearing set-up should be redesigned.
- Add heat-transfer fins in recuperator

The current recuperator design is really basic, its effectiveness can be greatly improved by adding i.e. heat transfer fins.

- Desing integrated sound suppressor
The test set-up has no sound suppressor at all. An absorption damper could be integrated within the recuperator.
- Add flow straightener to reduce the inlet swirl.
The tests which were conducted showed that a inlet-swirl was present.
- Improve measurement system
The turbine discharge temperature and pressure measurement showed a large error due to their positioning. Currently the sensors are placed at the end of a flexible coupling. By placing these sensors in front of the flexible coupling the read-out error can be removed.
- Airspeed measurement
By adding an airspeed measurement at the turbine inlet the choke, dynamic and static pressure can be calculated.
- Reduce interferences within measurement system
The measuring system suffered from interferences caused by the PWM-signal driving the fuelpumps. Especially the fuel flow measured contained lots of noise due to this interference.
- Change PWM controller to a pressure controller
The fuelpumps are controlled by a PWM signal. Besides the interference caused by the PWM signal, it is relatively inaccurate. A pressure controller would be more suitable.
- Improve Fluent combustion model
The inlet-swirl clearly influences the combustion process. The effects caused by this inlet-swirl can be studied using the Fluent combustion model.
- Change fuel pre-heater
The fuel line runs through the exhaust in order to pre-heat the fuel. When bio-ethanol is used, the fuel start to boil after a certain time. By changing the design of this fuel line, boiling can be prevented.
- Emissions measurement
To quantify the influence of the combustion liner on emissions, an emission measurement should be made.
- Optimize mixing and wall-cooling behaviour
The current combustion chamber design shows a hot core temperature at the end of the combustion chamber. The behaviour of the combustor can be optimized to enhance mixing and reducing the TIT and ensure sufficient wall-cooling.

Bibliography

- [1] Mengistu Tadesse Abebe. *Laminar Burning Velocity of Ethanol , Acetaldehyde and Ethanol- Acetaldehyde Flames*. PhD thesis, Lunds Universitet, 2013.
- [2] Ansys. *User ' s Guide*. 2009.
- [3] W. Bathie. *Fundamentals of Gas Turbines*. 1996.
- [4] M. P. Boyce. *Gas turbine engineering handbook*. Elsevier Science & technology, 4th edition, 2011.
- [5] Meherwan P. Boyce. *Gas Turbine Engineering Handbook*. Elsevier Inc., 3rd edition, 2006.
- [6] BSSA. British Stainless Steel Association.
- [7] Clara Moreno Castán. Market research : Micro gas turbine as range extender for electric vehicles. (October):1–73, 2015.
- [8] Chrysler. *History of Chryslers Corporation's gas turbine vehicles*. 1979.
- [9] Comsol. *COMSOL Multiphysics Reference Manual*. 2014.
- [10] Cycle Tempo and TU Delft. A program for thermodynamic modeling and optimization of energy conversion systems.
- [11] Danfoss. Techno Service.
- [12] Dieselnet. Dieselnet Emission legislation.
- [13] Mark Fernelius, Steven E Gorrell, John Hoke, and Fred Schauer. Effect of Periodic Pressure Pulses on Axial Turbine Performance. *49th AIAA/ASME/SAE/ASEE Joint Propulsion-Conference*, pages 1–15, 2013.
- [14] Linn Garborg. Physical Modeling of a Turbec T100 Microturbine. 1990.
- [15] K. K. Gupta, A. Rehman, and R. M. Sarviya. Bio-fuels for the gas turbine: A review. *Renewable and Sustainable Energy Reviews*, 14(9):2946–2955, 2010.
- [16] Injeti Gurrappa. *Gas Turbine Theory*. 4th edition, 1996.

- [17] By D C Haworth. A probability density function / flamelet method for partially premixed turbulent combustion. 2000.
- [18] M. K. Hossaini. Review of the New Combustion Technologies in Modern Gas Turbines. 2014.
- [19] Konstantinos G. Kyprianidis, Devaiah Nalianda, and Erik Dahlquist. A NO_x Emissions Correlation for Modern RQL Combustors. *Energy Procedia*, 75(x):2323–2330, 2015.
- [20] Ah Lefebvre, Dr Ballal, and Dw Bahr. *Gas turbine combustion: alternative fuels and emissions*. 2010.
- [21] Steve Letho. *Chrysler's Turbine Car: The Rise and Fall of Detroit's Coolest Creation*. Chicago Review Press, 2012.
- [22] Colin F McDonald. Recuperator considerations for future higher efficiency microturbines. *Applied Thermal Engineering*, 23(12):1463–1487, 2003.
- [23] A.M. Mellor. *Design of modern turbine combustors (Combustion Treatise)*. Academic Press Inc., 1990.
- [24] A.F Mills. *Basic Heat Mass Transfer*. Pearson Education (US), 2nd revisi edition, 1998.
- [25] N Peters. LAMINAR FLAMELET CONCEPTS IN TURBULENT COMBUSTION. pages 1231–1250, 1986.
- [26] James C. Polak, Donald L. Carriere, Y. Kemper, Charles E. Kraus, Peter Walzer, Robert A. Mercure, and John L. Wertz. *Advanced Gas Turbine Systems for Automobiles*. Warrendale, PA : Society of Automotive Engineers, 1980.
- [27] Adam Rasheed, Anthony H. Furman, and Anthony J. Dean. Pressure Measurements and Attenuation in a Hybrid Multitube Pulse Detonation Turbine System. *Journal of Propulsion and Power*, 25(1):148–161, 2009.
- [28] Adam Rasheed, Anthony H. Furman, and Anthony J. Dean. Experimental Investigations of the Performance of a Multitube Pulse Detonation Turbine System. *Journal of Propulsion and Power*, 27(3):586–596, 2011.
- [29] W.A. Rees, R.M. Junge, and General Electric company. *Thermodynamic analysis of intermittent combustion cycles*. Schenectady, oclc: 8411 edition, 1956.
- [30] Joost L.H.P. Sallevelt, Artur K Pozarlik, Martin Beran, and Lars-uno Axelsson. Numerical and Experimental Study of Ethanol Combustion in an industrial gas turbine. *Proceedings of ASME Turbo Expo 2013*, pages 1–11, 2013.
- [31] Scott Samuelsen. Rich Burn, Quick-Mix, Lean Burn (RQL) Combustor. *NETL Handbook*, (x):227–233, 1990.

-
- [32] Les Smith. Turbocharger heat transfer and mechanical losses influence in predicting engines performance by using one-dimensional simulation codes Ram o Jos e. 86:204–218, 2015.
 - [33] Bor Jang Tsai and Y. L. Wang. A novel Swiss-Roll recuperator for the microturbine engine. *Applied Thermal Engineering*, 29(2-3):216–223, 2009.
 - [34] J.A. Wüning and J.G. Wüning. FLAMELESS OXIDATION TO REDUCE THERMAL NO-FORMATION. 23:81–94, 1997.
 - [35] Joachim G Wüning. FLAMELESS COMBUSTION AND ITS APPLICATIONS. pages 1–12.

Appendix A

Morphological overviews

The following morphological overviews are used to determine the best configuration, engine type and configuration. Within the morphological overview criterion are graded with a value from 1 to 5. Each criteria has a specified weight factor, the overall grade determines the most optimal solution.

The first morphological overview is shown in Table A.1 and compares different types of powertrains. A range-extended powertrain is compared to an conventional ICE, EV, FCEV and a hybrid vehicle. The criteria are specified by eight people from within MTEE, these results have been averaged.

grade 1-5

Criteria\ car	Hybrid car	RE EV	EV	ICE	Fuel-cell	weight
Cost (for OEM)	4	4	4	3	1	3
Tax-benefits	4	4,5	5	2	4,5	2
engine's efficiency	2	3	5	3	4	1
size	1	2	2	3	2	2
weight	1	3	2	3	2	2
raw emissions (not tailpipe)	3,5	4	5	3	5	1
range	4	4	1	5	3	2
fuel price/km	3,5	4	5	3	4	2
maintenance cost	2	4	4	2	1	1
maintenance interval	3	4	4	3	2	1
reliability	4	5	3	4	3	1
lifetime	2,5	3	2	4	2	2
recharging time	5	4	1	5	5	2
noise & vibrations	3	4	5	2	5	1
charging infrastructure	5	5	2	5	1	2
future legislation proof	3	4	5	2	3	1

Table A.1: Mophological overview

Table A.2 shows grades with the weight factor processed. Eventually the highest grade belongs to the range-extended drivetrain.

Total (incl. weight)

Hybrid	RE	EV	ICE	Fuel-cell	
12	12	12	9	3	
8	9	10	4	9	
2	3	5	3	4	
2	4	4	6	4	
2	6	4	6	4	
3,5	4	5	3	5	
8	8	2	10	6	
7	8	10	6	8	
2	4	4	2	1	
3	4	4	3	2	
4	5	3	4	3	
5	6	4	8	4	
10	8	2	10	10	
3	4	5	2	5	
10	10	4	10	2	
3	4	5	2	3	
Total	84,5	99	83	88	73

Table A.2: Morphological overview

As discussed within Chapter 1 it is explained that the range-extender could use different types of engines. Each engine has specific advantages, to determine the best overall behaviour the morphological overview shown in Table A.3 is used. Currently conventional 4-stroke piston engines(ICE RE) are already being used for range-extender applications. This type of engine is compared to gas turbine(GT RE), Wankel and a hydrogen fuel-cell.

Criteria\engine	ICE RE	GT RE	wankel RE	fuelcell RE	weight
Cost	3	3,5	3,5	1	3
size	3	3	3,5	1	2
efficiency	4	3,5	3,5	4	2
price/litre fuel	4	4	3	2	2
weight	1	3	2	1	2
emissions	3	2	3	5	1
maintenance cost	2	4	1	1	1
start-up time	3	2	3	3	1
maintenance interval	3	4,5	2	2	1
reliability	4	5	3,5	3	2
integration	3	3	2	1	1
lifetime	3	4	2	2	1
noise & vibrations	3	3	3	5	1
auxiliary systems	2	3	2	1	1
time to market	4	3	3	1	1

Table A.3: Mophological overview

Table A.4 shows the total grade with its weight factor included. When the final grade is computed it becomes clear that a gas turbine range-extender would best suit the needs.

Total (incl. weight)

ICE RE	GT RE	Wankel RE	Fuelcell RE
9	10,5	10,5	3
6	6	7	2
8	7	7	8
8	8	6	4
2	6	4	2
3	2	3	5
2	4	1	1
3	2	3	3
3	4,5	2	2
8	10	7	6
3	3	2	1
3	4	2	2
3	3	3	5
2	3	2	1
4	3	3	1
total	67	76	62,5
			46

Table A.4: Mophological overview

Appendix B

Test results

B1 Plots

n_{TC} [RPM]

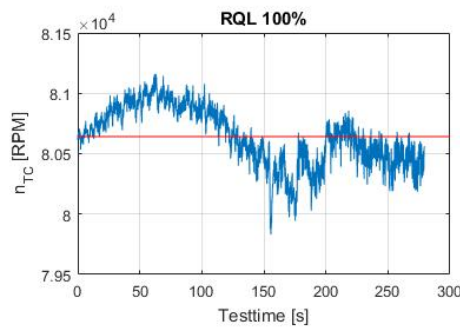
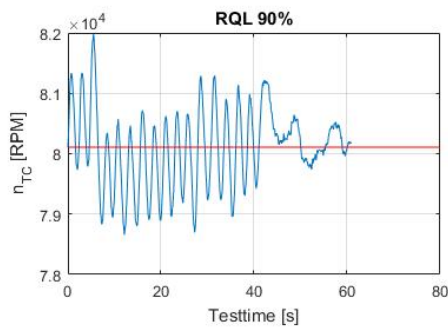
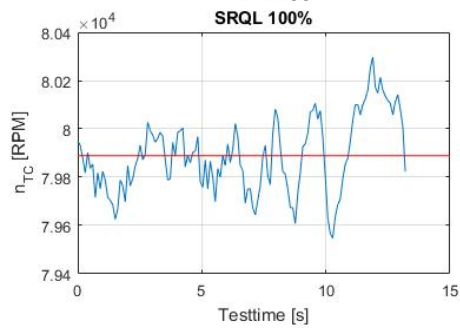
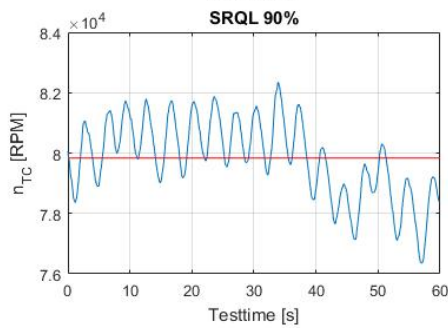
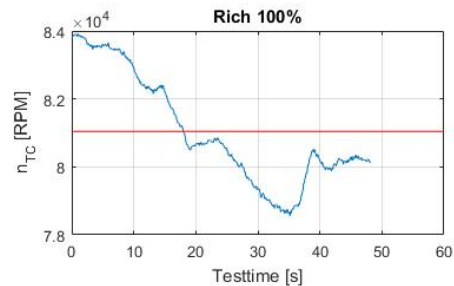
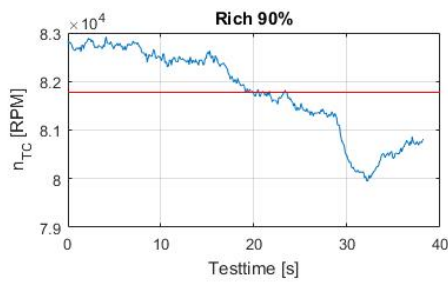


Figure B.1: RPM of the engine

Fuel flow [LPH]

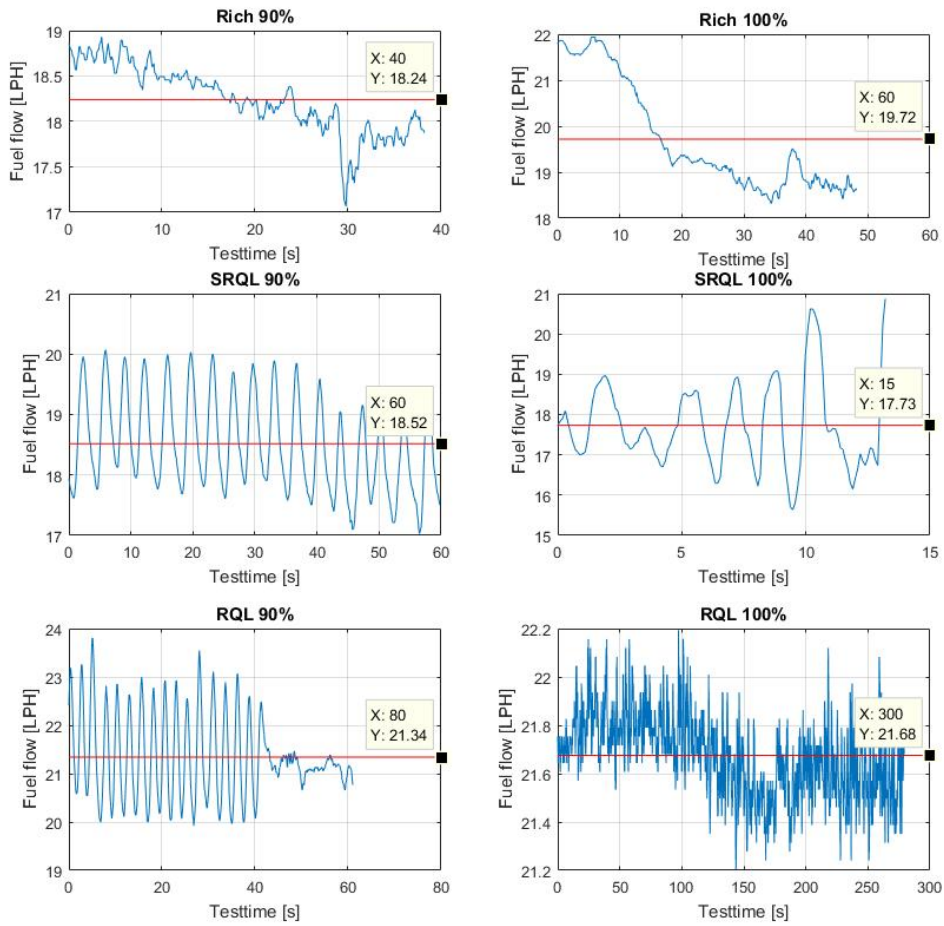


Figure B.2: fuel consumption

P_C OUT [mbar]

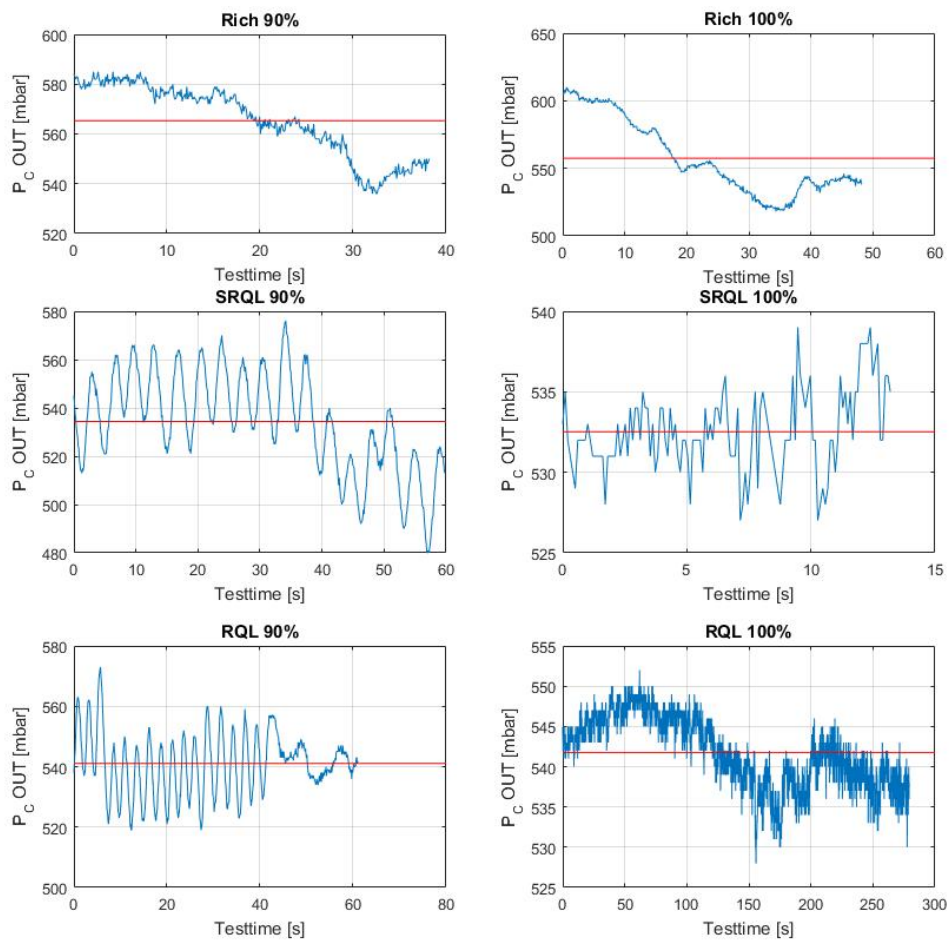


Figure B.3: Compressor out pressure

T_C OUT [°C]

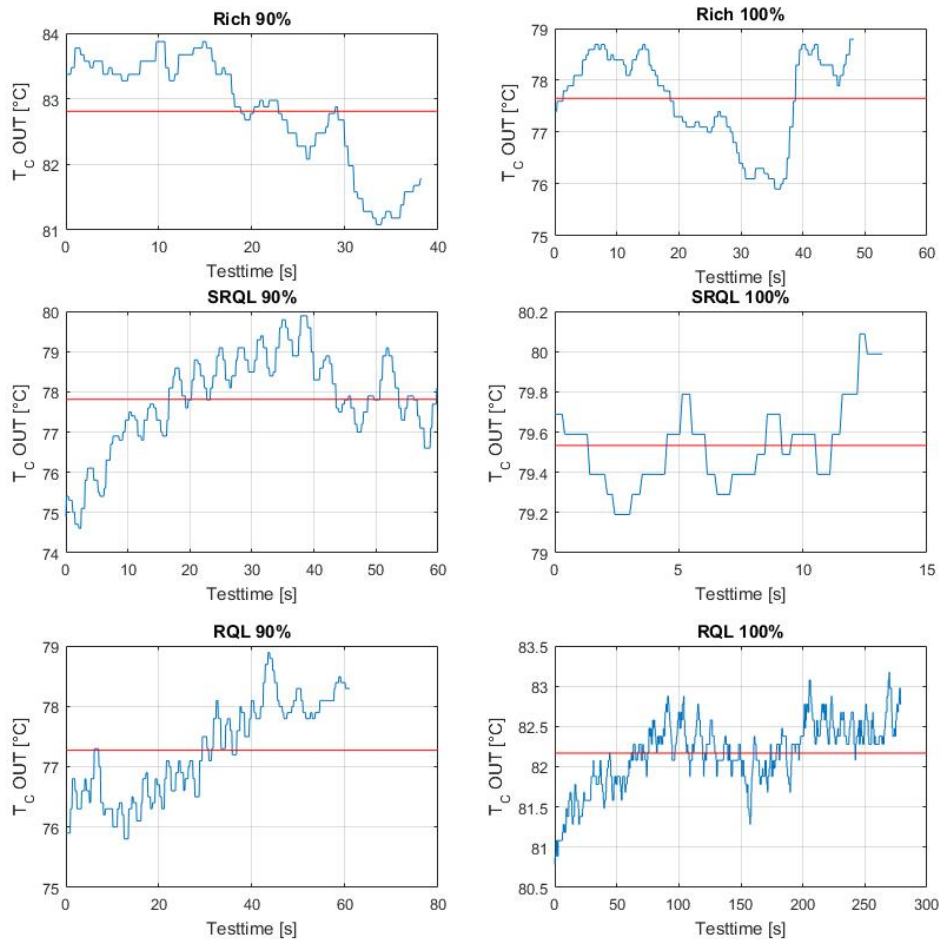


Figure B.4: Compressor out teperature

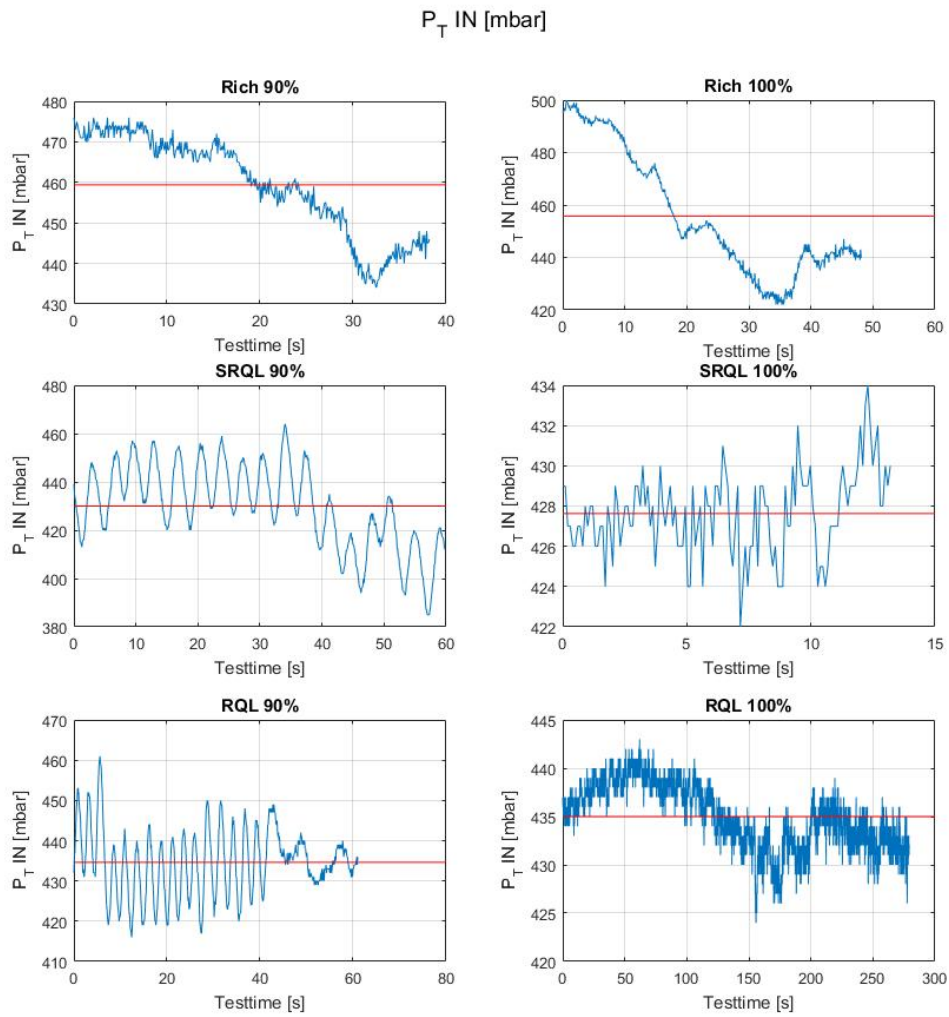


Figure B.5: Turbine in temperature

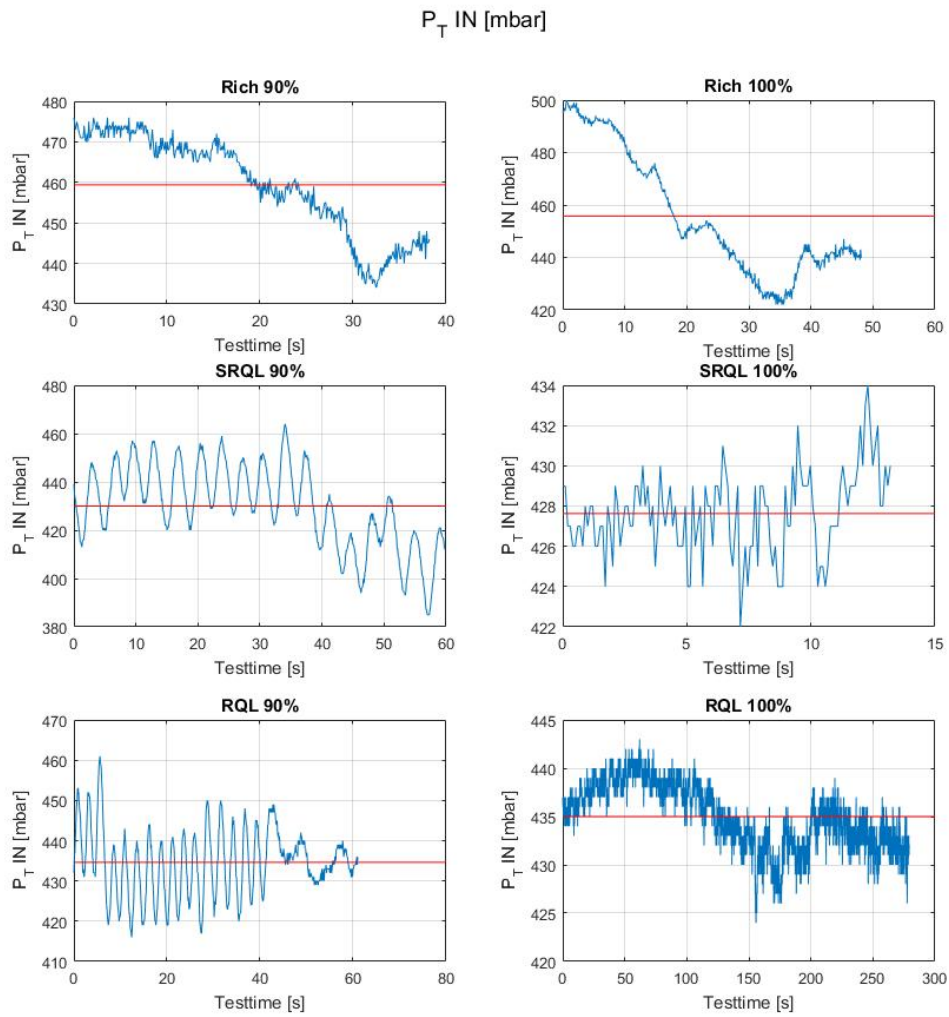


Figure B.6: Turbine in temperature

P_T OUT [mbar]

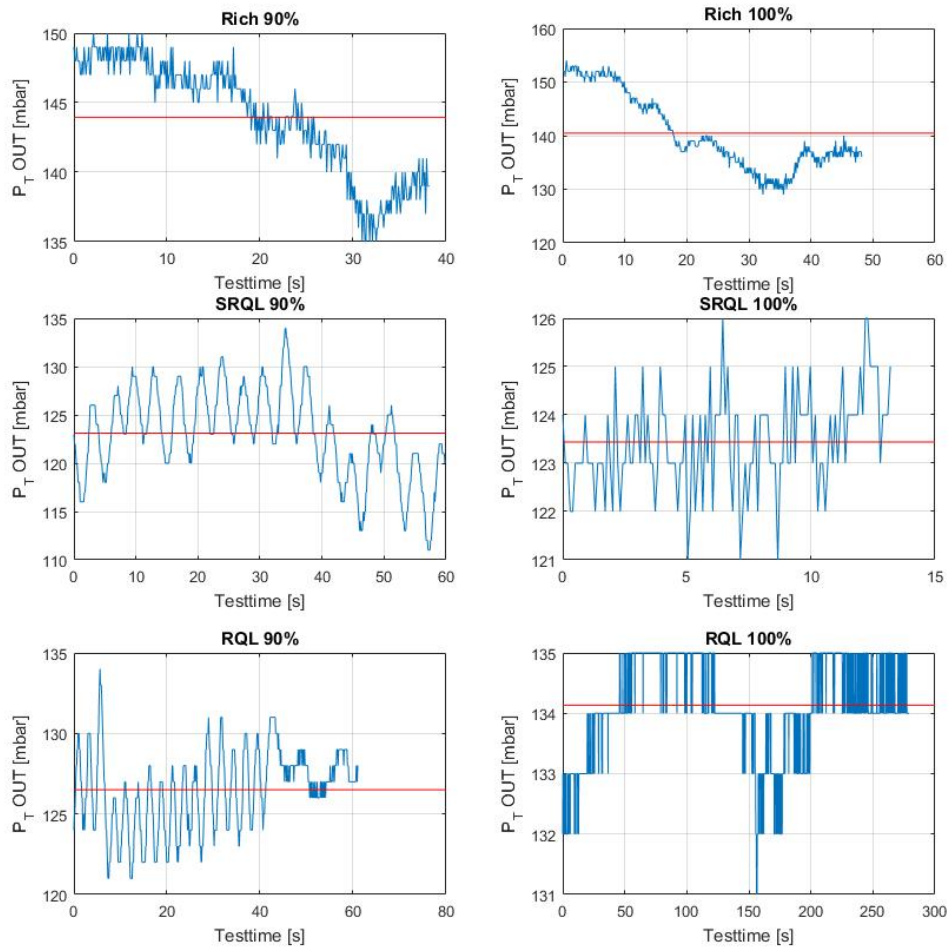


Figure B.7: Turbine out temperature

P_T OUT [mbar]

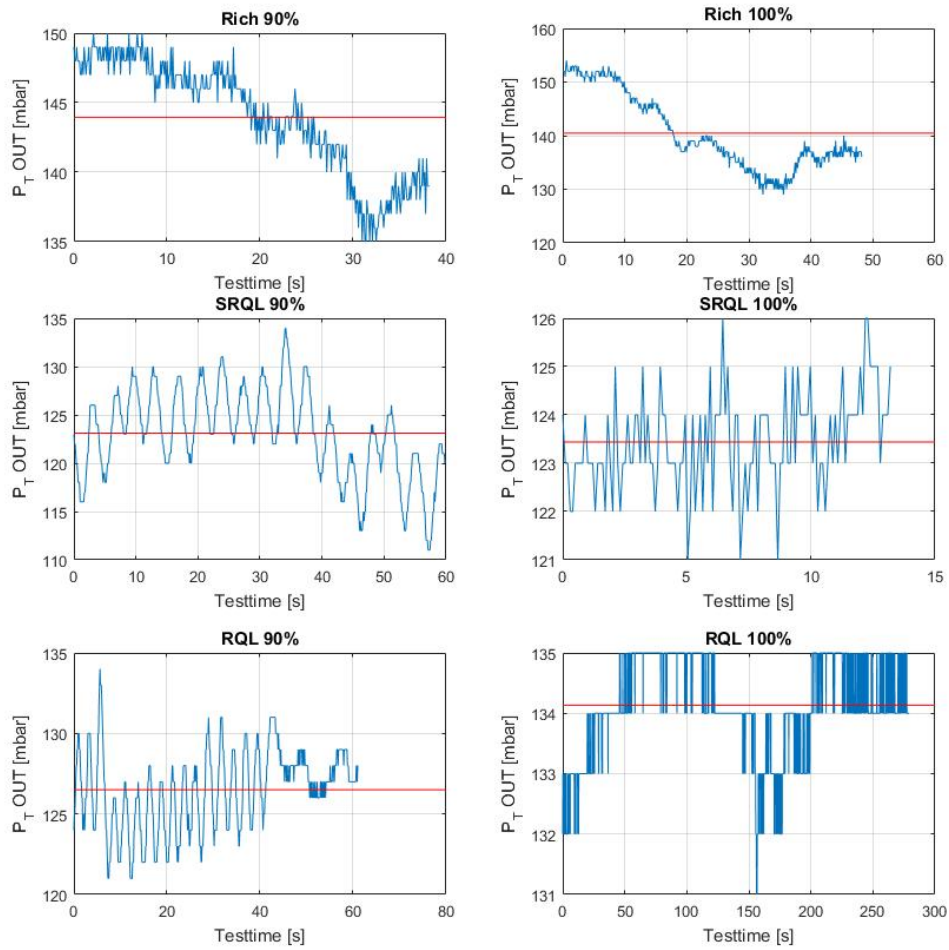


Figure B.8: Turbine out temperature

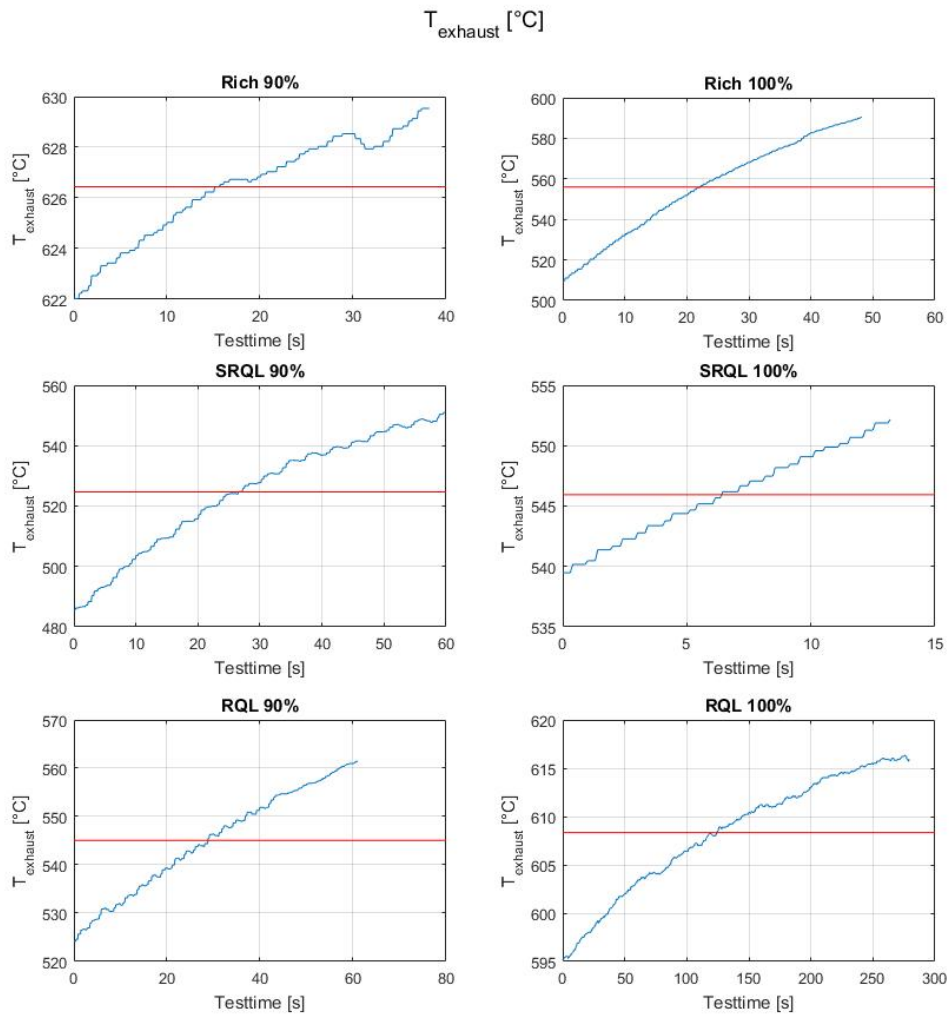


Figure B.9: Exhaust temperature

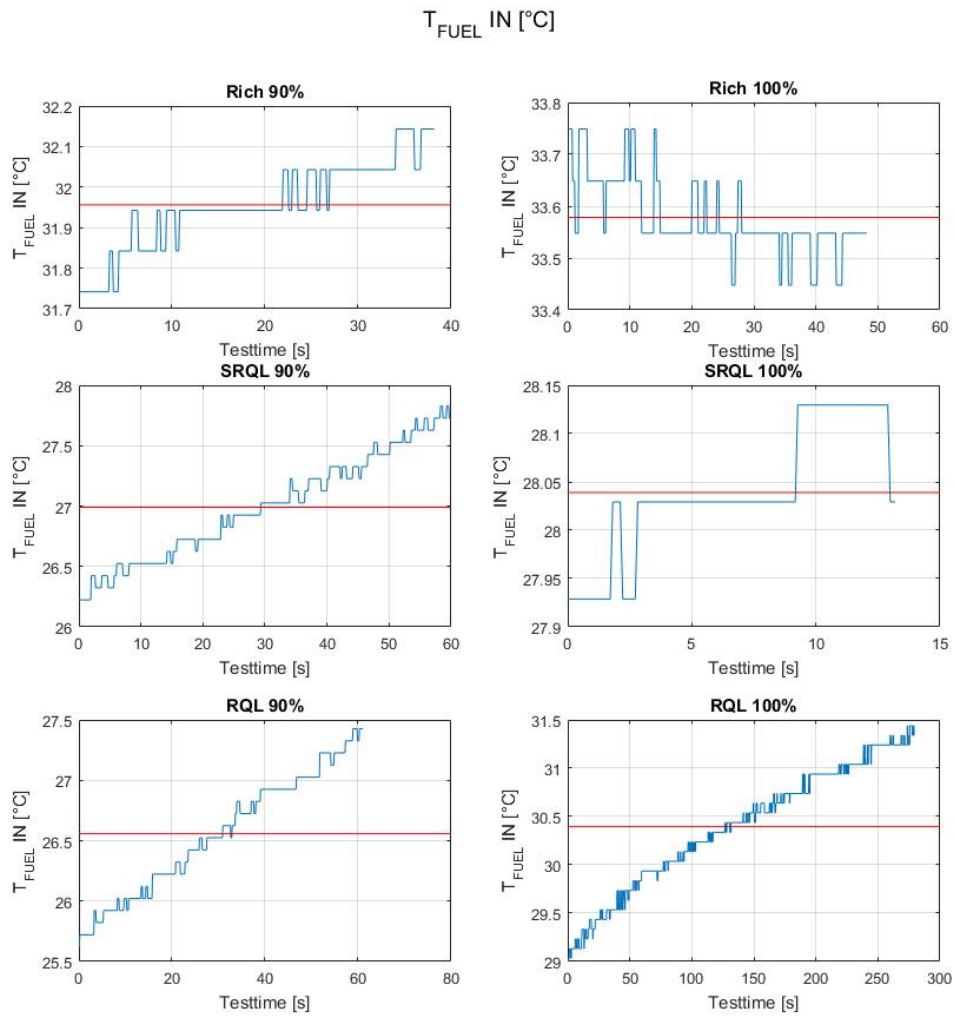


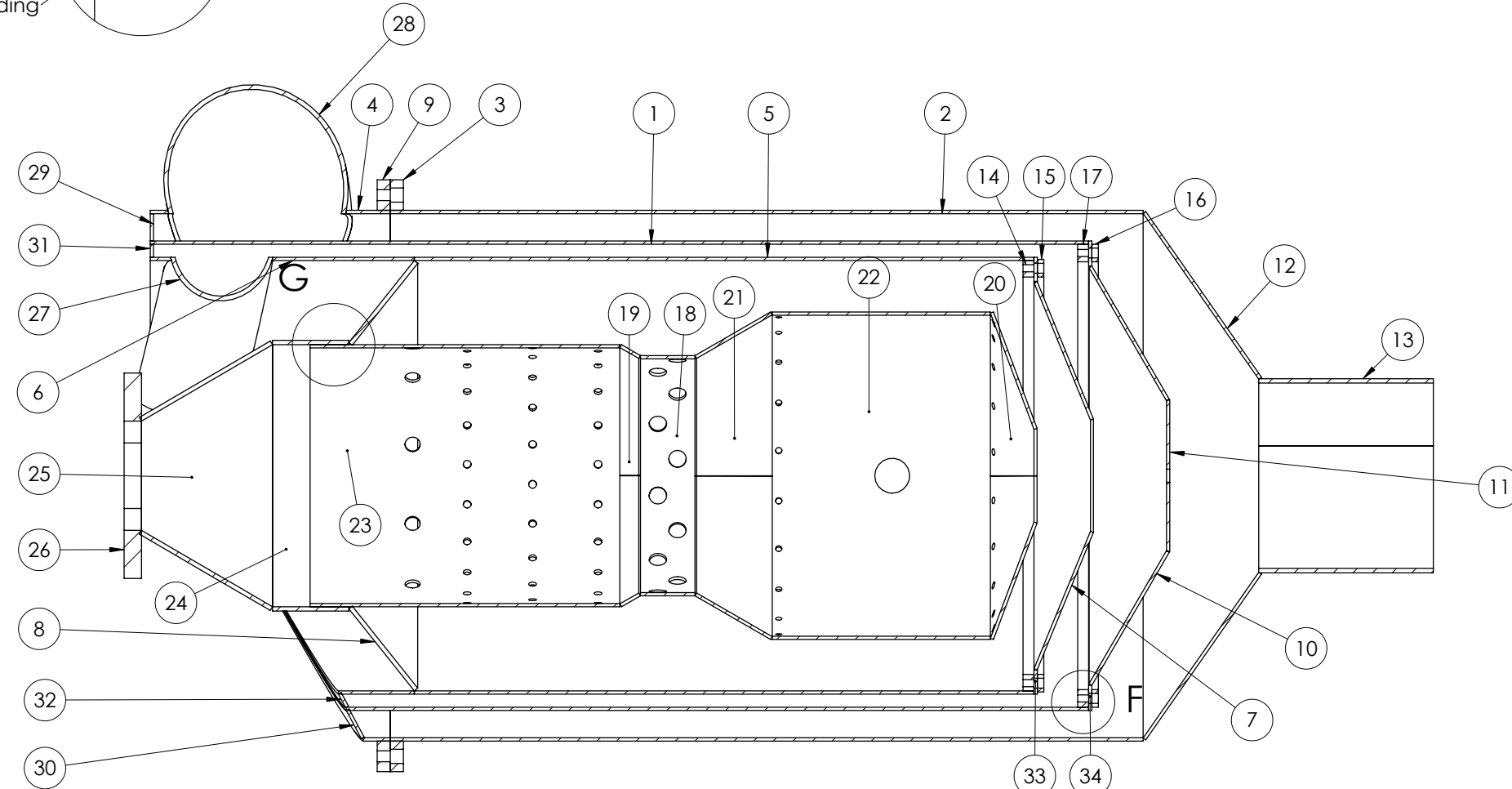
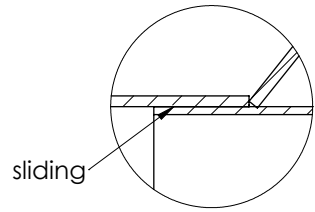
Figure B.10: Fuel temperature

Appendix C

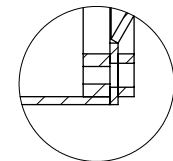
Drawings

DETAIL G

SCALE 1:1



SECTION E-E



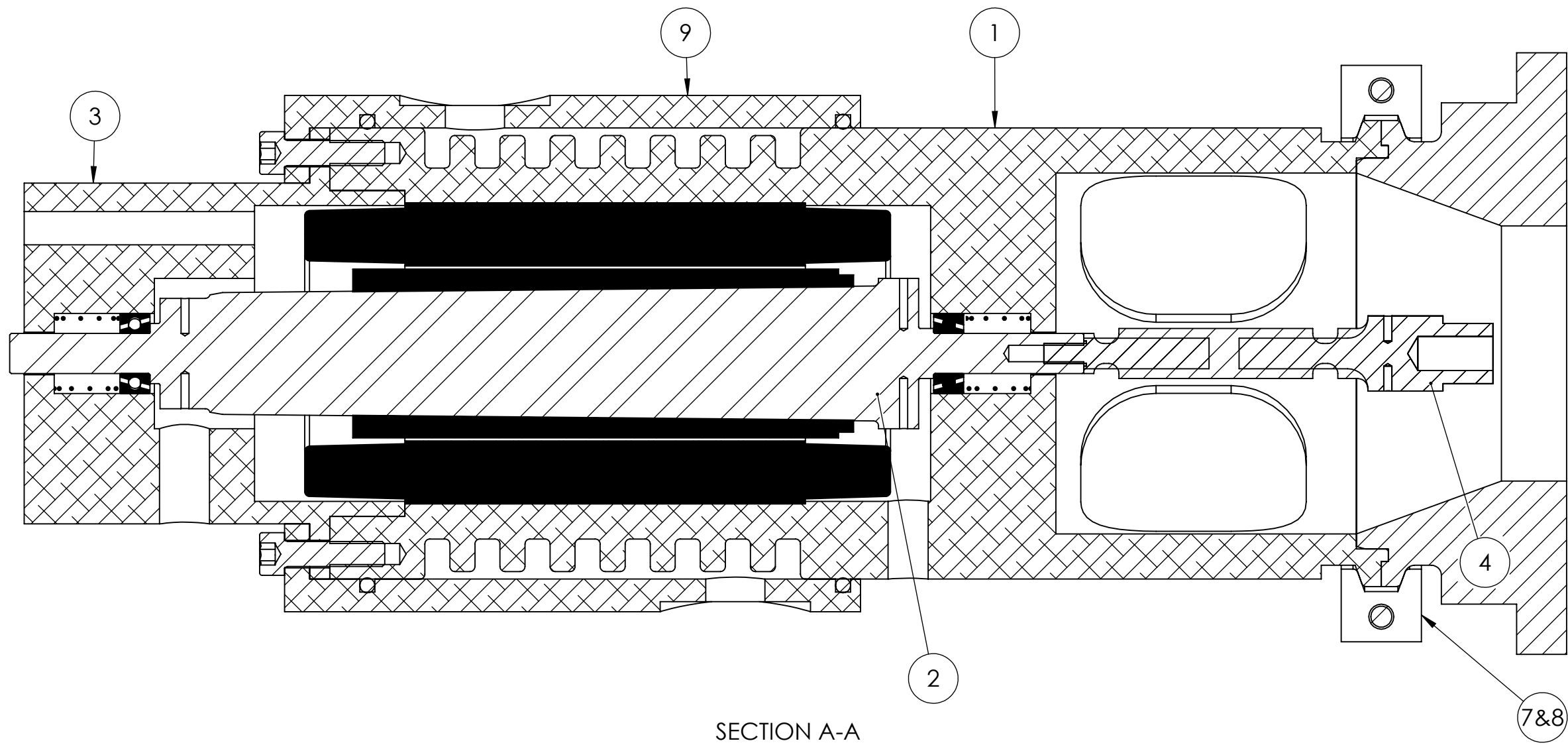
DETAIL F

SCALE 1:1

ITEM NO.	PART NUMBER	Thickness [mm]	DESCRIPTION
1	2nd_tube	1.5	
2	3rd_tube	1.5	
3	flange_holes	6	
4	3rd_tube_manifold	1.5	
5	1st_tube	1.5	
6	1st_tube_manifold	1.5	
7	1st_cone	1.5	
8	inner_cone	2	
9	flange_thread	6	
10	2nd_cone	1.5	
11	2nd_tube_cone_plate	1.5	
12	3rd_cone	1.5	
13	exhaust_tube	1.5	
14	1st_thread_ring	5	
15	1st_washer_ring	3	
16	2nd_washer_ring	3	
17	2nd_thread_ring	5	
18	middle_tube	1.5	
19	3rd_CC_cone	1.5	
20	front_cone	1.5	
21	2nd_CC_cone	1.5	
22	large_tube	1.5	
23	end_tube	1.5	
24	turbine_tube	2	
25	exhaust_flange_cone	2	
26	turbine flange	8	
27	bend_pipe	2	Lasbocht
28	exhaust_manifold_tube	2	Lasbocht
29	front_plate_large	1.5	
30	ellips_large2	1.5	
31	front_plate_small	1.5	
32	ellips_small	1.5	
33	1st_cone_hole_pattern	1.5	
34	2nd_cone_hole_pattern	1.5	

UNLESS OTHERWISE SPECIFIED: DIMENSIONS ARE IN MILLIMETERS SURFACE FINISH: TOLERANCES: LINEAR: ANGULAR:		FINISH:	DEBUR AND BREAK SHARP EDGES	DO NOT SCALE DRAWING	REVISION
DRAWN	NAME	SIGNATURE	DATE	TITLE:	
CHK'D					
APP'VD					
MFG					
Q.A				MATERIAL:	DWG NO.
				WEIGHT:	SCALE:1:2
					SHEET 1 OF 1

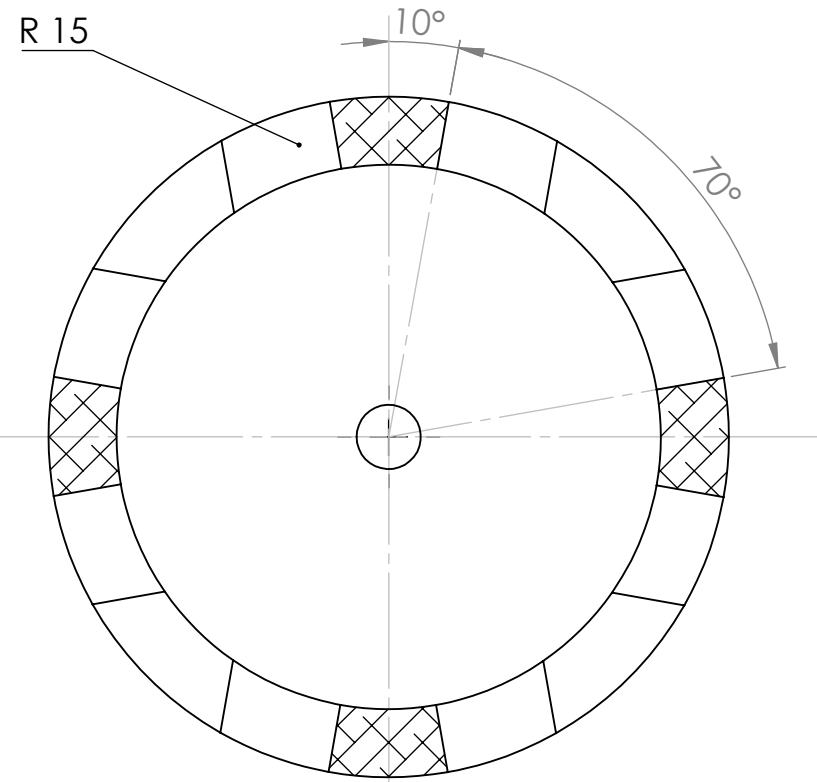
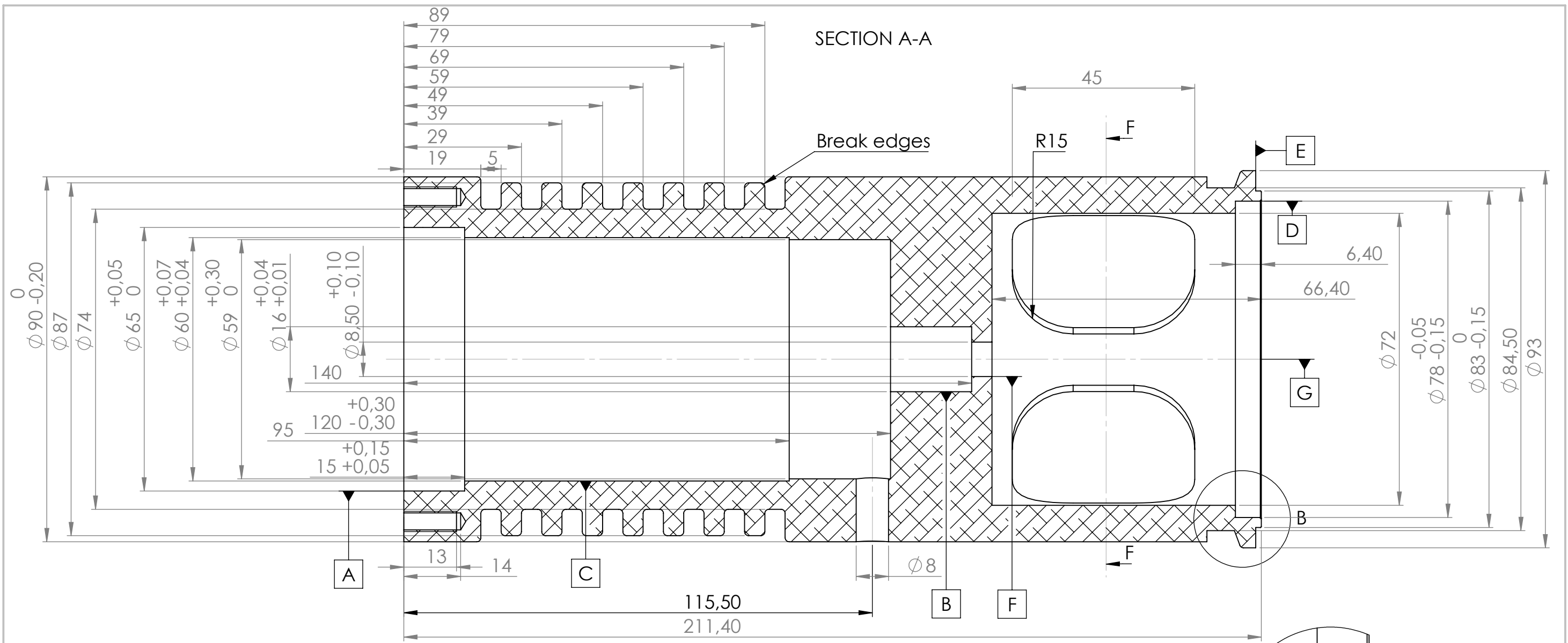
case_assembly_sheet_metal_weld_se



SECTION A-A

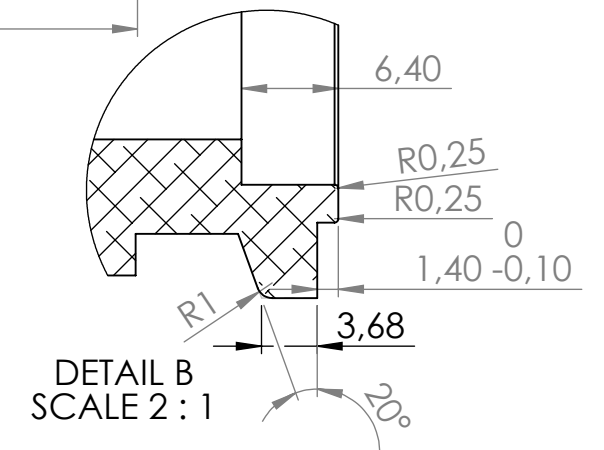
ITEM NO.	PART NUMBER	Material	QTY.
1	generator_housing		1
2	shaft_female_thread		1
3	generator_rear_cap		1
4	compressor_shaft_extension_long_2		1
7&8	clamp_ring_thread		1
8	clamp_ring		1
9	cooling_sleeve		1
13	Compressor_cover_mockup		1
14	compressor_shaft_generator_side		1
15	compressor_shaft_compressor_side		1

UNLESS OTHERWISE SPECIFIED: DIMENSIONS ARE IN MILLIMETERS				FINISH:		DEBUR AND BREAK SHARP EDGES		DO NOT SCALE DRAWING		REVISION	
SURFACE FINISH:											
TOLERANCES:											
LINEAR:											
ANGULAR:											
DRAWN		NAME	SIGNATURE	DATE					TITLE:		
CHK'D											
APPV'D											
MFG											
Q.A					MATERIAL:				DWG NO.		
									assembly_generator ^{A3}		
					WEIGHT:				SCALE:1:1		
									SHEET 1 OF 1		



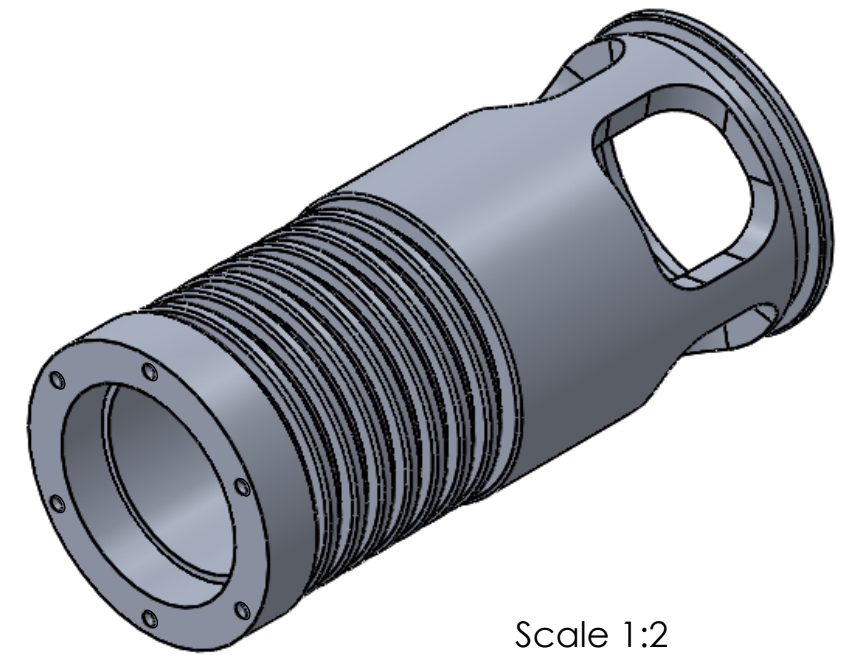
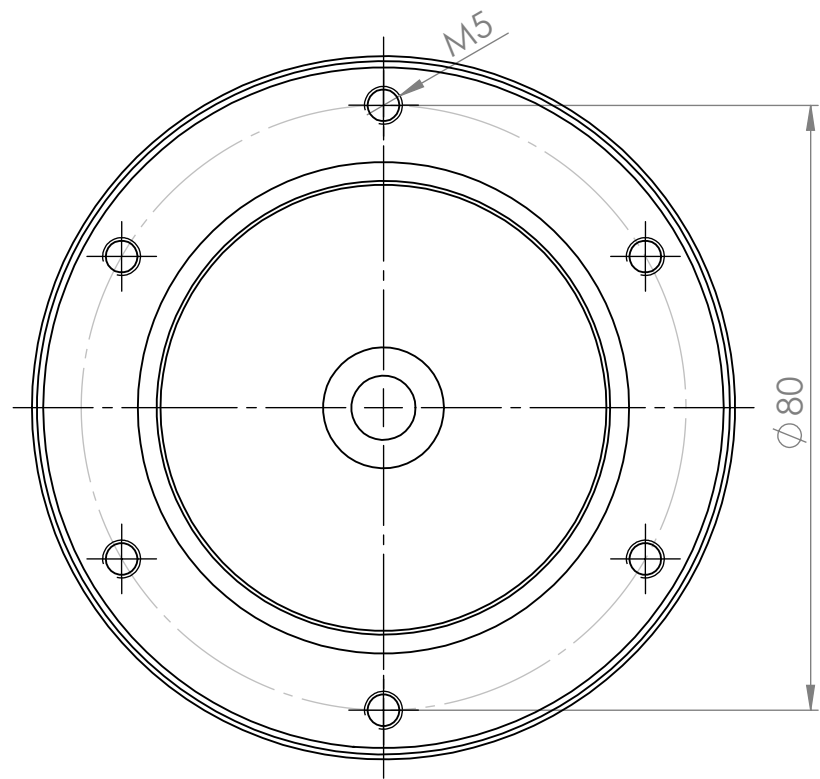
SECTION F-F

◎	0.02	A	B	C
⊥	0.01	B	C	G
≡	0.01	B	C	G
≡	0.01	B	F	G



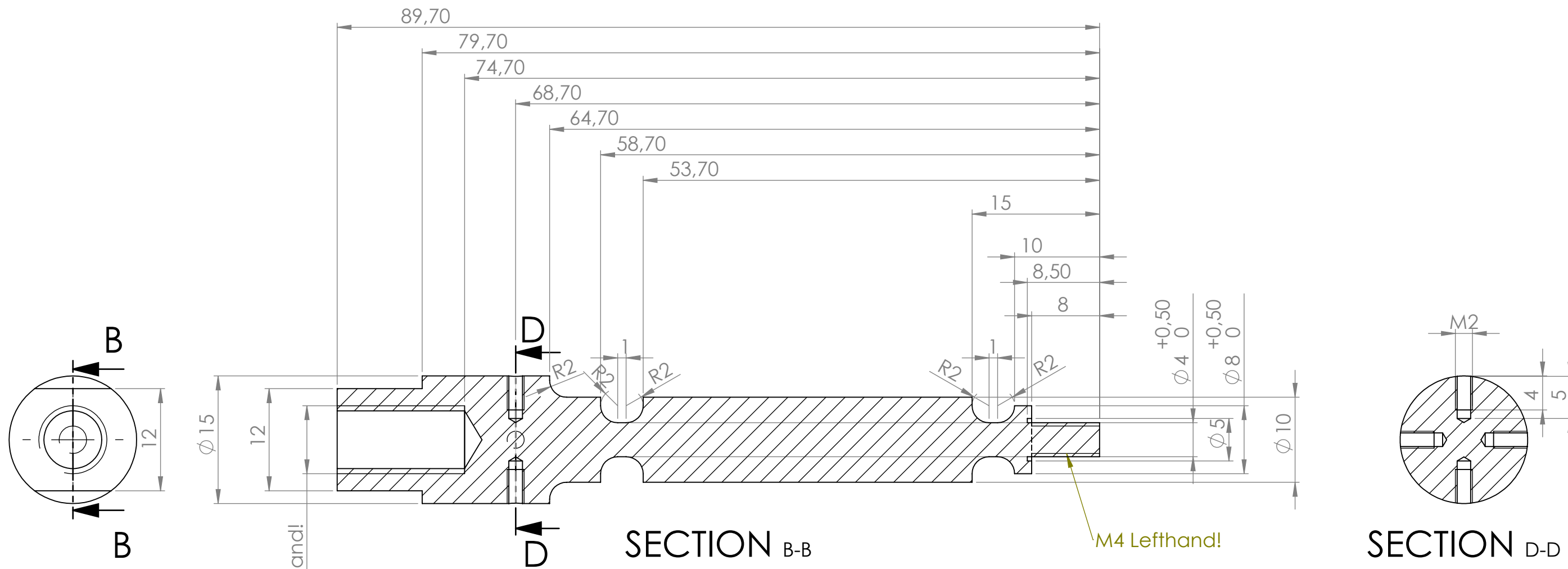
DETAIL B
SCALE 2:1

UNLESS OTHERWISE SPECIFIED: DIMENSIONS ARE IN MILLIMETERS SURFACE FINISH: TOLERANCES: LINEAR: ANGULAR:				FINISH:	DEBUR AND BREAK SHARP EDGES	DO NOT SCALE DRAWING	REVISION
DRAWN	NAME	SIGNATURE	DATE			TITLE:	
CHK'D							
APPV'D							
MFG							
Q.A				MATERIAL:		DWG NO.	
						generator_housing A3	
				WEIGHT:		SCALE:1:1	SHEET 1 OF 2

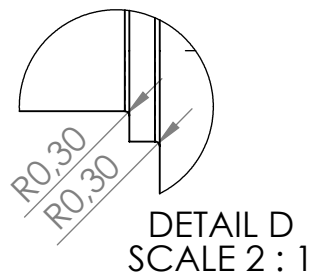
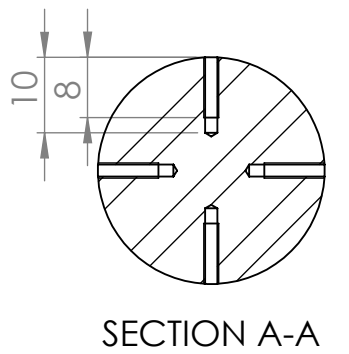
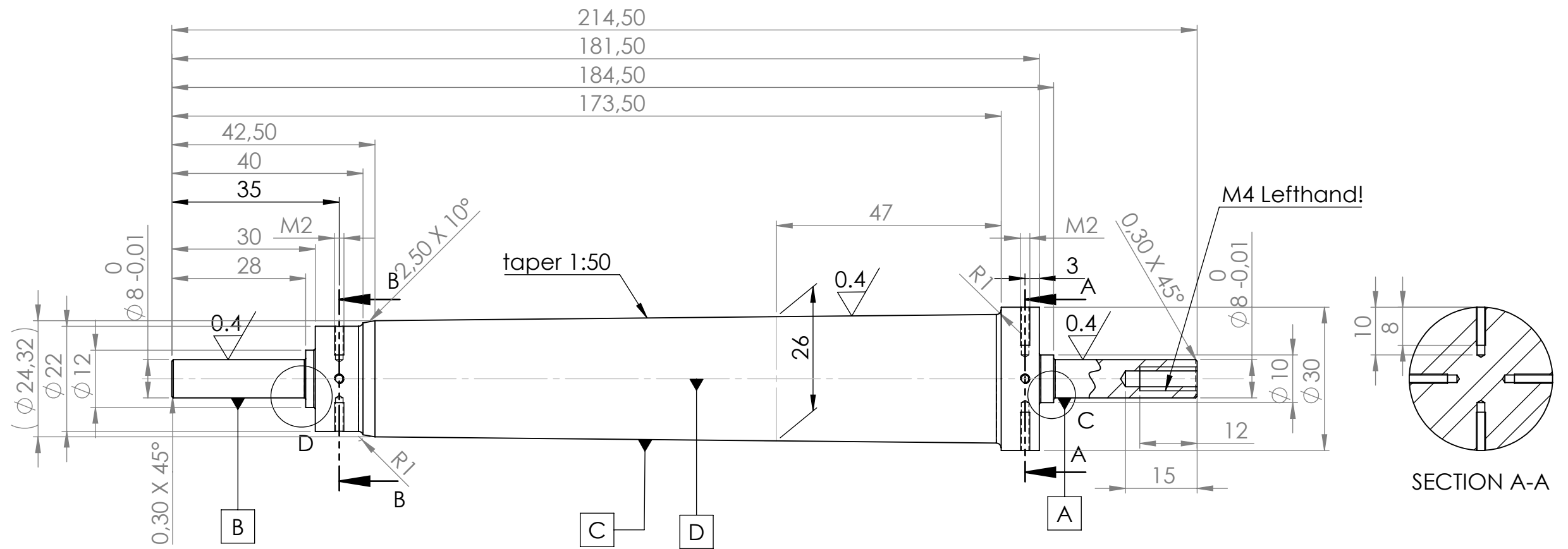
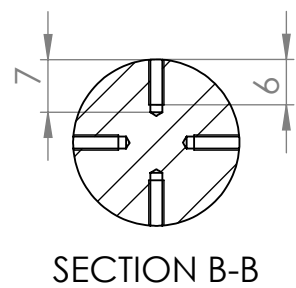


Scale 1:2

UNLESS OTHERWISE SPECIFIED: DIMENSIONS ARE IN MILLIMETERS SURFACE FINISH: TOLERANCES: LINEAR: ANGULAR:				FINISH:		DEBUR AND BREAK SHARP EDGES		DO NOT SCALE DRAWING		REVISION	
DRAWN				NAME		SIGNATURE		DATE		TITLE:	
CHK'D											
APPV'D											
MFG											
Q.A								MATERIAL:		DWG NO.	
										generator_housing ^{A3}	
								WEIGHT:		SCALE:1:1	
										SHEET 2 OF 2	

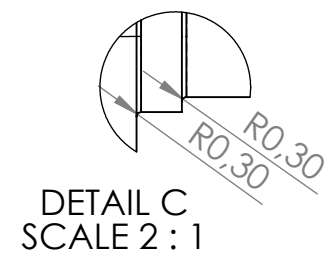


UNLESS OTHERWISE SPECIFIED: DIMENSIONS ARE IN MILLIMETERS SURFACE FINISH: TOLERANCES: LINEAR: ANGULAR:				FINISH:		DEBUR AND BREAK SHARP EDGES		DO NOT SCALE DRAWING		REVISION	
DRAWN				NAME		SIGNATURE		DATE		TITLE:	
CHK'D											
APPV'D											
MFG											
Q.A											
								MATERIAL:		DWG NO.	
								1.2510 compressor shaft extension 2 different dim lay		A3	
								WEIGHT:		SCALE:2:1	
										SHEET 1 OF 1	

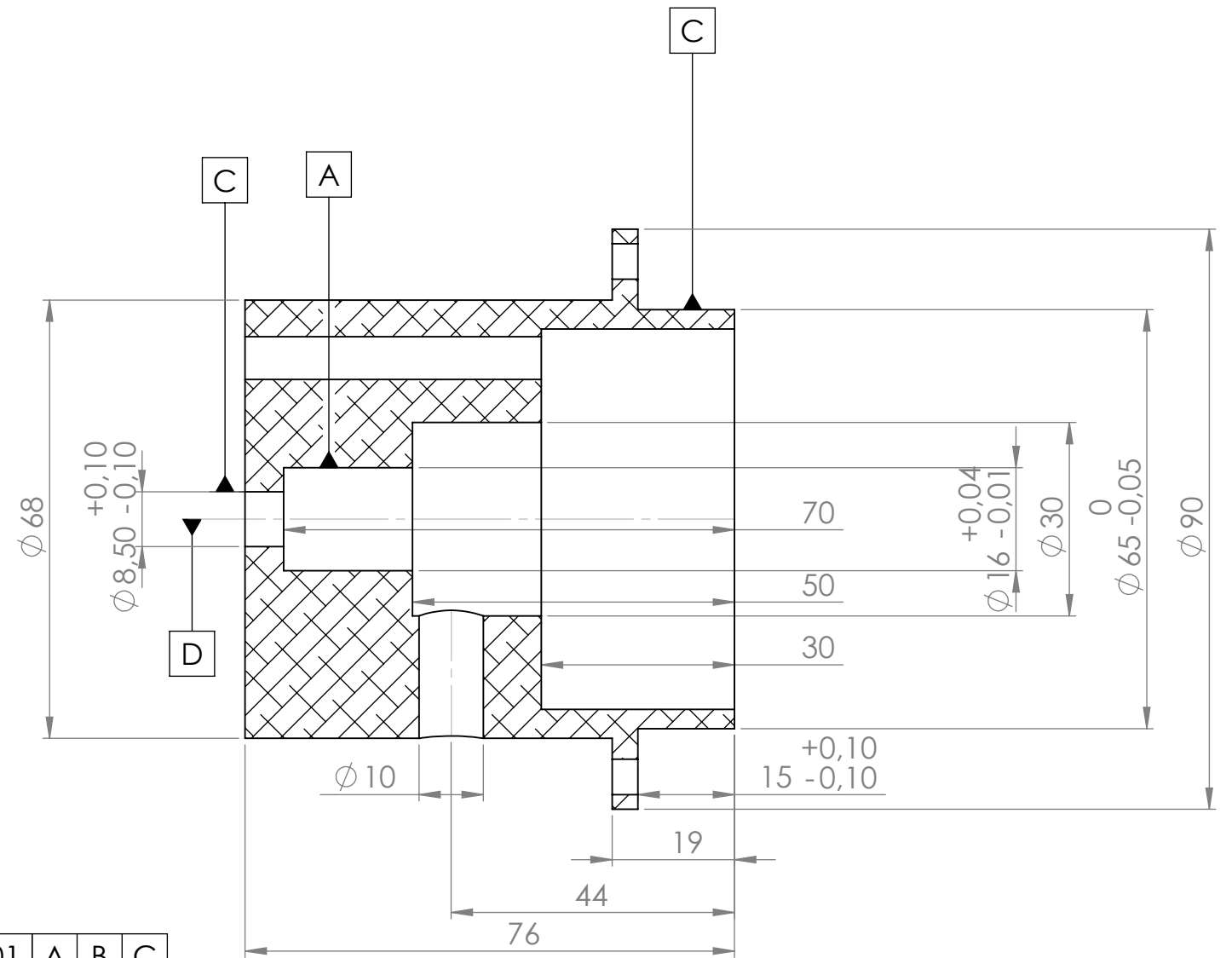
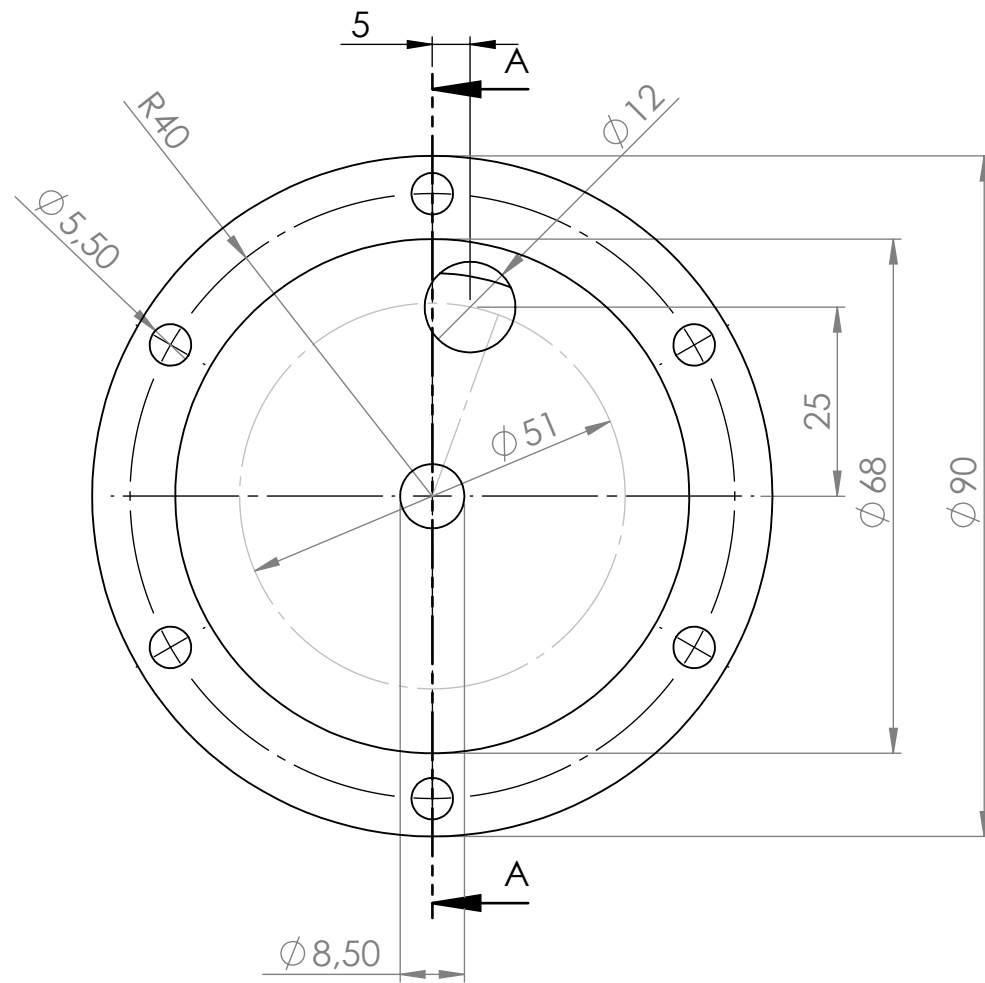


⊙	0.01	A	B	C
○	0.01	A	B	C
≡	0.01	A	C	D

A,B,C ground surfaces



UNLESS OTHERWISE SPECIFIED: DIMENSIONS ARE IN MILLIMETERS SURFACE FINISH: TOLERANCES: LINEAR: ANGULAR:				FINISH:		DEBUR AND BREAK SHARP EDGES		DO NOT SCALE DRAWING		REVISION	
DRAWN				SIGNATURE		DATE		TITLE:			
CHK'D											
APPV'D											
MFG											
Q.A								MATERIAL: 1.2510		DWG NO. Generator_as	
								WEIGHT:		SCALE:1:1	
										SHEET 1 OF 1	
										A3	

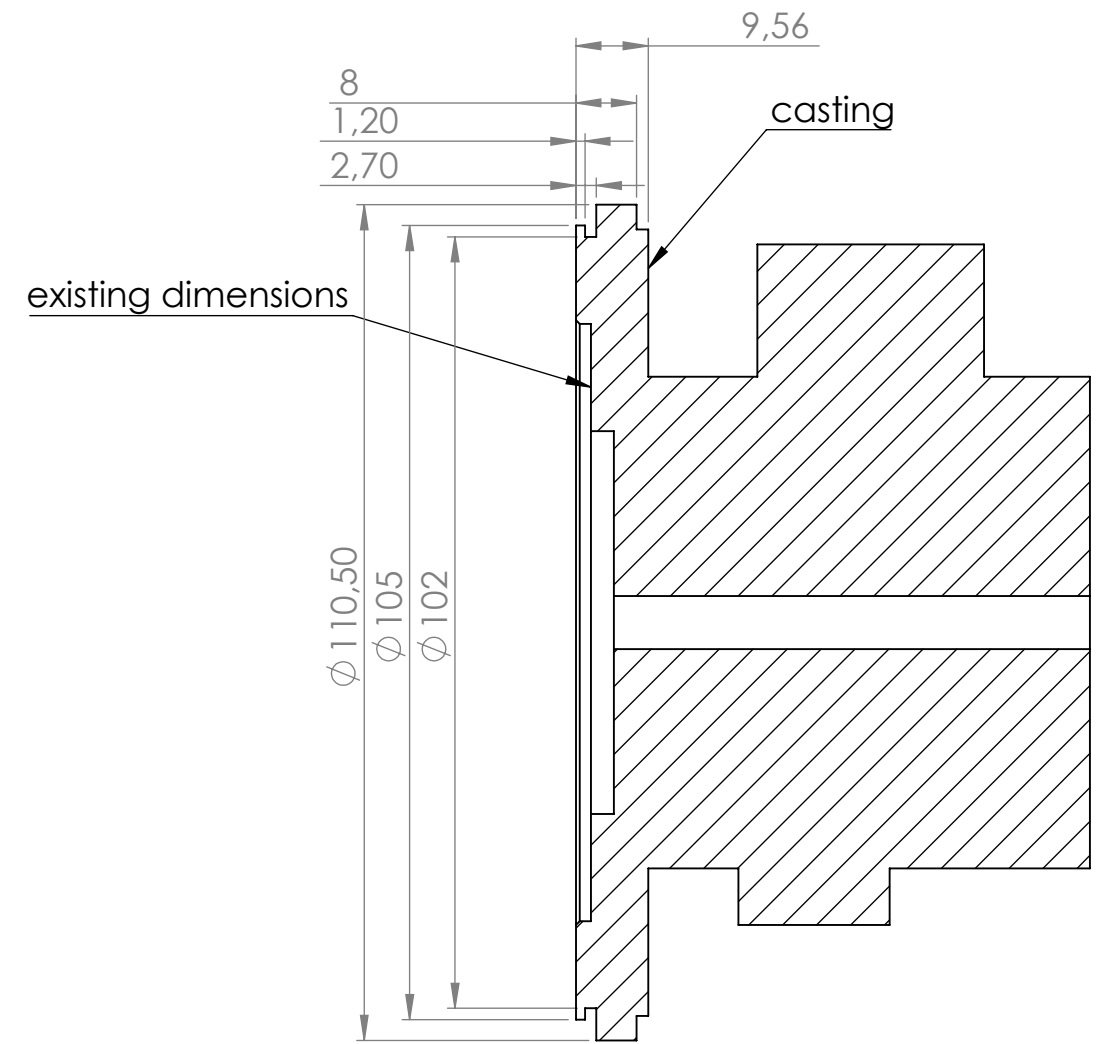
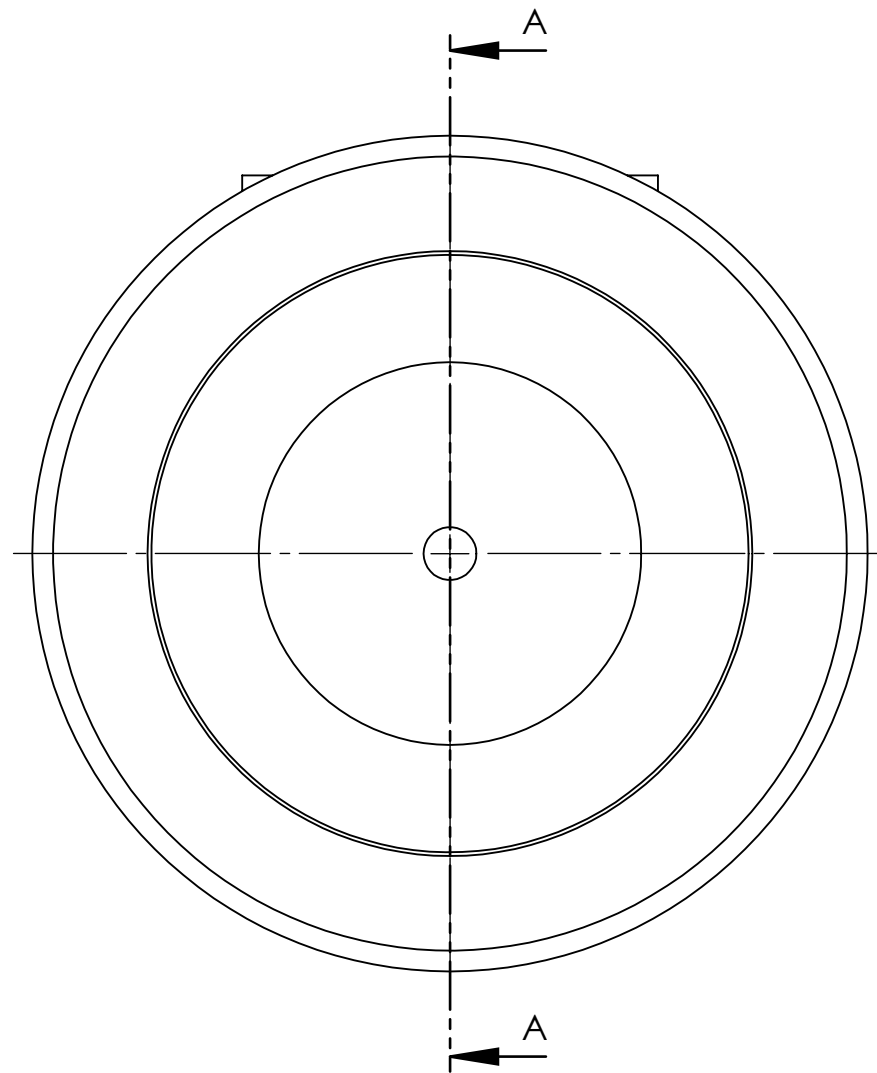


⊙	0.01	A	B	C
≡	0.01	A	C	D
○	0.01	A	C	

SECTION A-A

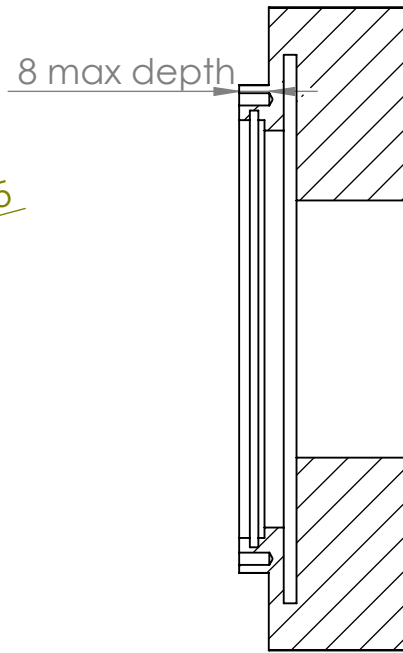
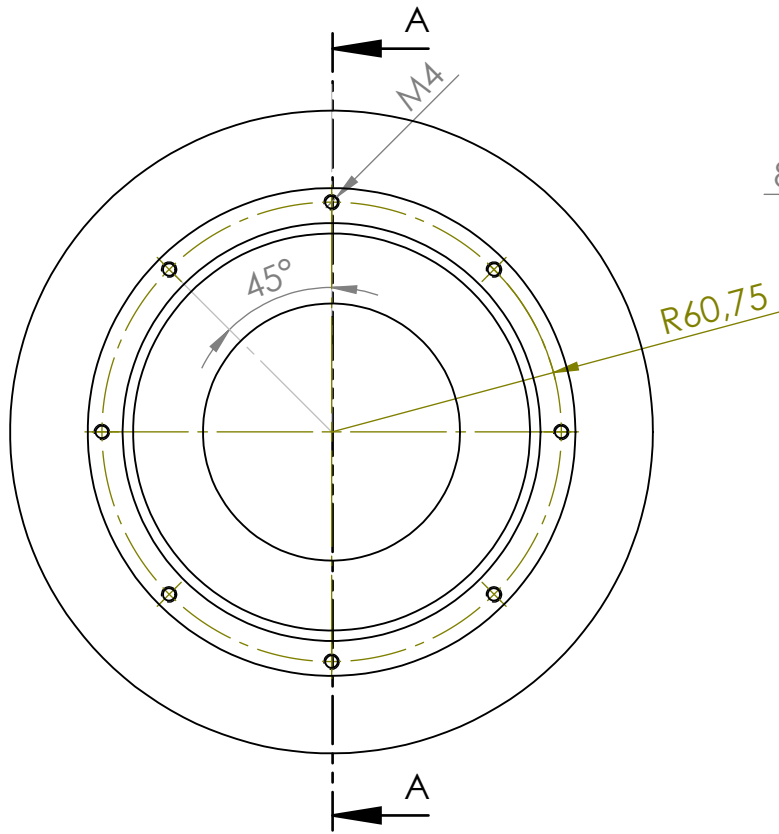
UNLESS OTHERWISE SPECIFIED: DIMENSIONS ARE IN MILLIMETERS SURFACE FINISH: TOLERANCES: LINEAR: ANGULAR:				FINISH:		DEBUR AND BREAK SHARP EDGES		DO NOT SCALE DRAWING		REVISION	
DRAWN				SIGNATURE		DATE		TITLE:			
CHK'D											
APPV'D											
MFG											
Q.A								MATERIAL: Aluminium		DWG NO: generator_rear_cap	
								WEIGHT:		SCALE:1:1	
										SHEET 1 OF 1	

A3



SECTION A-A

UNLESS OTHERWISE SPECIFIED: DIMENSIONS ARE IN MILLIMETERS SURFACE FINISH: TOLERANCES: LINEAR: ANGULAR:				FINISH:		DEBUR AND BREAK SHARP EDGES		DO NOT SCALE DRAWING		REVISION	
DRAWN				NAME		SIGNATURE		DATE		TITLE:	
CHK'D											
APPV'D											
MFG											
Q.A								MATERIAL:		DWG NO:	
										Cartridge_mockup A3	
								WEIGHT:		SCALE:1:1	
										SHEET 1 OF 1	



SECTION A-A

UNLESS OTHERWISE SPECIFIED:
 DIMENSIONS ARE IN MILLIMETERS
 SURFACE FINISH:
 TOLERANCES:
 LINEAR:
 ANGULAR:

FINISH:

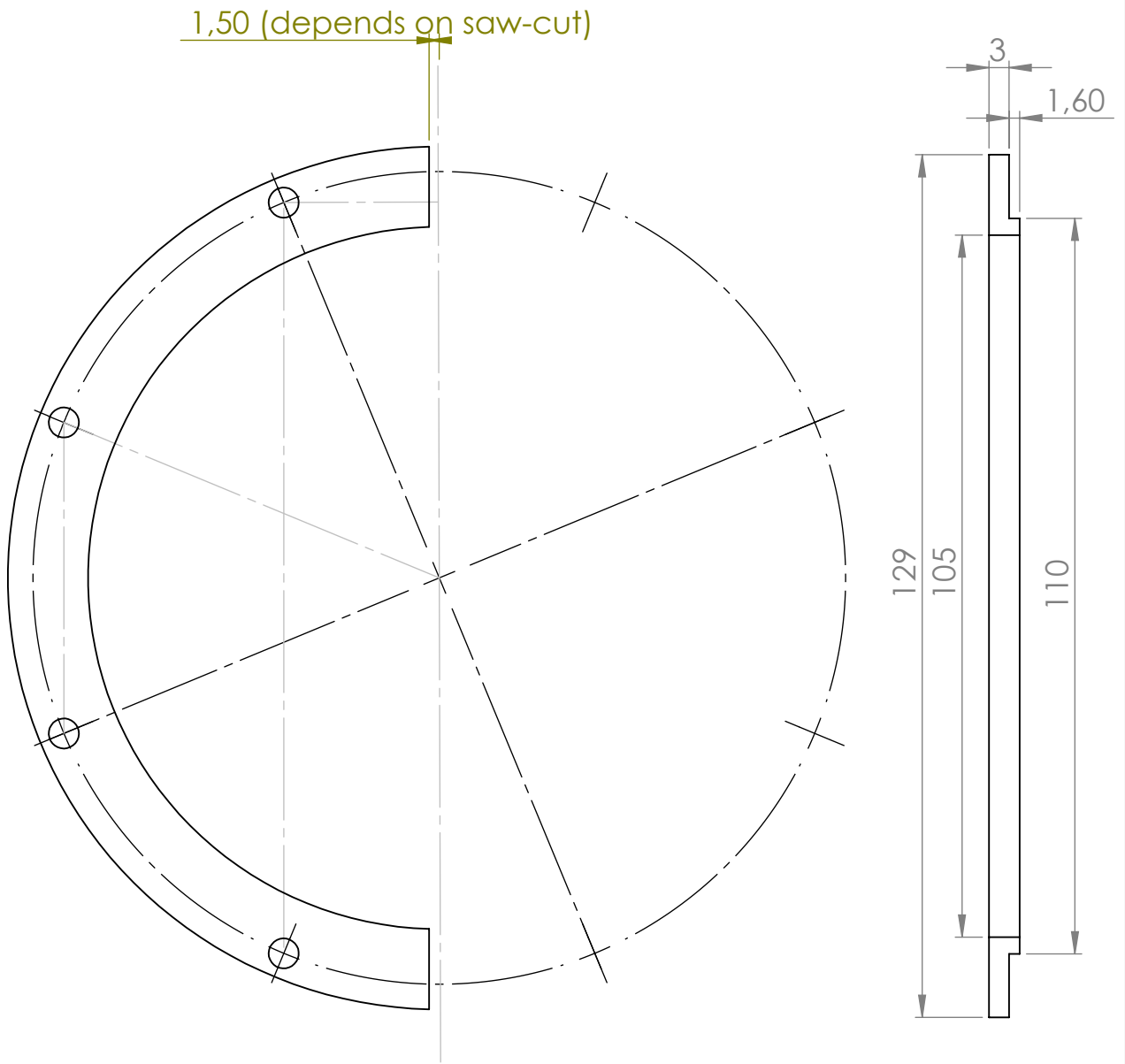
DEBUR AND
 BREAK SHARP
 EDGES

DO NOT SCALE DRAWING

REVISION

	NAME	SIGNATURE	DATE		
DRAWN					
CHK'D					
APPV'D					
MFG					
Q.A				MATERIAL:	
				WEIGHT:	

TITLE:	
DWG NO.	CC_mockup_fit
SCALE:1:2	A4
SHEET 1 OF 1	



UNLESS OTHERWISE SPECIFIED:
 DIMENSIONS ARE IN MILLIMETERS
 SURFACE FINISH:
 TOLERANCES:
 LINEAR:
 ANGULAR:

FINISH:

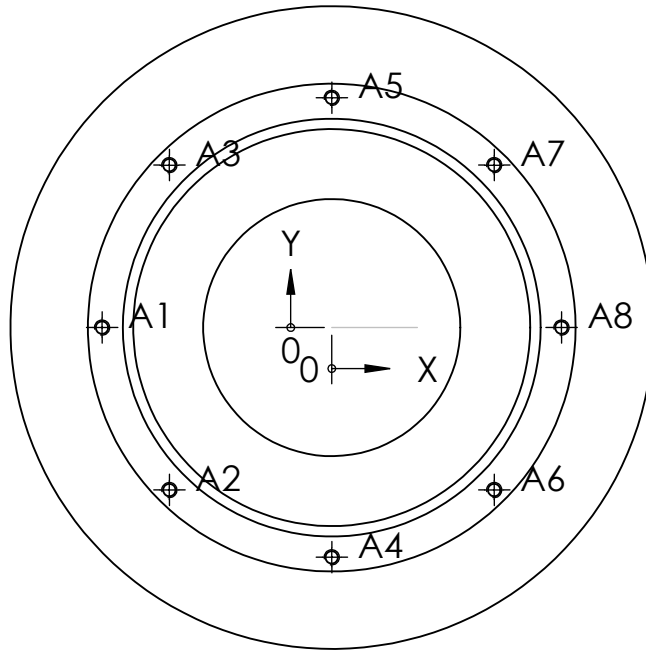
DEBUR AND
 BREAK SHARP
 EDGES

DO NOT SCALE DRAWING

REVISION

	NAME	SIGNATURE	DATE			
DRAWN						
CHK'D						
APPV'D						
MFG						
Q.A						
				MATERIAL:		
				6061?		
				WEIGHT:		

TITLE:	
DWG NO.	clamp_ring_comp_cover
SCALE:	1:1
SHEET	1 OF 1



TAG	X LOC	Y LOC	SIZE
A1	-60,7500	0	ϕ 3,30 ∇ 8 M4 - 6H ∇ 7
A2	-42,9567	-42,9567	ϕ 3,30 ∇ 8 M4 - 6H ∇ 7
A3	-42,9567	42,9567	ϕ 3,30 ∇ 8 M4 - 6H ∇ 7
A4	0	-60,7500	ϕ 3,30 ∇ 8 M4 - 6H ∇ 7
A5	0	60,7500	ϕ 3,30 ∇ 8 M4 - 6H ∇ 7
A6	42,9567	-42,9567	ϕ 3,30 ∇ 8 M4 - 6H ∇ 7
A7	42,9567	42,9567	ϕ 3,30 ∇ 8 M4 - 6H ∇ 7
A8	60,7500	0	ϕ 3,30 ∇ 8 M4 - 6H ∇ 7

UNLESS OTHERWISE SPECIFIED:
DIMENSIONS ARE IN MILLIMETERS
SURFACE FINISH:
TOLERANCES:
LINEAR:
ANGULAR:

FINISH:

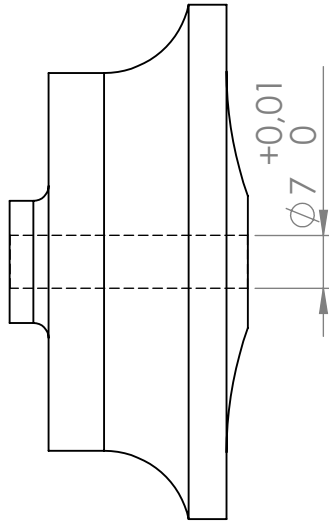
DEBUR AND
BREAK SHARP
EDGES

DO NOT SCALE DRAWING

REVISION

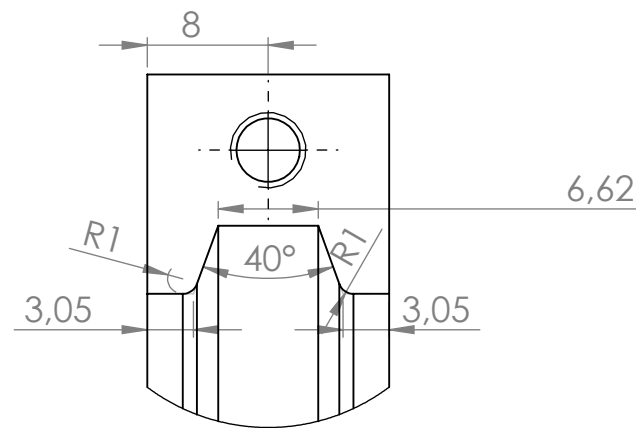
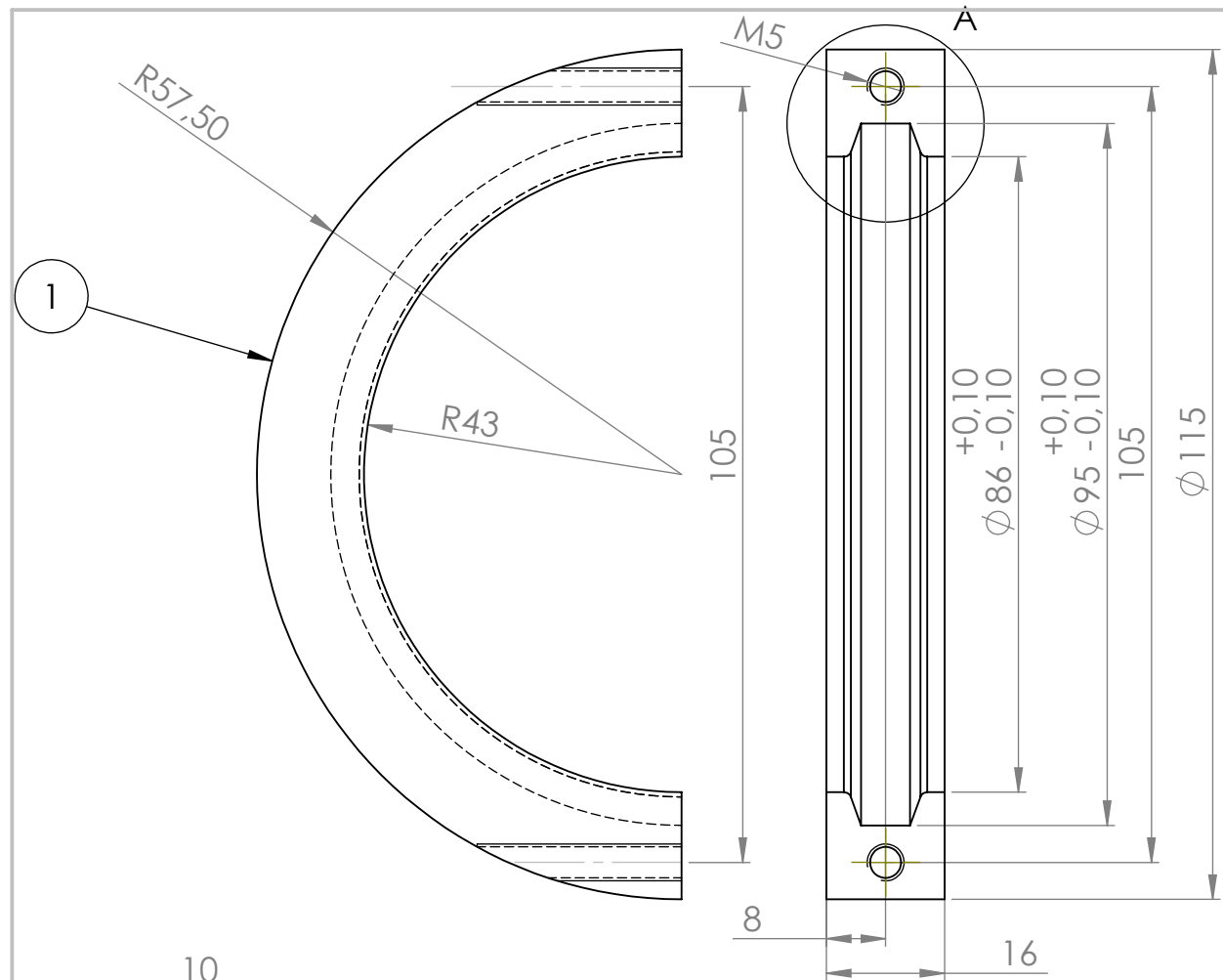
	NAME	SIGNATURE	DATE		
DRAWN					
CHK'D					
APPV'D					
MFG					
Q.A					
				MATERIAL:	
				WEIGHT:	

TITLE:	DWG NO.	SCALE:	SHEET
clamp_ring_hole_pattern		1:2	1 OF 1

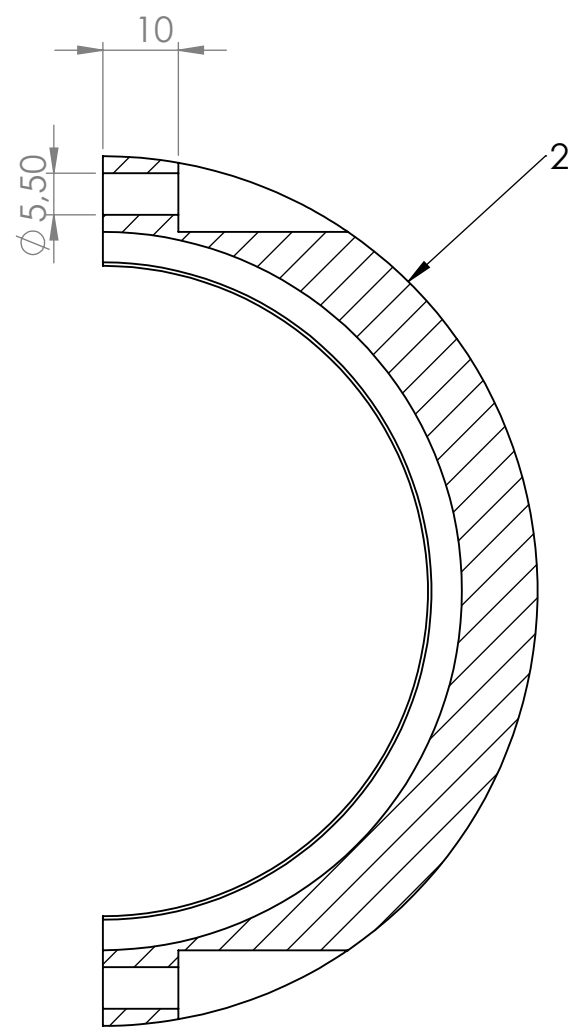


Ruimer $\phi 7 -0/+0.005$

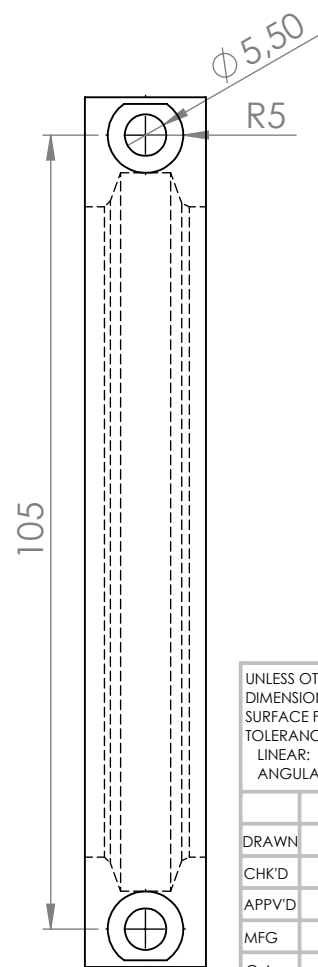
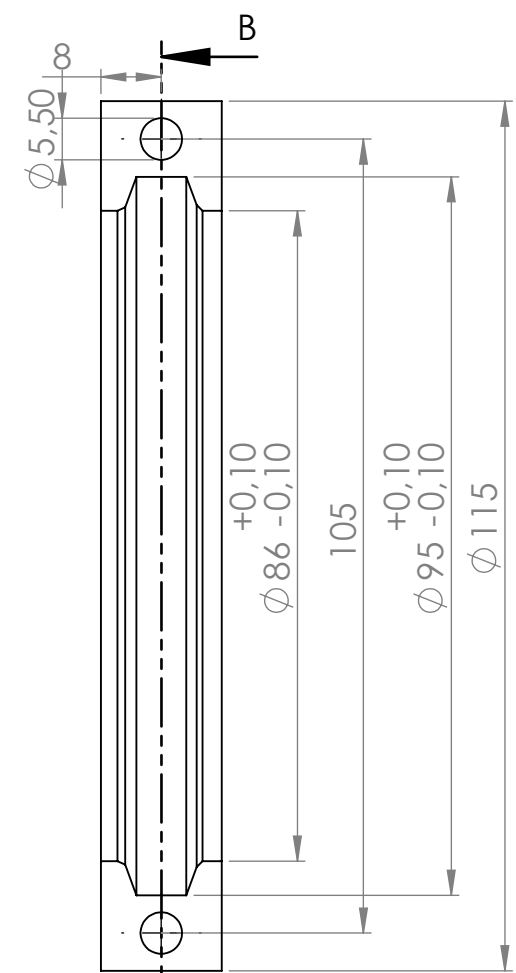
UNLESS OTHERWISE SPECIFIED: DIMENSIONS ARE IN MILLIMETERS SURFACE FINISH: TOLERANCES: LINEAR: ANGULAR:		FINISH:		DEBUR AND BREAK SHARP EDGES		DO NOT SCALE DRAWING		REVISION	
DRAWN		SIGNATURE		DATE		TITLE:			
CHK'D									
APPV'D									
MFG									
Q.A				MATERIAL:		DWG NO.		TD06H AM31	
						SCALE:1:1		A4	
				WEIGHT:		SHEET 1 OF 1			



DETAIL A
SCALE 2 : 1

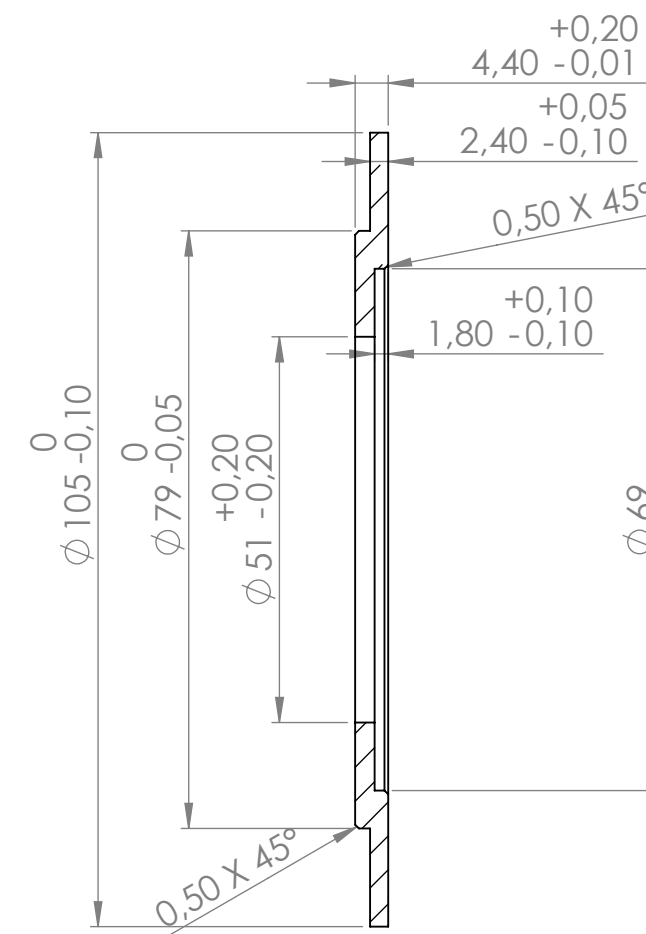
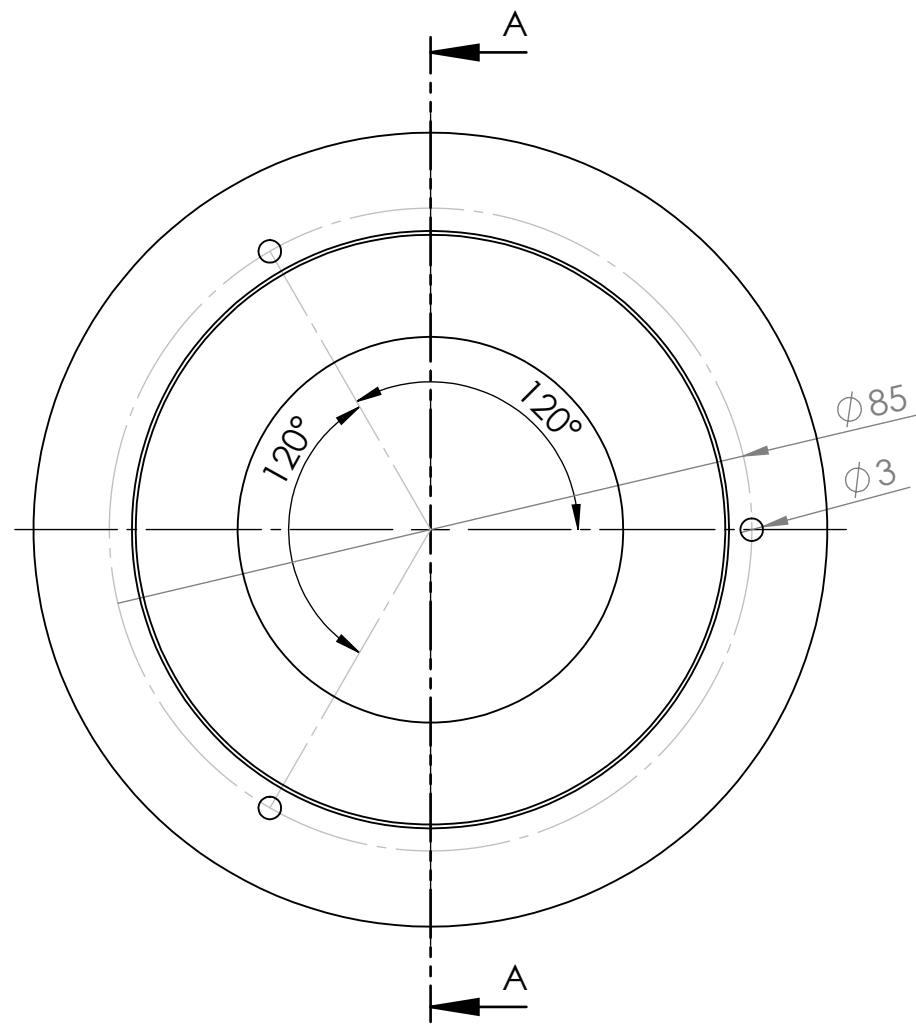


SECTION B-B



ITEM NO.	PART NUMBER	Material	QTY.
1	clamp_ring_thread	ST52	1
2	clamp_ring	ST52	1

UNLESS OTHERWISE SPECIFIED: DIMENSIONS ARE IN MILLIMETERS SURFACE FINISH: TOLERANCES: LINEAR: ANGULAR:				FINISH:	DEBUR AND BREAK SHARP EDGES	DO NOT SCALE DRAWING	REVISION
DRAWN	NAME	SIGNATURE	DATE			TITLE:	
CHK'D							
APPV'D							
MFG							
Q.A					MATERIAL:	DWG NO. clamp_ring_thread A3	
					WEIGHT:	SCALE:1:1	SHEET 1 OF 1



SECTION A-A

UNLESS OTHERWISE SPECIFIED: DIMENSIONS ARE IN MILLIMETERS SURFACE FINISH: TOLERANCES: LINEAR: ANGULAR:				FINISH:		DEBUR AND BREAK SHARP EDGES		DO NOT SCALE DRAWING		REVISION	
DRAWN				NAME		SIGNATURE		DATE		TITLE:	
CHK'D											
APPV'D											
MFG											
Q.A								MATERIAL:		DWG NO.	
								304		comp_washer	
								WEIGHT:		SCALE:1:1	
										SHEET 1 OF 1	
										A3	

Appendix D

Matlab Code

D1 Cycle Model

```
1 function [eff_overall, ...
    W_output,m_dot,v_dot2,rho_air2,rho_air4,fuel_consumption]= GTfunc(x)
2
3 %INPUTS ;
4 v_dot1 = x(1); %[kg/sec]
5 PR = x(2);
6 eff_comp = x(3);
7 T6 = x(4);
8 T4 = x(5);
9 eff_turb = x(6);
10 ER = x(7);
11 eff_shaft = x(8);
12 eff_generator = x(9);
13 eff_combustion= x(10);
14 C_fuel = x(11); % 45*10^6 for kerosene %[MJ/L]
15 rho_fuel = x(12); %[kg/L]
16 T1 = x(13); %[K]
17
18 %rho_air = 1.225; %[kg/m^3]
19 k_293 = 1.4;
20 k_1273 = 1.4;
21 Cp_293 = 1.005; %[kJ/kgK]
22 Cp_400 = 1.07; %[kJ/kgK]
23 Cp_1123 = 1.18; %[kJ/kgK]
24
25
26 %% compressor
27
28 % v_dot= 0.283; %[m^3/sec]          %%% INPUT!!!!
29 % m_dot = v_dot*rho_air; %[kg/sec]
30 P1 = 1; %[bar]
31 P2 = PR*P1; %[bar]
32
```

```

33 rho_air1=rhoair(P1,T1)
34
35 m_dot= v_dot1*rho_air1; %[m^3/sec]
36 h1 = T1*Cp_293;
37
38
39 %%T2 calculation
40 %computing T2 isentropic
41 T2s= T1*PR^((k_293-1)/k_293); %[K]
42
43 %computing actual T2
44 T2= (T2s-T1)/eff_comp+T1 %[K]
45 h2= (Cp_400)*T2;
46
47 W_comp = -m_dot*(h2-h1)
48
49 %% scroll
50
51 rho_air2 = rhoair(P2,T2);
52
53 A2= pi*(24.5e-3)^2; %[mm^2]
54
55 v_dot2= m_dot/rho_air2;
56 v2 = v_dot2/A2
57
58
59 %% Combuster
60
61 h4 = T4*Cp_1123;
62
63
64 rho_air4 = rhoair(ER,T4);
65
66 r4= 40e-3;
67 A4= pi*r4^2; %[mm^2]
68
69 v_dot4= m_dot/rho_air4;
70 v4 = v_dot4/A4
71
72
73 %% Turbine
74
75 syms mf_dot real
76
77 T5s = T4*(1/ER)^((k_1273-1)/k_1273);
78 T5 = T4-eff_turb*(T4-T5s)
79
80 h5 = T5*Cp_1123;
81
82 W_turb = (m_dot+mf_dot)*(h4-h5)
83
84
85 rho_air5 = rhoair(ER,T5)
86 %% Recuperator

```



```

87
88 if T5<T6
89     display('ERROR negative heat flux over recuperator')
90     return
91
92 else
93
94 T3 = T2 + T5 - T6
95
96 eff_recup = 100*(Cp_400*(T3-T2))/(Cp_400*(T5-T2)); % [%]
97
98 %% Combustion chamber
99
100
101
102
103 Q_in= m_dot*Cp_1123*(T4-T3); %[KJ/sec]
104
105
106 fuel_consumption = 3600*Q_in/(eff_combustion*C_fuel); %[L/hr]
107
108 mf_dot = ((rho_fuel/1000)*fuel_consumption)/(3600); %[kg/sec]
109
110
111 %% Power output
112
113 W_output = eff_shaft*eff_generator*(eval(W_turb)+W_comp);
114
115 eff_overall = (W_output/Q_in)*100; % [%]
116
117 eval(W_turb)
118
119 end

```

```

1 clear
2 close all
3 clc
4
5 %% TD-06 ->1/2Power
6
7
8 %INPUTS ;
9 v_dot1 = 0.1647; %[m^3/sec]
10 PR = 2.035;
11 eff_comp = 0.77;
12 T6 = 540+273;
13 T4 = 850+273;
14 eff_turb = 0.74;
15 ER = 0.9*PR;%1.8;
16 eff_shaft = 0.98;
17 eff_generator = 0.95;
18 eff_combustion = 0.95;

```

```

19 RPM = 105*10^3;
20 C_fuel = 20*10^3; %[kJ/L]
21 rho_fuel = 1346; %[kg/m^3]
22 T1 = 15+273; %[K]
23
24
25 %% Test configuration
26
27 % %INPUTS ;
28 % v_dot1 = 0.1492; %[m^3/sec]
29 % PR = 2.1;
30 % eff_comp = 0.74;
31 % T6 = 300+273;
32 % T4 = 850+273;
33 % eff_turb = 0.74;
34 % ER = 0.9*PR;%1.8;
35 % eff_shaft = 0.98;
36 % eff_generator = 0.95;
37 % eff_combustion = 0.9;
38 % RPM = 105*10^3;
39 % C_fuel = 20*10^3; %[kJ/L]
40 % rho_fuel = 700; %[kg/m^3]
41 % T1 = 15+273; %[K]
42
43 %% general function
44 x=[ v_dot1 PR eff_comp T6 T4 eff_turb ER eff_shaft eff_generator ...
    eff_combustion C_fuel rho_fuel T1];
45
46 [eff_overall, ...
    W_output,m_dot,v_dot2,rho_air2,rho_air4,fuel_consumption]=GTfunc(x);
47
48 Flow_para = m_dot*sqrt(T4)/(PR/0.98);
49 CRPM = RPM/sqrt(T4);
50
51 m_dotfuel = fuel_consumption*rho_fuel/1000 %[kg/hr]
52 sigma_mass = (m_dot*3600)/m_dotfuel
53 sigma_volume = (v_dot2*3600)/(fuel_consumption/1000)
54 Stoichratio = 9;
55 phi = 1.8;
56 Stoichm = Stoichratio*m_dotfuel/(3600*m_dot)*100; %[%]
57 Swirl_m= m_dotfuel/3600*Stoichratio/phi; % mass of air needed for rich ...
    combustion going through swirler [kg/sec]
58 Swirl_mp= 100-((m_dot-Swirl_m)/m_dot)*100
59
60 %% Display results
61
62 disp(['Power ' num2str(W_output) ' kW'])
63 disp(['Efficiency ' num2str(eff_overall) ' %'])
64 disp(['Fuel consumption ' num2str(fuel_consumption) ' L/hr'])
65 disp(['Turbine flow parameter ' num2str(Flow_para)])
66 disp(['Corrected RPM ' num2str(CRPM)])

```

```

1 clear all
2 close all
3 clc
4
5 mdot=0.1993;
6 Cp_400 = 1070;
7 Cp_1173= 1400;
8 k = 0.0313;
9 Pr = 0.69;
10 mu = 22.5e-6;
11
12 Ti1 = 370;
13 To1 = 990;
14 Tcase = (Ti1+To1)/2;
15
16 r1=202e-3/2;
17 r2=208e-3/2;
18 L =450e-3;
19
20 At=2*pi*r2*L; % heat transfer area
21 Af= pi*(r2^2-r1^2); %flow area
22 P = 2*pi*(r1+r2);
23
24 Dh = 4*Af/P; %hydraulic diameter
25
26 Re = (mdot/Af)*Dh/mu;
27
28 f = (0.790*log((Re)/log(exp(1)))-1.64)^-2;
29
30 Nu= 0.023*(Re^0.8)*(Pr^0.4);
31
32 hc=(k/Dh)*Nu
33
34
35 Ti2=Tcase-(Tcase-Ti1)*exp((-1*hc*At)/(mdot*Cp_400))
36
37
38 Q=(Ti2-Ti1)*mdot*Cp_400
39
40 eff_recup = 100*(Ti2-Ti1)/(To1-Ti1)
41
42 dTi=Ti2-Ti1
43 dh=dTi*Cp_400
44 dTo= dh/Cp_1173

```

D2 Recuperator Calculations

The behaviour of the recuperator is modelled using the equations 3.13. The geometry is simplified to a construction of two concentric tubes. For the calculation the following assumptions have been made:

- Fuel mass flow is neglected
The mass flows through the cold and hot sides are assumed equal.
- Constant Cp
The Cp is assumed constant over the hot and cold side
- constant k
The thermal conductivity is assumed constant over the hot and cold side
- Constant Prandtl number
- No heatloss to the outside world
- Thermal conductivity within stainless steel sheets is assumed to be very high in comparison to the air properties.

The thermal resistance thin stainless steel boundary can be neglected as the thermal conductivity is high and it acts lumped.

The applied boundary conditions can be found in Table 6.6

Parameter	Value
\dot{m}	0.1993 kg/s
Diameter 1	202 mm
Diameter 2	208mm
Diameter 3	240 mm
Length	450 mm
k cold	0.0313 W/mK
k hot	0.0627 W/mK
Pr	0.69
Cp hot	1.4 kJ/kgK
Cp cold	1.07 kJ/kgK

Table D.1: Boundary conditions used for recuperator calculations

When the equations mentioned earlier are applied the recuperator behaviour generates the results as seen in table 4.2.

D3 Matching model

```

1 clear
2 close all
3 clc
4
5 TIT = 700+273; % INPUT [K]
6 PR = 1.55; % INPUT
7 v_dot = 0.1; % INPUT m3/sec
8 rho = 1.225;
9 m_dot = rho*v_dot; %[kg/sec]
10
11 % TIT = 850+273; % INPUT [K]
12 % PR = 2.035; % INPUT
13 % v_dot = 0.1647; % INPUT m3/sec
14 % rho = 1.225;
15 % m_dot = rho*v_dot; %[kg/sec]
16
17 % Cp_1273 = 1.18;
18 % nt = 0.64
19 % Pt = m_dot*Cp_1273*1273*(1-(1/1.9)^(0.4/1.4))*nt
20
21 Poi = 0.9*PR;
22 flowpoi = m_dot*sqrt(TIT)/(PR/0.98)
23 RPMoi = 105000;
24 CRPMoi = RPMoi/sqrt(TIT)
25 v_dotoi= v_dot
26
27 %% Compressor
28
29 % TD06H_16KX3s(PR, v_dotoi, RPMoi)
30
31
32
33 %% Turbine
34 % TD04HL_F70(Poi, flowpoi, RPMoi, TIT)
35 %
36 % TD05H_AM(Poi, flowpoi, RPMoi, TIT);
37 %
38 % TD06_F14(Poi, flowpoi, RPMoi, TIT);
39 %
40 TD07S_F13(Poi, flowpoi, RPMoi, TIT);

```

D4 Post-process script

```

1 function [fft_block, fft_time, fft_freq, max_amp] = compute_fft(block, ...
    Tend, fs, NFFT, useHanning, usedB)

```

```

2 % [fft_block, fft_time, fft_freq, max_amp] = compute_fft(block, Tend, ...
   fs, NFFT, useHanning, usedB)
3 % The function 'compute_fft' computes the Fast Fourier Transform of a data
4 % block and can optionally return the maximum amplitude of this FFT.
5 % The Hanning window and a log10 scaling are used automatically, but ...
   can be
6 % switched off.
7 if nargin < 6
8     usedB = 1;
9 end
10 if nargin < 5
11     useHanning = 1;
12 end
13 if nargin < 4 || NFFT == 0
14     NFFT = size(block,1);
15 end
16
17 nblocks = size(block, 2);
18
19 tloss = Tend/(2*nblocks);
20 fft_time = linspace(tloss, Tend-tloss, nblocks);
21
22 fft_freq = linspace(0,fs/2,NFFT/2);
23
24 if useHanning
25     hanWin = hanning(size(block,1),'periodic');
26     repBlk = repmat(hanWin, 1, nblocks);
27     block = block .* repBlk;
28 end
29
30 % FFT computation
31 fft_block = fft(block,NFFT);
32 fft_block = (useHanning+1)*abs(fft_block)/size(block,1)*2;
33 fft_block = fft_block(1:length(fft_freq),:);
34 max_amp = max(fft_block);
35 if usedB
36     fft_block = 20*log10(fft_block);
37 end
38
39 end

```

```

1 clear all
2 close all
3 clc
4
5 load('Usable_data.mat')
6 fieldnames = fieldnames(Usable_data);
7
8 RE100 = fieldnames{1};
9 RE90_1 = fieldnames{2}; % Not being used
10 RE90_2 = fieldnames{3};
11 RD_1 = fieldnames{4}; % Not being used

```

```

12 RD_2 = fieldnames{5};
13 SRQLE90 = fieldnames{6};
14 SRQLE100_2 = fieldnames{7};
15 SRQLE100_1 = fieldnames{8}; % Not being used
16 RE100_N4 = fieldnames{9}; % Not being used
17 RQLE90 = fieldnames{10};
18 RQLE100 = fieldnames{11};
19
20 % Tests used for plotting
21 fields=[3 1 6 7 10 11];
22
23 var = cell(11,1);
24 var{1} = 'Testtime';
25 var{2} = 'T_FUEL_IN';
26 var{3} = 'P_C_OUT';
27 var{4} = 'T_C_OUT';
28 var{5} = 'P_T_IN';
29 var{6} = 'T_T_IN';
30 var{7} = 'n_TC2';
31 var{8} = 'T_X_1';
32 var{9} = 'AI_V_2';
33 var{10}= 'P_T_OUT';
34 var{11}= 'T_T_OUT';
35
36 %% filter
37
38 for i=fields;
39 for j=2:1:11 ;
40 a = 1;
41 b = ones(1,8)*1/8;
42 Usable_data.(fieldnames{i}).(var{j})= ...
    filter(b,a,Usable_data.(fieldnames{i}).(var{j}));
43 Usable_data.(fieldnames{i}).(var{j})= ...
    Usable_data.(fieldnames{i}).(var{j})(20:end,1);
44 end
45 end
46
47 fieldnames_neat{1}= 'Rich 90%'
48 fieldnames_neat{2}= 'Rich 100%'
49 fieldnames_neat{3}= 'SRQL 90%'
50 fieldnames_neat{4}= 'SRQL 100%'
51 fieldnames_neat{5}= 'RQL 90%'
52 fieldnames_neat{6}= 'RQL 100%'
53
54
55 %% FFT and plot
56
57 figure
58 y=0;
59 for i=fields
60 y=y+1;
61 subplot(3,2,y)
62 q=0;
63 for p=2:1:11

```

```

64 q=q+1;
65 X=Usable_data.(fieldnames{i}).(var{p});
66
67 fs = 10;           % Sampling frequency
68 T = 1/fs;         % Sampling period
69 L = length(X);    % Length of signal
70 t = (0:L-1)*T;    % Time vector
71 X=X(1:length(t));
72 nfft=0;
73
74 [fft_out, fft_time, fft_freq, max_amp] = compute_fft(X, t(end), fs, ...
    nfft, 0, 0);
75 fft_outh = compute_fft(X, t(end), fs, nfft, 1, 0);
76 % FT=fft(X);
77
78 semilogy(fft_freq, abs(fft_out))
79 axis([0 1 10e-6 10e6])
80 xlabel('Frequency [Hz]')
81 ylabel('Magnitude')
82 grid on
83 hold on
84 legendlist{q}=var{p};
85 % title((fieldnames{i}));
86 title((fieldnames_neat{y}));
87 end
88 legend(legendlist, 'location', 'SouthEastOutside')
89 end

```

```

1  %%% Import data excel files
2  %%% made by: Patrick Dettmers
3  %%% 13-6-2015
4
5  clear
6  close all
7  clc
8
9  %%
10
11 display('Start importing data-file')
12 filename = 'GT_ReX_AllTests.xls';
13
14 [status,sheetnames] = xlsfinfo(filename);
15
16 for j=1:length(sheetnames)
17 sheetname= sheetnames{j};
18 [data,name,row] = xlsread(filename, (sheetname));
19
20 names = row(1,:);
21 units = row(2,:);
22
23
24 %% generate structure

```



```

25
26     for i=1:1:length(names);
27
28         name=names{i};
29         Testdata.(sheetname).(name)=data(:,i);
30
31
32     end
33
34 end
35
36 save('Testdata','Testdata')
37
38
39 %% Remove unwanted data
40
41 %limits
42 Lim(1,:) = [410  910];
43 Lim(2,:) = [1796 2700];
44 Lim(3,:) = [1400 1800]; %[559 1600];
45 Lim(4,:) = [2000 2400];
46 Lim(5,:) = [1150 1500]; % [3200 3600]; %[1200 2200];
47 Lim(6,:) = [717 1333]; % best [2500 3000]; [600 900];
48 Lim(7,:) = [1200 1350]; %[623 852];
49 Lim(8,:) = [100 300];
50 Lim(9,:) = [39 400];
51 Lim(10,:) = [1496 2124]; %[1150 1350];
52 Lim(11,:) = [2736 5546]; %[4500 5546];
53
54 %removed data-sets
55 rem_data = [2 4 8]';
56
57 % Adjust data-structure
58
59 for k=1:1:length(sheetnames)
60     sheetname= sheetnames{k};
61     for p=1:1:length(names);
62         name=names{p};
63         Usable_data.(sheetname).(name) = ...
            Testdata.(sheetname).(name) (Lim(k,1):Lim(k,2));
64
65         for n=1:1:length(rem_data)
66             if k == rem_data(n);
67                 Usable_data.(sheetname).(name) = zeros((Lim(k,2)-Lim(k,1)),1);
68             else
69                 end
70         end
71     end
72 end
73
74 save('Usable_data','Usable_data')
75
76
77

```

```

78
79
80
81 display('finished exporting .mat file')

```

```

1  %%% plot measured data
2  %%% made by: Patrick Dettmers
3  %%% 13-6-2015
4
5  clear
6  close all
7  clc
8
9  %% load data file
10
11 addpath('line_fewer_markers_v4');
12 load('Usable_data.mat');
13 load('Testdata.mat');
14
15 % Usable_data=Testdata
16
17 fieldnames = fieldnames(Usable_data);
18
19 RE100 = fieldnames{1};
20 RE90_1 = fieldnames{2}; % Not being used
21 RE90_2 = fieldnames{3};
22 RD_1 = fieldnames{4}; % Not being used
23 RD_2 = fieldnames{5};
24 SRQLE90 = fieldnames{6};
25 SRQLE100_2 = fieldnames{7};
26 SRQLE100_1 = fieldnames{8}; % Not being used
27 RE100_N4 = fieldnames{9}; % Not being used
28 RQLE90 = fieldnames{10};
29 RQLE100 = fieldnames{11};
30
31 % Tests used for plotting
32 fields=[1 3 5 6 7 10 11];
33
34 var = cell(11,1);
35 var{1} = 'Testtime';
36 var{2} = 'T_FUEL_IN';
37 var{3} = 'P_C_OUT';
38 var{4} = 'T_C_OUT';
39 var{5} = 'P_T_IN';
40 var{6} = 'T_T_IN';
41 var{7} = 'n_TC2';
42 var{8} = 'T_X_1';
43 var{9} = 'AI_V_2';
44 var{10} = 'P_T_OUT';
45 var{11} = 'T_T_OUT';
46 % var{12} = 'P_{drop CC}[%]';
47

```

```

48 var_neat = cell(11,1);
49 var_neat{1} = 'Testtime [s]';
50 var_neat{2} = 'T_{FUEL} IN [C]';
51 var_neat{3} = 'P_{C} OUT [mbar]';
52 var_neat{4} = 'T_{C} OUT [C]';
53 var_neat{5} = 'P_{T} IN [mbar]';
54 var_neat{6} = 'T_{T} IN [C]';
55 var_neat{7} = 'n_{TC} [RPM]';
56 var_neat{8} = 'T_{exhaust} [C]';
57 var_neat{9} = 'Fuel flow [LPH]';
58 var_neat{10}= 'P_{T} OUT [mbar]';
59 var_neat{11}= 'T_{T} OUT [C]';
60 % var_neat{12}= 'P_{drop CC}[%]';
61
62 fieldnames_neat{1}= 'Rich 90%'
63 fieldnames_neat{2}= 'Rich 100%'
64 fieldnames_neat{3}= 'SRQL 90%'
65 fieldnames_neat{4}= 'SRQL 100%'
66 fieldnames_neat{5}= 'RQL 90%'
67 fieldnames_neat{6}= 'RQL 100%'
68
69 % correct fuel flow for energy content
70 D_energy    = 39e3; % MJ/Liter
71 E100_energy = 21.28e3; % MJ/Liter
72 E90_energy  = 19.67e3; % MJ/Liter
73
74 % moving average filter
75 for i=fields;
76 for j=9 ;
77 a = 1;
78 b = ones(1,8)*1/8;
79 Usable_data.(fieldnames{i}).(var{j})= ...
    filter(b,a,Usable_data.(fieldnames{i}).(var{j}));
80 % Usable_data.(fieldnames{i}).(var{j})= ...
    Usable_data.(fieldnames{i}).(var{j})(20:end,1);
81 end
82 end
83
84
85 % % compute pressure drop over liner
86 % v=0;
87 % for i=fields
88 % v=v+1;
89 % P_drop(1:length(Usable_data.(fieldnames{i}).(var{3})),v) = ...
    (100*(Usable_data.(fieldnames{i}).(var{3})-Usable_data.(fieldnames{i}).(var{5}))...
90 %     ./Usable_data.(fieldnames{i}).(var{3}));
91 %
92 % Usable_data.(fieldnames{i}).(var{11})= ...
    P_drop(1:length(Usable_data.(fieldnames{i}).(var{3})),v);
93 % end
94
95
96
97 % compute mean RPM

```

```

98 % memory allocation
99 Mean_RPM = ones(1,7);
100 q=0;
101 for i=fields;
102 q=q+1;
103     Mean_RPM(q)=mean(Usable_data.(fieldnames{i}).(var{7}));
104
105 end
106
107 %% average to single point
108
109
110 % for i=fields
111 % for h=1:1:length(var)
112 %     ...
113     Averaged_data.(fieldnames{i}).(var{h})=mean(Usable_data.(fieldnames{i}).(var{h}));
114 % end
115
116 % v=0;
117 % for i=fields
118 % v=v+1;
119 % p=0;
120 % for h=1:1:length(var)
121 %     p=p+1;
122 %     Table_data(p,v) = Averaged_data.(fieldnames{i}).(var{h});
123 % end
124 % end
125 % Table_data(1:11,2:8)=Table_data
126 % Table_data=mat2cell(Table_data,11,8)
127 % Table_data(1:11,1)=var_neat;
128 %
129 % filename = 'average_table.xlsx';
130 % xlswrite(filename,Table_data)
131
132 %
133 % for i=fields;
134 % if i== 1||i==7||i==11
135 %     comp_factor=E100_energy;
136 % else
137 % end
138 % if i== 3||i==6||i==10
139 %     comp_factor=E90_energy;
140 % else
141 % end
142 % if i== 5
143 %     comp_factor=D_energy;
144 % else
145 % end
146 %
147 % ...
148     Usable_data.(fieldnames{i}).(var{9})=Usable_data.(fieldnames{i}).(var{9})*comp_factor/6;
149 % end

```

```

150 % convert L/min to L/h
151 for i=fields
152 Usable_data.(fieldnames{i}).(var{9})=Usable_data.(fieldnames{i}).(var{9})*60;
153 end
154
155
156
157
158 % compute turbine corrected RPM
159 colorscheme_data = [{'r.'} {'b.'} {'k.'} {'y.'} {'g.'} {'c.'} {'m.'}];
160 % colorscheme_area = [{'r'} {'g'} {'k'} {'g'} {'r'} {'g'} {'r'}]; % ...
    sorted by fuel type
161 colorscheme_area = [{'b'} {'b'} {'b'} {'g'} {'g'} {'r'} {'r'}]; % ...
    sorted by CC type
162 colorscheme_lin = [{'-r*'} {'-g*'} {'-k*'} {'g'} {'r'} {'gs'} {'rs'}];
163
164 % memory allocation
165 corrected_RPM=ones(2811,7);
166 q=0;
167 for i=fields
168 q=q+1;
169 for r=1:length(Usable_data.(fieldnames{i}).(var{7}));
170 corrected_RPM(r,q)= ...
    Usable_data.(fieldnames{i}).(var{7})(r)/sqrt(Usable_data.(fieldnames{i}).(var{6})(r)+27);
171
172 end
173 end
174
175 %% plot energy input (fuel) vs corrected RPM
176 if 0
177
178 figure
179 q=0;
180 for i=fields
181 q=q+1;
182 plot(corrected_RPM(1:length(Usable_data.(fieldnames{i}).(var{9})),q),Usable_data.(fieldnames{i}).(var{9}));
183 axis([2200 2600 50 150]);
184 grid on;
185 hold on;
186 lin_fit = ...
    polyfit(corrected_RPM(1:length(Usable_data.(fieldnames{i}).(var{9})),q),Usable_data.(fieldnames{i}).(var{9}));
187 x=linspace(2200,2600,length(Usable_data.(fieldnames{i}).(var{9})));
188 y=lin_fit(1)*x+lin_fit(2);
189 % plot(x,y,(colorscheme_lin{q}))
190 line_fewer_markers(x, y, 20,(colorscheme_lin{q}));
191 hold on;
192
193 X=corrected_RPM(1:length(Usable_data.(fieldnames{i}).(var{9})),q);
194 [K,V]=convhull(corrected_RPM(1:length(Usable_data.(fieldnames{i}).(var{9})),q),Usable_data.(fieldnames{i}).(var{9}));
195 % ...
    plot(corrected_RPM(1:length(Usable_data.(fieldnames{i}).(var{9})),q),Usable_data.(fieldnames{i}).(var{9}));
196 % hold on
197 patch(X(K),Usable_data.(fieldnames{i}).(var{9})(K),(colorscheme_area{q}),'Facealpha',0.3);
198 xlabel('corrected turbine RPM [RPM K^{0.5}]')

```

```

199 ylabel('Burner power [kW]')
200 legendlist{3*q-2} = fieldnames{i};
201 legendlist{3*q-1} = fieldnames{i};
202 legendlist{3*q} = fieldnames{i};
203 end
204 title('Energy/RPM plot')
205 legend(legendlist, 'Location', 'NorthEastOutside');
206
207
208 end
209
210 %% plot data all test for 1 paramater
211 if 1
212
213 fields=[3 1 6 7 10 11];
214
215
216 y=0;
217 for j= 2:1:length(var)
218 y=y+1;
219 figure
220 p=0;
221 for i=fields
222 p=p+1;
223 t=linspace(0,length(Usable_data.(fieldnames{i}).(var{1}))(20:end,1))/10,length(Usable_data.(
224 subplot(3,2,p)
225 plot(t,Usable_data.(fieldnames{i}).(var{j}))(20:end,1))
226 mu = mean(Usable_data.(fieldnames{i}).(var{j}))(20:end,1));
227 hline = reline([0 mu]);
228 hline.Color = 'r';
229 grid on
230 % title(fieldnames{i});
231 title((fieldnames_neat{p}));
232 supitle(var_neat{j});
233 xlabel(var_neat{1});
234 ylabel(var_neat{j});
235
236
237
238 n(i)=mean(Usable_data.(fieldnames{i}).n_TC2);
239
240 end
241
242 end
243
244 end
245 %% plot data all parameters of 1 test
246 if 0
247
248 Y=11; %fieldname (Testcase)
249 figure
250 plot(Testdata.(fieldnames{Y}).n_TC2);
251
252 figure

```

```
253 u=0;
254 for j= 2:1:length(var)
255 u=u+1;
256 subplot(4,3,u);
257 plot(Usable_data.(fieldnames{Y}).(var{j}));
258 mu = mean(Usable_data.(fieldnames{Y}).(var{j}));
259 hline = reffline([0 mu]);
260 hline.Color = 'r';
261 title(var{j});
262 suptitle(fieldnames{Y}) ;
263 grid on;
264 end
265
266 figure
267 u=0;
268 for j= 2:1:length(var)
269 u=u+1;
270 subplot(4,3,u)
271 plot(Testdata.(fieldnames{Y}).(var{j}));
272 mu = mean(Testdata.(fieldnames{Y}).(var{j}));
273 hline = reffline([0 mu]);
274 hline.Color = 'r';
275 title(var{j});
276 suptitle(fieldnames{Y}) ;
277 grid on
278 end
279 hold off
280
281
282 %%%
283 figure
284 u=0;
285 for j= 2:1:length(var)
286 u=u+1;
287 subplot(4,3,u);
288 plot(Usable_data.(fieldnames{5}).(var{j}));
289 mu = mean(Usable_data.(fieldnames{5}).(var{j}));
290 hline = reffline([0 mu]);
291 hline.Color = 'r';
292 title(var{j});
293 suptitle(fieldnames{5});
294 grid on;
295 end
296 %%%
297
298
299 end
```

Appendix E

Generator data

Outer diameter	22 mm
Inner diameter	8 mm
Thickness	7 mm
Limiting speed (grease)	124 kRPM
Dynamic load	336 kgf
Basic load	173 kgf
Contact angle	15 degrees
Race material	440C
Rolling element material	Si ₃ N ₄
Enclosure	Open, full complement

Table E.1: Specifications of D608/602C hybrid full complement angular contact bearing

- Built-in motor
- Motor design
- High-speed motor
- Services

Postfach
CH-4313 Möhlin
Switzerland

Tel.: +41 (0)61 855 92 92
Fax: +41 (0)61 855 92 99
E-Mail: info@EundA.ch
Internet: www.EundA.ch

data sheet type mSpW 6/8 - 2 - a10 ENCA

DBL 151515

2 pole model

The e + a - medium - frequency motor elements are wound stators and PM-rotors, of which high-speed synchronous motors can be made.

winding: insulation class F, maximal permissible heating up 120K with a coolant temperature of 20°C
 connection leads: insulation class H, Teflon insulated
 rotor: material : permanent magnets, max. temperature 150°C circumferential speed: v = 192.4 m/s

material of shaft: magnetic hollow shaft: none
 cooling method: water

For machining and handling of the motorelements it's categorial necessary to note the precautions !
 Electrical data only valid with the according inverter data !

speed	n	1/min * 10 ³	105			
frequency	f	Hz	1750			
power	P_{S1}	kW	10			
peak power		kW				
voltage	U	V	280			
current	I	A	22			

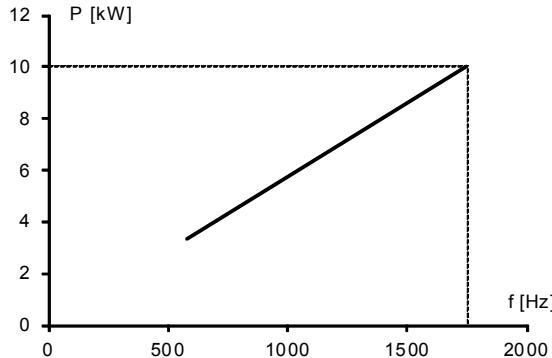
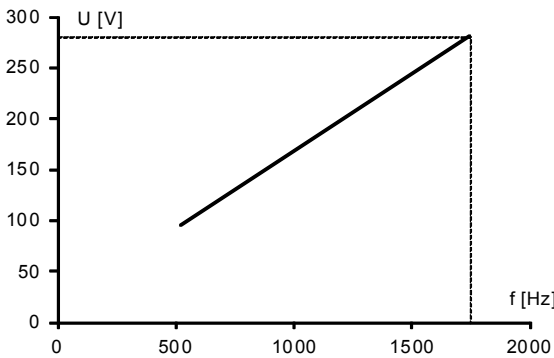
ID-Nr. a10/10S2
 KD-Nr. S: _____
 R: _____

The power apply to sinusoidal current and sinusoidal voltage.

With an operation at static frequency inverter the currents can be 10-15% higher depending on execution.

The **input power** in VA is calculated to: $S = \sqrt{3} \cdot U \cdot I$.
 Once the motor assembly is finished by the customer, the respective tests according to the norm **EN 60034-1** have to be conducted.

In any case the effective applied voltage must suit for reaching the power.

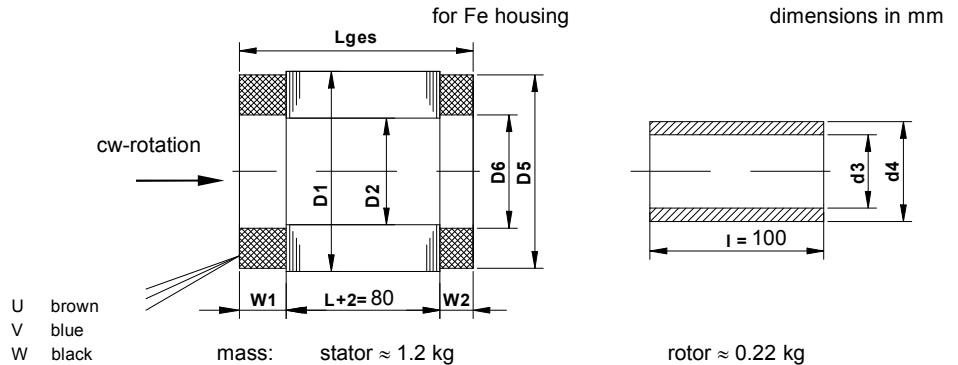


The torque computes itself to:

$$M = \frac{9550 \cdot P}{n} \quad [\text{Nm}]$$

- with label on Enca
- 2 thermo sensor KTY 84-130

Enca-design



connection leads	length	400 mm	D1= 60 +0.051/+0.032	D5= 58	W1= 20 0/-1	d4≈ 33.7 not to machine
	cross section	1.23 mm ²	Finished by e+a			
	diameter	2.4 mm	D2= 35 JS9	D6= 36	W2= 17 0/-1	d3≈ 26 according to e+a drawing no.: 100912-004.021

cable outlet according to e+a drawing no.: 290505-004.011.001

push-in path = 7 distance to push the rotor onto the conus of the shaft max. permissible oil pressure
 Pmax = 1150 bar

²⁾ finished by customer

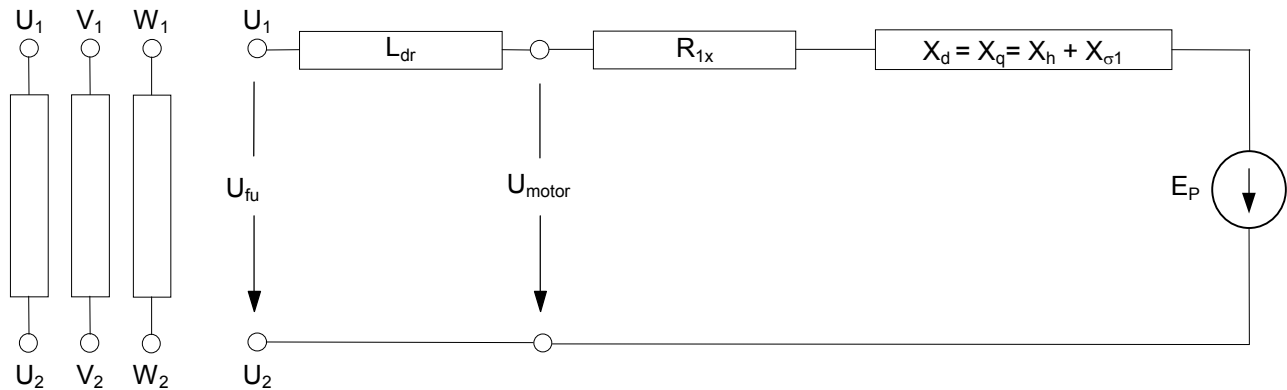
Synchronmotor-Ersatzschaltbilddaten synchronous motor equivalent circuit diagram data



Motor Typ **mSpW 6/8-2-a10 ENCA**
motor type

Datenblatt **DBL 151515**
data sheet

Einphasiges Ersatzschaltbild / one-phase equivalent circuit diagram



Bezeichnung description	Formelz. symbol	Wert value	Einheit unit	Bemerkung remarks
Nennleistung / rated power	P_N	10	kW	S1-Betrieb / S1 duty
Motorspannung / motor voltage	U_{motor}	162	V	
Nennfrequenz / rated frequency	f_N	1750	Hz	
Nennstrom / rated current	I_N	22	A	
Schaltungsart / circuit connection	Y oder /or D	Y		
Umrichter-Ausgangsspannung / inverter output voltage	U_{fu}	162	V	
Vorschalttdrossel / series choke	L_{dr}	0	mH	
Ständerwiderstand kalt (20°) phase stator resistance, cold (20°)	R_{1x}	0.0781	Ω	
Ständerstreureaktanz / phase stator leakage reactance	$X_{\sigma1}$	0.56	Ω	
Hauptfeldreaktanz / phase main field reactance	X_h	4.07	Ω	
Synchrone Motorreaktanz synchronous phase motor reactance	$X_d = X_q$	4.63	Ω	
Polradspannung / magnet wheel voltage	E_p	185	V	
Spannungskonstante / back EMF constant	k_E	3.05	V/krpm	bei 100°C / at 100°C
Drehmomentkonstante / torque constant	k_M	0.0413	Nm/A	
Maximale Umrichter-Ausgangsspannung maximum inverter output voltage	$U_{fu,max}$	280	V	verkettet phase-to-phase
Motorhauptfeldinduktivität / motor main field inductance	L_h	0.369	mH	
Motorstreuinduktivität / motor leakage inductance	$L_{1\sigma}$	0.0508	mH	

Motordaten / motor data

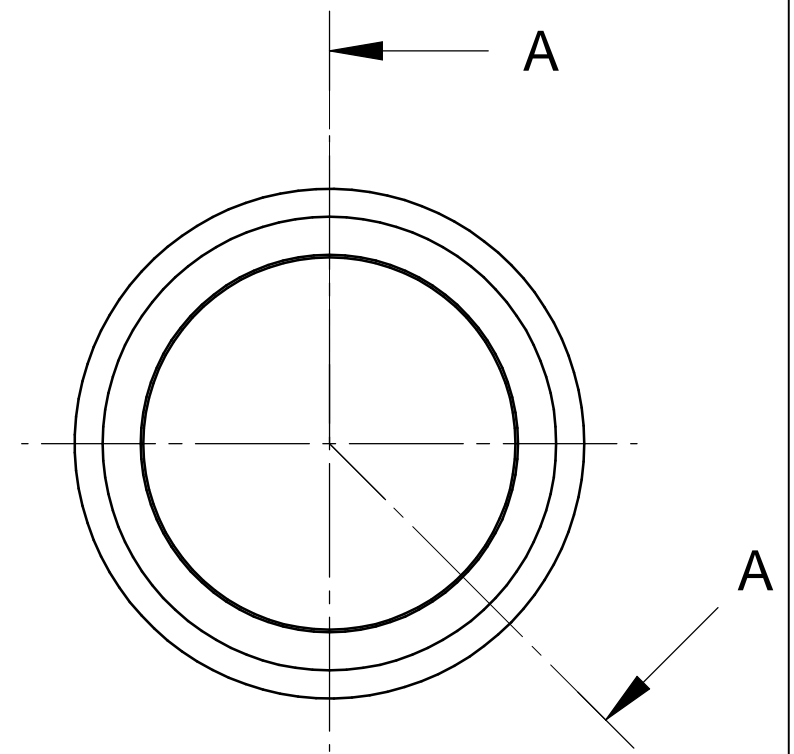
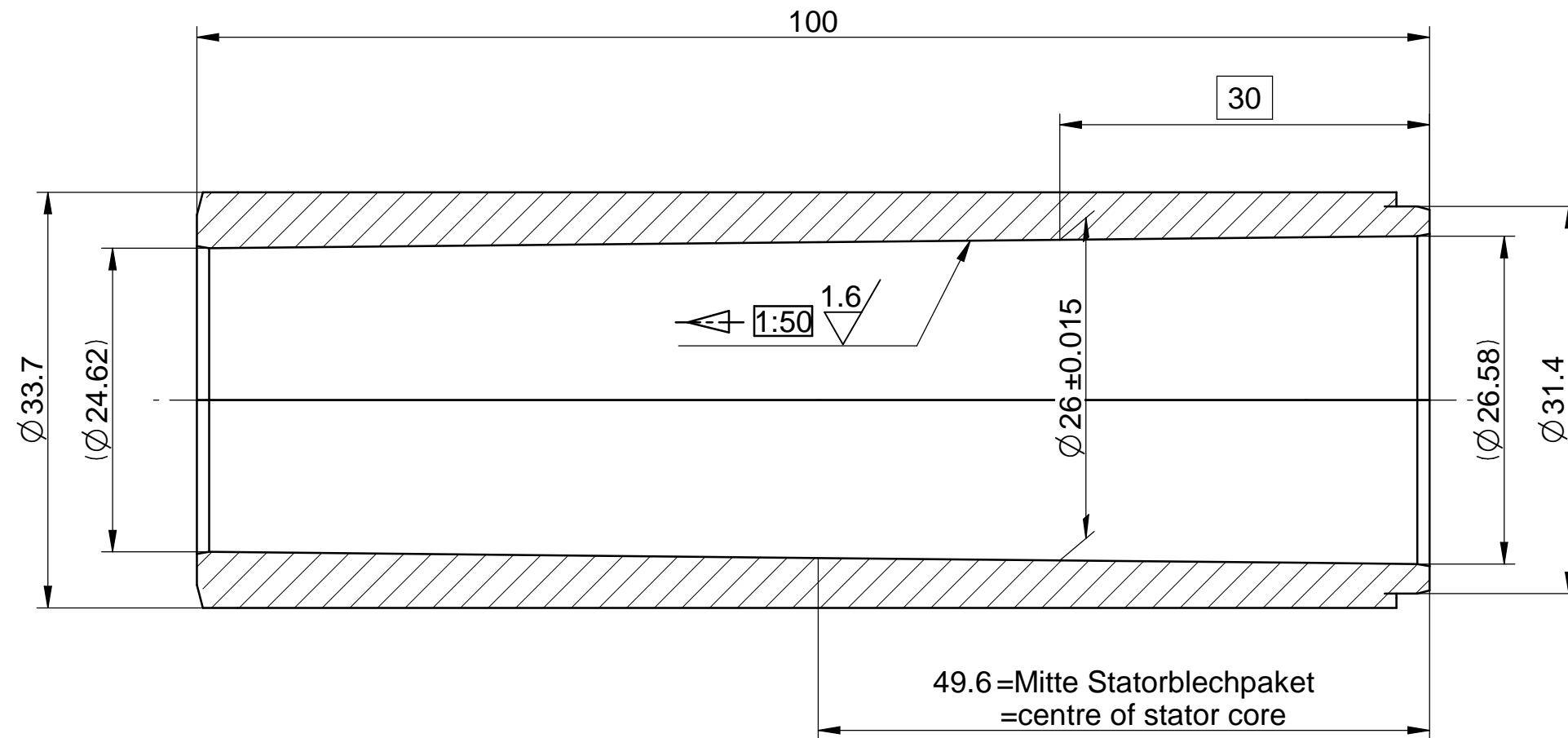
Drehzahl / speed	105000						min ⁻¹
Frequenz / frequency	1750						Hz
Leistung / power S1	10						kW
Spannung / voltage	280						V
Strom / current	22						A

Confidential

04.02.2016 / neda

Rotor mSpW 6/8-2-a10

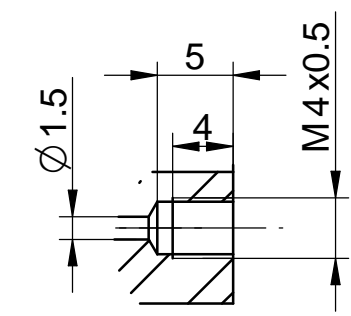
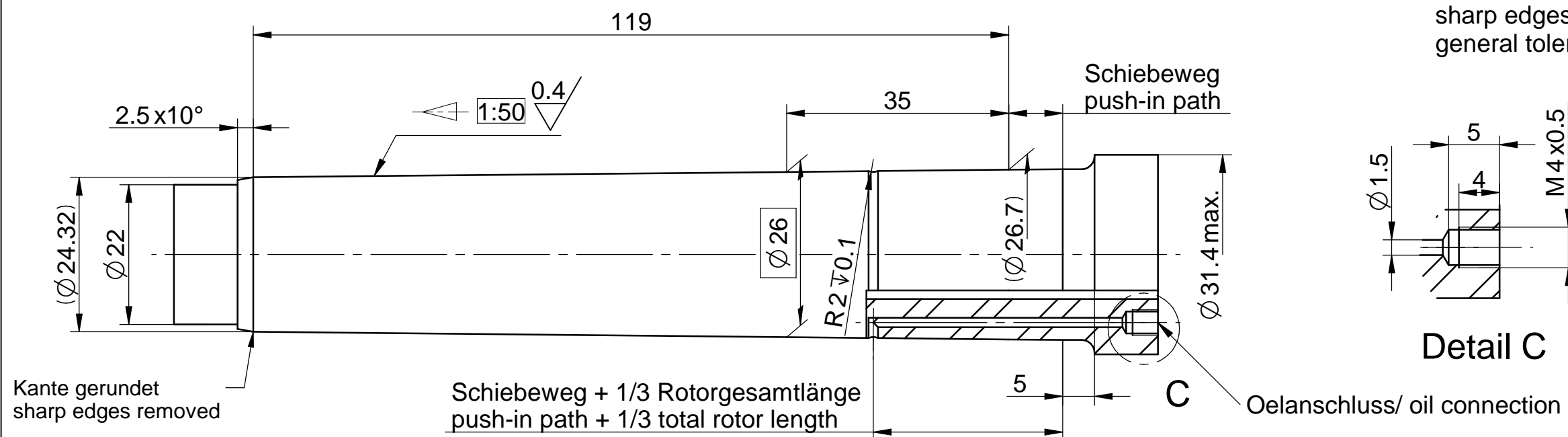
Confidential



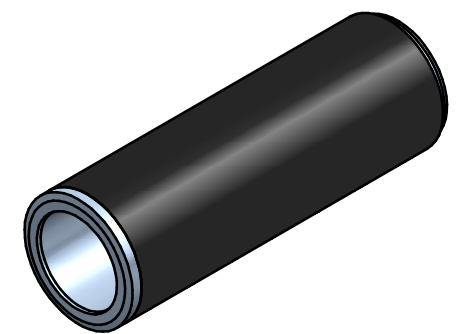
Rotor nicht gewuchtet
Kanten gebrochen 0.2...0.5x45°
Allgemeintoleranzen nach ISO 2768-mH

Rotor not balanced
sharp edges removed 0.2...0.5x45°
general tolerances according to ISO 2768-mH


Wellenbeispiel / example of shaft:



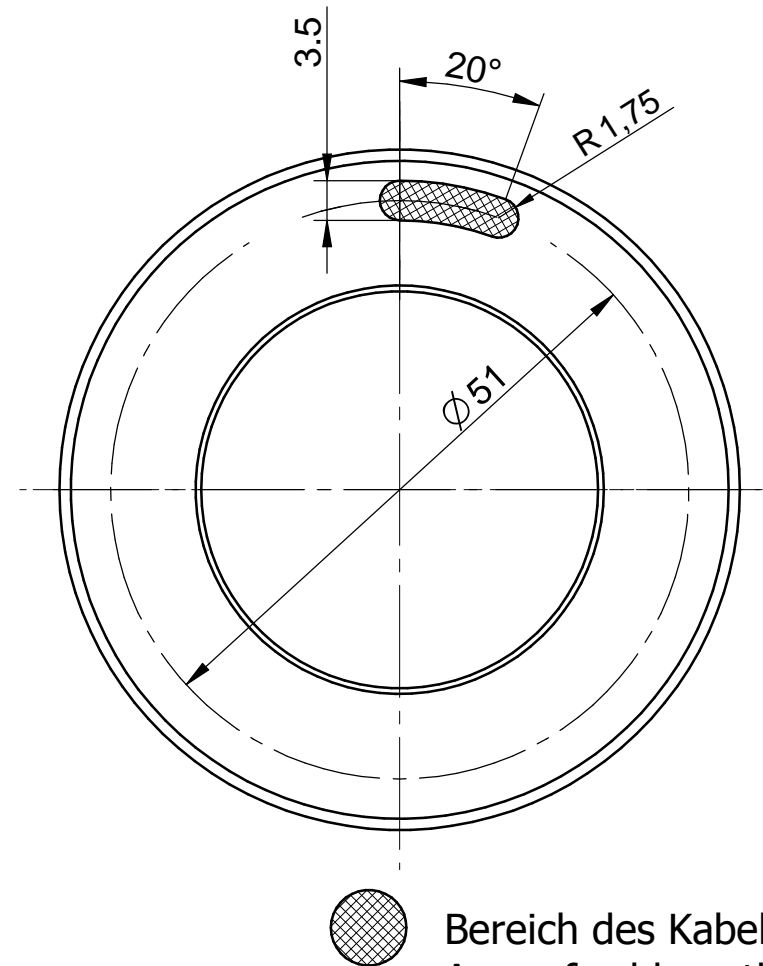
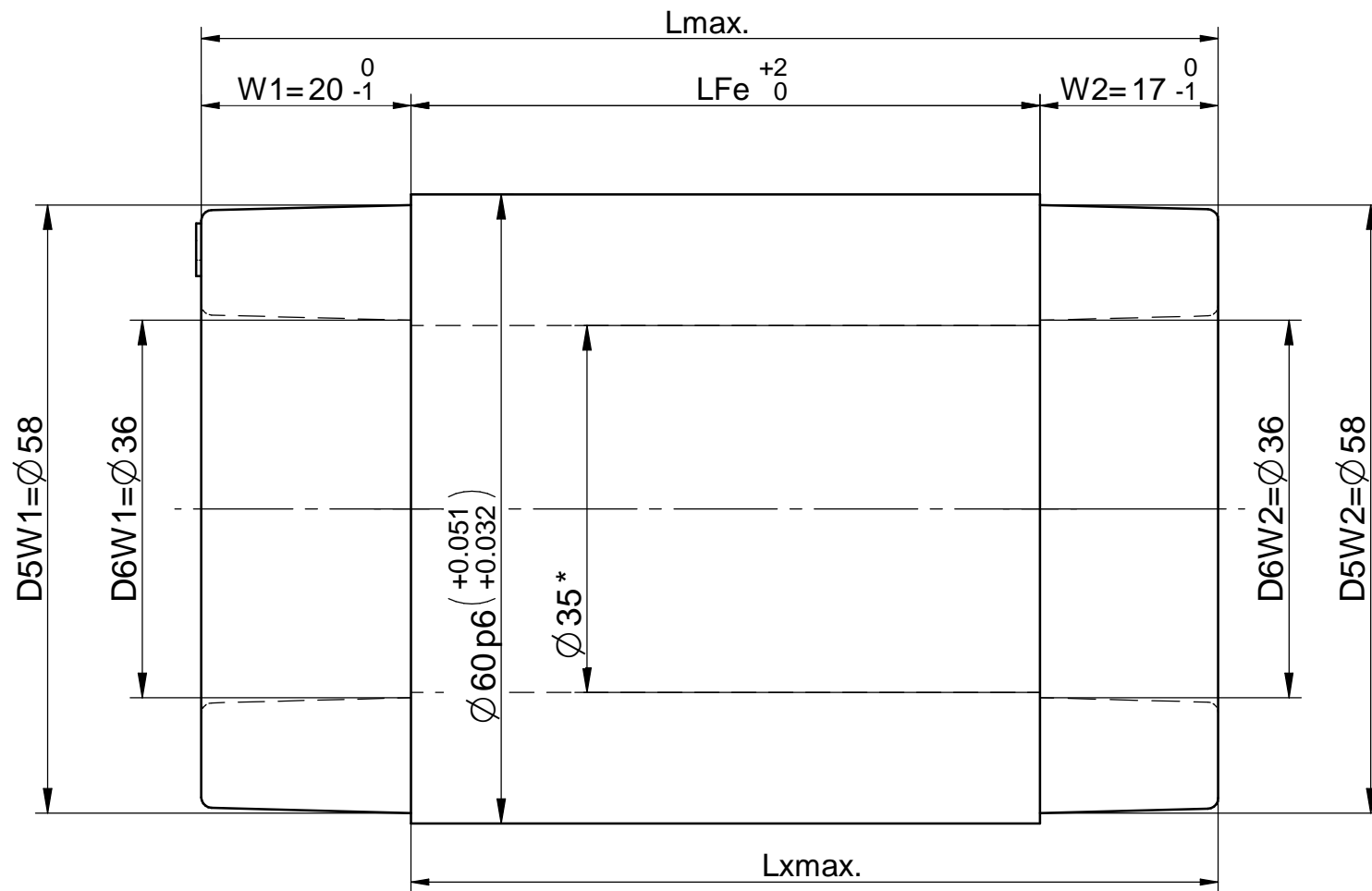
Detail C

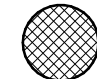


Massblatt e+a Motorelemente

	mSpW 6/8-2-a10	Masstab 2:1
	100912-004.021	Revision 001
		Stand 11.09.2012

Stator mSpW 6/..-2-a..Enca



 Bereich des Kabelabganges
 Area of cable outlet

Anschlüssen max.
 Power leads up to max.
 3x AWG16
 oder
 6x AWG20
 inkl. 3 Fühler/ Sensor

Material PTFE
 Tmax.= 260°
 Litze versilbert
 silver plated wire

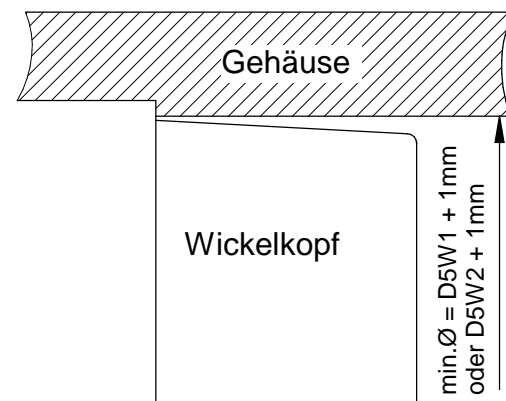
Biegeradien min.
 feste Verlegungen 3x Ø
 freie Verlegung 5x Ø

bending radius min.
 at fixed laying 3x Ø
 at free laying 5x Ø

*Die Bohrung ist nicht kleiner als ein Zylinder mit Ø 34.9

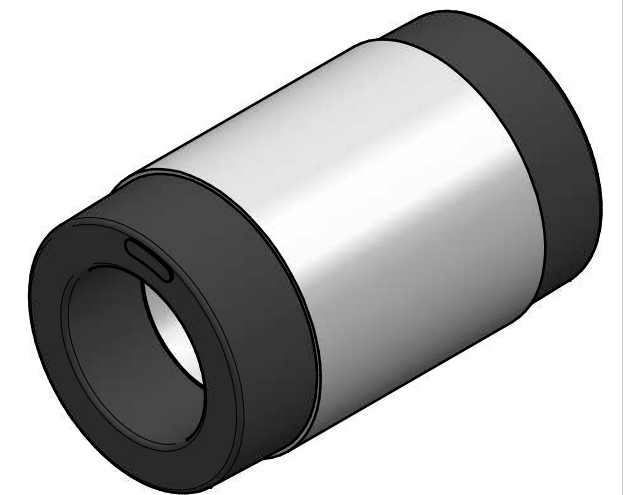
*The ID of the stator lamination core is not smaller than Ø 34.9

Einbaubeispiel:




LFe	Lmax.	Lxmax.
20	58	38
30	68	48
40	78	58
45	83	63
60	98	78
80	118	98

Alle Masse / all dimensions in mm



Confidential

Massblatt e+a Motorelemente

 Elektromaschinen und Antriebe	mSpW 6/..-2-a..Enca	Masstab 1.5:1
	290505-004.011.001	Revision 001
		Stand 30.04.2015

Diese Darstellung ist unser geistiges Eigentum. Sie darf ohne unsere schriftliche Zustimmung weder irgendwo kopiert, noch zur Anfertigung des Werkes gebracht oder Dritten bekanntgegeben werden.

The information contained in this drawing is limited to the recipient only. It is strictly confidential and is not to be reproduced nor transmitted to an unauthorized party.